NOVA SCHOOL OF SCIENCE & TECHNOLOGY

DEPARTAMENT OF CHEMISTRY

ANDRÉ TEIXEIRA DIAS

BSc in Biochemistry

GOLD NANOPROBES FOR MOLECULAR DETECTION OF SNPS RELATED TO LACTOSE INTOLERANCE

MASTER IN BIOTECHNOLOGY

NOVA University Lisbon
December, 2021

DEPARTAMENT OF
CHEMISTRY

GOLD NANOPROBES FOR MOLECULAR DETECTION OF SNPS RELATED TO LACTOSE INTOLERANCE

ANDRÉ TEIXEIRA DIAS

BSc in Biochemistry

Adviser: José Ricardo Ramos Franco Tavares,
Associate Professor, NOVA University Lisbon

Co-advisers: Maria Enea
PhD Researcher, NOVA University Lisbon

Examination Committee:

Chair: Carlos Alberto Gomes Salgueiro,
Associate Professor, FCT-NOVA

Rapporteurs: Miguel Peixoto,
PhD Researcher, FCUP

Adviser: José Ricardo Ramos Franco Tavares,
Associate Professor, NOVA University Lisbon

MASTER IN BIOTECHNOLOGY

NOVA University Lisbon
December, 2021

Gold nanoprobes for molecular detection of SNPs related to lactose intolerance

Agradecimentos

Ao Professor Ricardo Franco,
pela oportunidade, tempo despendido e interesse em estar a par do trabalho desenvolvido.

À Maria Enea,
pela amabilidade, interesse e paciência para discutir qualquer assunto e acima de tudo pela enorme ajuda prestada que tornou a realização desta tese possível. Desejo-te tudo de bom.

Aos membros do laboratório 603,
pelo ambiente acolhedor, todas as conversas sérias e menos sérias, a ajuda fornecida e por tornarem este percurso mais interessante.

À Professora Eulália Pereira e os membros do projeto NANOMODE,
pelas ideias, debates e ajuda no decorrer da dissertação.

Aos meus amigos,
por tornarem o meu percurso tão mais acolhedor.

À Matilde,
por todo o apoio e carinho que me proporciona.

À minha família,
por todos os valores que me transmitiram.

Aos meus pais,
por tudo.

Abstract

Lactose intolerance is a condition that affects millions of people around the world. The current diagnosis methods have shortcomings, namely high costs and long processing times. As such, innovative detection mechanisms should be developed to allow fast, reliable, and inexpensive diagnosis in a point-of-care format. The utilization of gold nanoparticles could overcome these limitations due to their aggregation-dependent colorimetric properties. The developed work focused on their use for the diagnostic of lactose intolerance through the single nucleotide polymorphism associated with European populations (C/T -13910 LCT).

Gold nanoparticles with different diameters (15 or 40 nm) were synthesized, characterized and functionalized (salt-aging or pH method). The functionalization was performed using a 5' or 3' thiol-modified oligonucleotide. The salt-aging method yielded better results for 15 nm gold nanoparticles, while the pH method worked better for 40 nm gold nanoparticles.

The evaluation of several DNA targets through non-cross-linking method showed that anti-parallel hybridization resulted in DNA duplexes with greater stability and stronger colorimetric distinction, when compared to parallel hybridization.

Cross-linking and non-cross-linking methodologies were then applied to the optimized conditions. The cross-linking method revealed that nanoprobes obtained using the 3' thiol-modified oligonucleotide had problems with hybridization, requiring further optimization. From the non-cross-linking method, it was possible to conclude that the 40 nm nanoprobes led to better colorimetric distinction between the complementary and mutated samples (upwards of 60%) and improved statistical significance in comparison to 15 nm nanoprobes. For the tested conditions, smaller DNA targets (40 b.p.) resulted in better colorimetric distinction compared to larger DNA targets (120 b.p.). The differences seen also improved with the increase of DNA target concentration (from 0.25 up to 100 ng/μL).

These results demonstrate the capabilities of 40 nm nanoprobes for detection of lactose intolerance and highlight the importance of optimizing the length and concentration of the DNA target.

Keywords: Gold nanoparticles; Single nucleotide polymorphism; Lactose intolerance; Point-of-care detection system

Resumo

A intolerância à lactose é uma condição que afeta milhões de pessoas em todo o mundo. Os mecanismos de deteção utilizados possuem alguns aspetos que devem ser melhorados, como custos elevados e longo tempo de processamento. Assim sendo, mecanismos de deteção inovativos devem ser desenvolvidos para possibilitar um diagnóstico rápido, reprodutível e barato num formato *point-of-care*. A utilização de nanopartículas de ouro pode colmatar estas limitações devido às suas propriedades colorimétricas dependentes da agregação. O trabalho desenvolvido focou-se no seu uso para o diagnóstico de intolerância à lactose através do polimorfismo de base única associado a populações Europeias (C/T -13910 LCT).

Nanopartículas de ouro com diferentes diâmetros (15 ou 40 nm) foram sintetizadas, caracterizadas e funcionalizadas (método *salt-aging* ou pH). A funcionalização foi realizada utilizando oligonucleótidos modificados com um grupo tiol a 5' ou 3'. O método de *salt-aging* produziu melhores resultados para nanopartículas de ouro de 15 nm, enquanto o método de pH funcionou melhor para nanopartículas de ouro de 40 nm.

A testagem de diversos alvos de DNA através do método de *non-cross-linking* demonstrou que hibridização antiparalela resulta em duplexes de DNA mais estáveis e com melhor distinção colorimétrica, quando comparado com hibridização paralela.

Os métodos de *cross-linking* e *non-cross-linking* foram de seguida aplicadas às condições otimizadas. Os ensaios de *cross-linking* revelaram que as nanosondas obtidas através do oligonucleótido modificado com grupo tiol a 3' tinha problemas com hibridização, requerendo mais otimização. Através do método *non-cross-linking* foi possível concluir que as nanosondas de 40 nm levaram a uma melhor distinção colorimétrica entre amostras com DNA complementar e DNA mutado (até 60 %) e uma significância estatística melhorada, quando comparado com as nanosondas de 15 nm. Para as condições testadas, alvos de DNA curtos (40 p.b.) resultaram numa distinção colorimétrica superior, quando comparado com os alvos de DNA longos (120 p.b.). As diferenças visualizadas também melhoraram com o aumento da concentração do DNA alvo (de 0.25 até 100 ng/µL).

Estes resultados demonstram as capacidades das nanosondas de 40 nm para a deteção de intolerância à lactose e realçam a importância da otimização do tamanho e concentração do DNA alvo.

Palavras-chave: Nanopartículas de ouro; Polimorfismo de base única; Intolerância à lactose; Sistema de deteção *point-of-care*

Table of contents

Figure Index

Table Index

Abbreviations

3’ SH-OL	Thiol-modified oligonucleotide with thiol modification at 3’ end
5’ SH-OL	Thiol-modified oligonucleotide with thiol modification at 5’ end
ATH	Adult-type hypolactasia
Au-nanoprobe	Gold nanoprobe
AuNP	Gold nanoparticle
b.p.	Base pairs
CL	Cross-linking
CLD	Congenital lactase deficiency
DLS	Dynamic light scattering
ELS	Electrophoretic light scattering
LI	Lactose intolerance
LSPR	Localized surface plasmon resonance
NCL	Non-cross-linking
NP	Nanoparticle
NPL	Non-persistent lactase
OL	Oligonucleotide
PB	Phosphate buffer
PL	Persistent lactase
RT-PCR	Real-time polymerase chain reaction
SA	Salt-aging
SDS	Sodium dodecyl sulphate
SH	Secondary hypolactasia
SH-OL	Thiol-modified oligonucleotide
ssDNA	Single strand DNA
TCEP	Tris(2-carboxyethyl) phosphine
UV-Vis	Ultraviolet-visible spectroscopy

Chapter 1

Introduction

1.1. Lactose intolerance

Over the last decade, lactose intolerance (LI) has seen an uprise in public discussion due to the increasing concern over healthy eating habits and overall wellbeing [1]. Although this topic has seen expanded discussion, its argument is often guided by misinformation, leading to diverging public opinions and, consequently, unrequired adjustments in one's diet. Due to this mystification surrounding LI, some people actively stop consuming milk from an animal source on the premise that some relatives or friends made this change and felt better after doing so. This is supported by the significant reduction in milk consumption that has been seen in the last few years, with a nearly 11 % reduction in 2016 alone [2]. Even though some people make this change consciously, based on their personal needs or beliefs, a portion of the population does so on the assumption that it improves their health, without scientific reasoning behind it. As such, it is vital to shed light on this subject and lead people to make rational choices instead of blindly following public opinions, which frequently have warped notions of the science behind such conditions.

On the other hand, the symptoms of LI, such as stomach pain, cramps and bloating, as well as gas and diarrhoea, can be particularly cumbersome [3]. These symptoms can be attributed to a multitude of conditions. When coupled with the fact that LI is highly disseminated, with certain populations reaching near 70 % incidence [4], a need for a proper diagnosis is an urging reality. This could ensure the individuals' wellbeing with adequate dietary adjustments only if necessary.

There are several concepts, such as hypolactasia, commonly utilised to describe LI. Nevertheless, these have slight nuances that set them apart from the proper definition. For example, a lactose-intolerant individual is someone that possesses abdominal symptoms that characterise LI [5], regardless of the specific condition behind it. Hypolactasia represents a specific condition that can lead to LI [6].

Despite the condition afflicting the patient, two distinct phenotypes are usually utilized to differentiate adult populations across the world according to their lactose digesting enzyme. These will be further explored.

1.1.1. Basic principles and ancient phenotype

Lactose is a disaccharide whose source is tightly bound to mammals' milk [7], since it is the primary source of carbohydrates in early years of development. It is composed of galactose and glucose [8], as seen in Figure 1.1. Its production is dependent on a protein complex constituted by α-lactalbumin and galactosyltransferase. Only when the two are present can lactose be synthetised by the mammary glands of mammals, since the binding of α-lactalbumin induces a conformational change that alters the substrate specificity of galactosyltransferase to glucose [9].

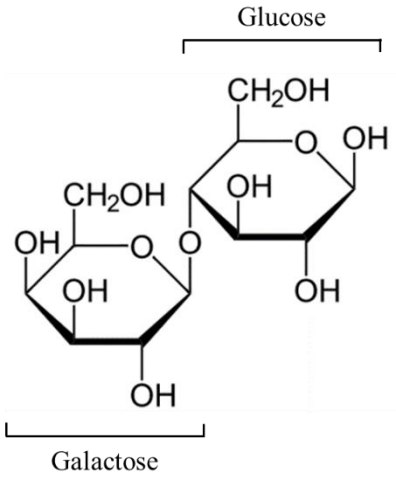

Figure 1.1 – Structural depiction of the lactose dimer and its two monomers, galactose and glucose.

In order to understand the origin of LI, it is crucial to establish that lactase is the enzyme responsible for the digestion of lactose in humans. If a loss of this enzyme occurs, it can lead to LI.

Our ancestors only produced this enzyme in early development to allow the digestion of lactose present in breast or mammal milk, the primary food source at this stage, but saw a massive decline in its production upon further growth. This ancestral phenotype is designated non-persistent lactase (NPL) [10].

Somewhere in Human development, individuals with persistent lactase (PL), who present lactase activity throughout their lifetime, appeared. These individuals are speculated to be a product of induced mutagenesis. This mutation is theorized to have developed in specific geographic populations over the need to utilise mammal milk as one of the primary sources of carbon hydrates over the course on an individual's life [11]. This adaptative mutation ensured the survival of certain populations where other options, such as agriculture, were not available.

1.1.2. Lactose intolerance types

LI is the name utilized to describe the broad problem. The general condition can be subdivided into two: primary, further divided into congenital lactase deficiency (CLD) and adult-type hypolactasia (ATH), and secondary hypolactasia (SH) [12].

CLD is considered a rare condition, as it is a recessive autosomal genetic transmitted form of LI [13]. This condition is the most extreme of the family, with a total or nearly total loss of lactase production seen from the point of birth, where even the ingestion of breast milk for the growing child is not advised.

ATH is also a product of a recessive autosomal genetic mutation but it is a far more common condition, since it derives from the ancestral lineage [14]. It is less aggressive than CLD since it is characterised by a reduction in lactase activity after the breastfeeding period due to genetic programming, which to this day remains a mystery. This is the condition associated with the NPL phenotype.

Lastly, SH, unlike the primary type, is often transitory, as it is a result of perturbations at the intestinal mucosa, which can arise from a multitude of reasons: bacteria overgrowth; parasitosis; drug and alcohol ingestion, among others [15]. Currently, this is the only treatable type.

A summary of these conditions and their characteristics can be seen in Table 1.1.

Table 1.1 – Types of LI, their origin, incidence, consequences and manifestation period. Information taken from reference 13.

Lactose intolerance			
		CLD	**ATH**
Primary	Origin	Mutations at LCT gene	Mutations at MCM6 gene
	Incidence	Rare	Common
	Consequences	No lactase production	Loss of lactase production
	Manifestation	At point of birth	After breastfeeding
		SH	
Secondary	Origin	Gut microbiome perturbation	
	Incidence	Common	
	Consequences	Punctual loss of lactase production	
	Manifestation	Possible throughout whole life	

The lactase enzyme is codified in the LCT gene, localized in the 2q21 locus along the chromosome 2. Its regulation is tied to the MCM6 gene, adjacently localized in the same locus, due to the presence of a regulator region that acts over the LCT gene [16], as evidenced in Figure 1.2. A mutation in either gene has implications towards the existence of LI.

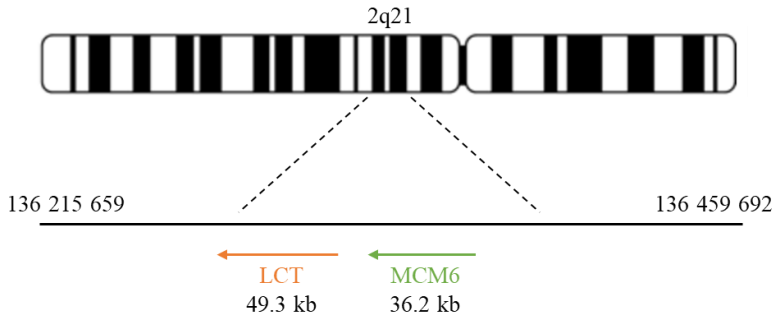

Figure 1.2 – LCT and MCM6 gene encoding regions in chromosome 2.

(1) Congenital lactase deficiency

CLD is associated with mutations at the LCT gene that lead to a loss of production of lactase from the point of birth. A total of five mutations are associated with this condition, three leading to premature truncation of lactase and two that result in amino acid substitutions [17]. The mutations that lead to premature truncation are as follows: a nonsense mutation c.4170T→A; a deletion of four nucleotides c.4998_5001del TGAG; a two-nucleotide deletion c.653_654del CT. On the other hand, the mutations that result in amino acid substitutions are as follows: a transversion c.804G→C, which alters a histidine to a glutamine; a transition c.4087G→A, that modifies a serine for a glycine. The estimated incidence of this condition is 1:60000 for Finland individuals [18], making it extremely rare.

(2) Adult-type hypolactasia

ATH is associated with single nucleotide mutations at the MCM6 gene, which leads to a loss of the production of lactase over an individual's life, starting at 5 years of age. There are many polymorphisms associated with this condition but two are of greater importance: C/T at nucleotide -13910 and G/A at nucleotide -22018. European individuals with ATH are homozygous to both C-13910 (CC) and G-22018 (GG), with a 100 and 97% correlation, respectively [19].

The C/T polymorphism is located in a transcriptional enhancer sequence which, in the case of C-13910, leads to a normal activation of the LCT gene, making it transcriptional inactive after weaning. This results in the NPL phenotype. Contrarily, T-13910 leads to a stronger activation of the LCT gene, resulting in a transcriptional active gene after weaning, which characterizes the PL phenotype. It is also important to note that heterozygous individuals (CT / GA) possess an intermediary lactase activity and are more prone to developing SH than their homozygous counterparts (TT / AA) [20]. A summary of this information can be seen in Table 1.2.

Table 1.2 – C/T and G/A polymorphisms and their resulting phenotypes. Information taken from reference 20 and 21.

Genotype		Phenotype
C/T -13910	CC	Non-persistent lactase (LI - ATH)
	CT	Persistent lactase (LT)
	TT	Persistent lactase (LT)
G/A -22018	GG	Non-persistent lactase (LI - ATH)
	GA	Persistent lactase (LT)
	AA	Persistent lactase (LT)

Three other mutations were later discovered, inherent from different populations, namely Africa and the Middle East. These discoveries reinforced the theory that LI was a product of induced mutagenesis.

ATH is estimated to be present in near 70 % of the adult population [4], although some populations have extremely variable incidences, arguably due to the mutagenesis that led to PL in certain regions of the world. The latter phenotype is strongly associated with Caucasian individuals, descendent of Northern Europe populations, as evidenced by Figure 1.3. These populations strongly developed livestock and milk consumption 10000 years ago. On the other hand, in regions that relied more in agriculture, this phenotype is scarcer [11].

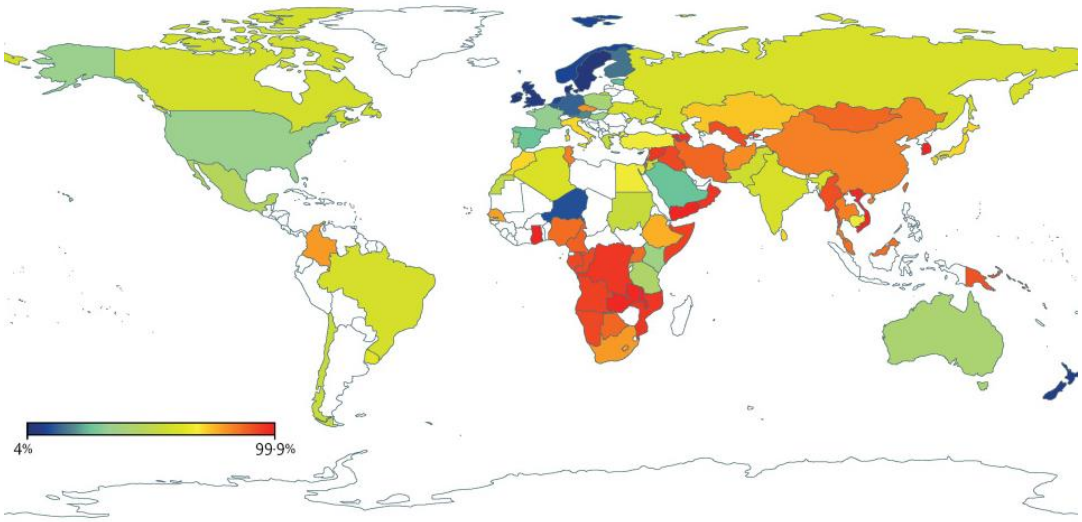

Figure 1.3 – World map with the incidence of lactose malabsorption according to country. Image adapted from reference 4.

1.1.3. Clinical diagnostic for the detection of lactose intolerance

In the clinical practice, patients with digestive symptoms of unknown causes are firstly evaluated for food intolerances, including gluten and lactose, as these are the most common [21]. If the patient's symptoms align with LI, a lactose-free diet is suggested for a period of two weeks, after which, the persistence of the symptoms is evaluated.

For a more precise diagnosis, capable of confirming the presence of LI or obtaining additional information, such as the amount of lactase being produced or the cause of the intolerance, other techniques can be used: Jejunal/Duodenal biopsy; Lactose tolerance test; Milk tolerance test; Hydrogen breath test; DNA sequencing.

(1) Jejunal/Duodenal biopsy

The first accurate method capable of detecting LI was the jejunal biopsy [22]. This assay consisted in performing a direct biochemical lactase assay on a jejunal sample. Even though it had a high sensitivity, it was substituted by the endoscopic duodenal biopsy due to its invasiveness.

In the endoscopic duodenal biopsy, the same principle is applied but to samples taken from the duodenum [23]. It is considered a less invasive method presenting good specificity and sensitivity especially in cases of severe LI. Nevertheless, it presents a major disadvantage since the lactase activity measured in this digestive zone is 40 % lower [24], which can difficult the diagnosis. Therefore, new diagnostic methods that exclude the need of biopsies are often preferred.

(2) Lactose tolerance test and milk tolerance test

Both lactose and milk tolerance tests are based on the same principle: evaluate the glucose levels after the consumption of a lactose solution or milk, respectively [24]. Following either's ingestion, a blood sample is taken from the patient, and the glucose levels are measured. If the glucose levels rise slowly or do not rise at all, the patient is diagnosed with LI due to their inability to transform lactose into glucose.

The main advantage of these tests is their large acceptance by the patients as these are less invasive compared to jejunal/duodenal biopsies. On the other hand, they rely on the consumption of lactose, which can be sufficient to induce uncomfortable symptoms in lactose intolerant patients.

(3) Hydrogen breath test

The hydrogen breath test is widely used for the screening of LI for the general population [25]. It relies on the determination of hydrogen, carbon dioxide and methane liberated through the lungs, after the consumption of a lactose solution [26]. After the ingestion of the lactose solution, the patient's breath is measured using a breathalyser, with subsequent measurements being taken in 15-minute intervals for several hours. If the patient is lactose intolerant, the levels of liberated gases should rise. This rise is a sign of bacterial lactose fermentation, which takes place in the intestinal flora, when lactose is not properly digested.

Similarly to the previous methods, the disadvantage of the test is the need for ingestion of a lactose solution, which can give rise to unwanted symptoms. Its reliability can also be questioned since false negatives can occur if the patient is under the effect of antibiotics or its colonic pH is very low [26].

(4) DNA sequencing

The development of the genetic branch of science led to the creation of new detection techniques. After the discovery of the PL alleles, new types of assays that relied on the use of the patient's DNA were established. Real-time polymerase chain reaction (RT-PCR) is one of these techniques, which can be effective in detecting LI [27].

The RT-PCR presents a special advantage over the conventional methods since it allows the discrimination of which type of LI affects the patient. This technique enables examining the key DNA segments responsible for different LI types. Even if the patient does not possess the mutations that indicate LI, but its symptoms align with this condition, it can be attributed to disruptions in gut microbiota, effectively discerning between all types of the disease.

The main advantages of this technique are its non-invasiveness and that the diagnosis is lactose ingestion free, providing better comfort to the patient [24]. On the other hand, it is quite a complex assay that requires specialized equipment and personnel, making the diagnosis more time consuming and expensive. As such, it is not the first choice for the diagnosis of LI.

There are several aspects that can and should be improved in the LI diagnostic in order to meet current world's needs, where commodity and time are more valuable than ever before. Upon an analysis of the available methods, it becomes evident that they are extremely time consuming, since the time required for acquiring the results varies from several hours, for the hydrogen breath test, to several days or weeks, for the remaining tests. It should also be noted that some of these tests require the consumption of lactose, which can have mild effects on the patients' health. Others are very invasive, which can turn patients away from conducting the proper diagnosis. Most important of all, all procedures require either expensive equipment or specialized personnel, which can be extremely rare in countries with less financial means. As such, the development of a new method that allows for a quick response time, avoids lactose consumption, presents itself as a cheaper alternative with unparallel commodity, is a fundamental improvement over the existing methodologies.

1.2. Gold nanoparticles

Gold nanoparticles (AuNPs) have been extensively explored in the last decades, either as a platform to allow administration of certain molecules [28], or as a detection mechanism [29]. At the nanoscale (from 1 to 100 nm [30]) gold (Au) presents a new set of chemical, electrical and optical properties that arise from superficial and quantum confinement effects [31]. Even though there are many types of metallic nanoparticles (NPs), AuNPs are the most attractive due to their optical properties, explained by the localized surface plasmon resonance phenomenon, as well as a good shelf-life, easiness to synthetise and functionalize with other molecules and low toxicity [32].

1.2.1. Localized surface plasmon resonance and its factors

The localized surface plasmon resonance (LSPR) phenomenon provides an intense colour to metallic NP colloidal suspensions, making the absorption and dispersion coefficient of the NPs extremely high in the visible region of the radiation spectrum, resulting in a characteristic peak in the Ultraviolet-visible zone. For example, for 15 nm spherical AuNPs, the band originated due to the LSPR occurs near 520 nm [33]. This effect arises from the interaction between the electromagnetic field of the incident light and the free electrons of the valence band of the NPs [34], as presented in Figure 1.4.

There are several factors that significantly affect the beforementioned phenomenon: size, shape, interparticle distance – intrinsic parameters; interactions between NPs and its media, evaluated by the refractive index – extrinsic parameters. The refractive index and NP size have a less pronounced effect, while their shape and interparticle distance induce greater changes in their Ultraviolet-visible spectroscopy (UV-Vis) spectra [35].

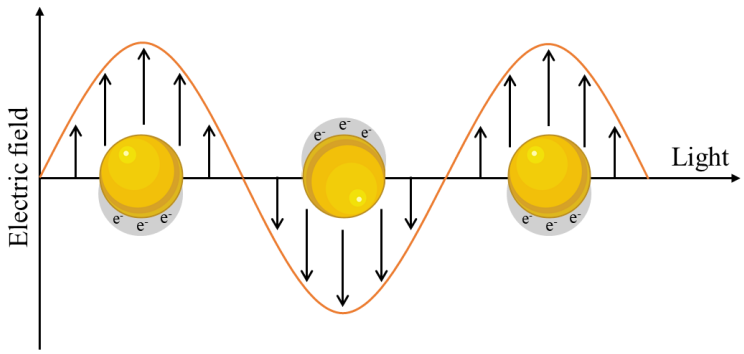

Figure 1.4 – LSPR phenomenon induced in a AuNP by an external electrical field. Assets for the image were taken from Biorender.

(1) Size

Several studies have demonstrated that NP size impacts their UV-Vis spectra. For example, for spherical AuNPs, which possess only one absorption peak, it is possible to verify that their optical properties are tightly dependent on their diameter, since size variation leads to slight changes of the LSPR peak.

As they get bigger, a red shift can be seen in their absorption peak, as seen in Figure 1.5 (A). The red shift occurs because more light is dispersed by the NPs due to their growing size [36]. This results in a smaller frequency of the plasmon resonance, leading to a less energetic peak.

Even though this is the most predominant effect of NP size, there are other aspects to keep in mind. The extinction coefficient of larger NPs is several fold greater than that of smaller NPs [37], conferring a stronger colour to their solution when concentration is normalized. This phenomenon, illustrated in Figure 1.5 (B), is of extreme importance in colorimetric assays. The size of the NPs also affects how they interact with the human body [38], which is particularly significant when trying to breach specific barriers in the human body and assess their diverging toxicity levels. This effect is important when mentioning applications that rely on NPs' administration in the human body.

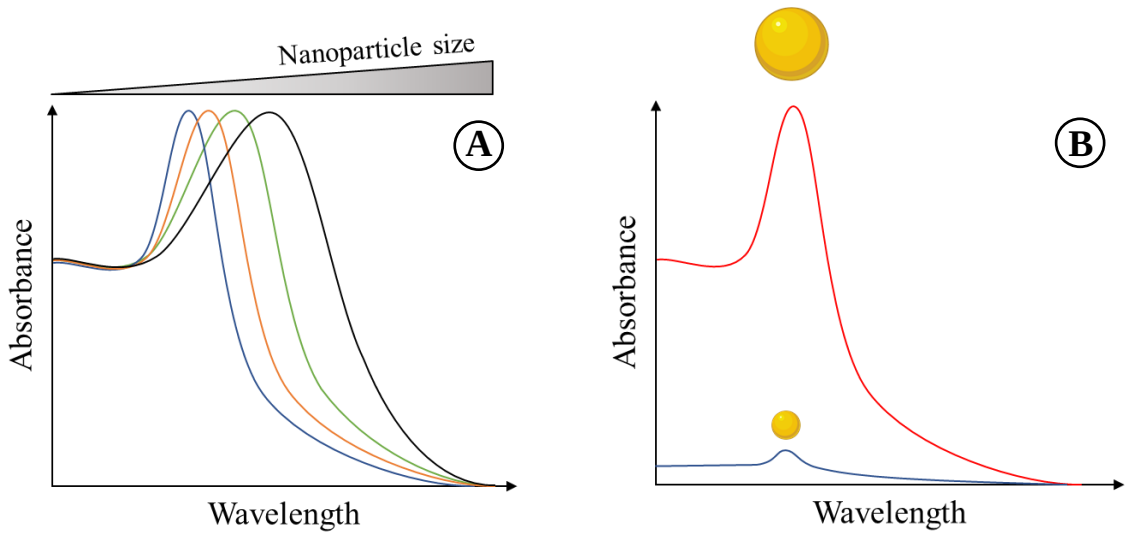

Figure 1.5 – Effect of NP size on (A) – Maximum absorbance peak, where a red shift is seen, as NP size increases; (B) – Extinction coefficient, where an increase in the coefficient is seen, as NP size increases. Assets for the image were taken from Biorender.

(2) Shape

Unlike spherical NPs that only have one absorption peak, due to their high symmetricity, NPs of other shapes give rise to more than one absorption peak in their UV-Vis spectra [39]. As an example, nanorods have two absorption peaks, consequence of two distinct dipole modes of the plasmon resonance, longitudinal and transverse [40], which are a result of their shape, as seen in Figure 1.6.

As NPs' shape gets more asymmetrical, as is the case of nanostars, new dipolar modes arise, resulting in more absorption peaks and, consequently, more complex spectra [41]. When a high number of peaks appear, they tend to superimpose each other, resulting in new bands.

NPs' shape also affects how they interact with the human body: nanostars, despite their pointy ends, have been shown to have a less pronounced toxicity on endothelial cells [42]; nanorods, with their smaller y axis, also display less toxicity than their nanosphere counterpart [43]. Another interesting property of nanostars is their Raman-enhancing ability, allowing the development of different detection assays that utilize this technique [44]. The red shift of their absorption peak makes them absorb more infrared light, capable of penetrating tissues, and have been extensively studied in hyperthermia assays for the destruction of tumours [45].

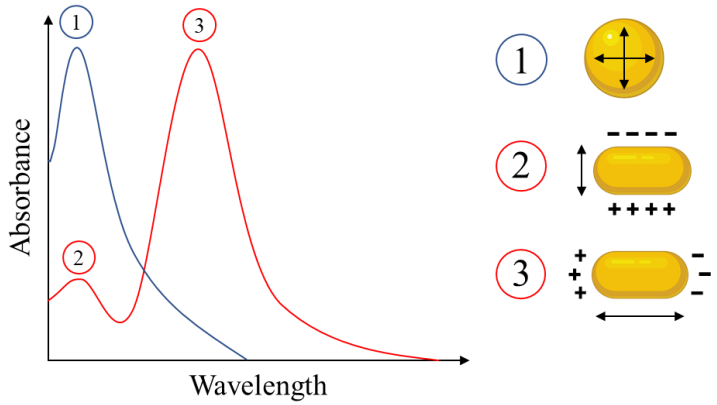

Figure 1.6 – Effect of Au nanomaterial shape on the UV-Vis spectra. Non-symmetrical shapes originate several absorption peaks, due to the existence of several dipolar modes: (1) Absorption peak that originates from the only dipolar mode of AuNPs; (2) Absorption peak that originates from the transverse dipolar mode of nanorods; (3) Absorbance peak that originates from the longitudinal dipolar mode of nanorods. Assets for the image were taken from Biorender.

(3) Interparticle distance

Interparticle distance is a topic of great importance when discussing NPs. As they get closer, they can reach a certain threshold where their repulsive forces will no longer be sufficient to avoid aggregation. When aggregation occurs, the electromagnetic interactions between NPs lead to plasmon excitation, resulting in more intense and energetic electric fields that originate hotspots, name given to superimposing resonance plasmons, that are of extreme importance for colorimetric assays [46].

On an UV-Vis level, NP aggregation leads to a less energetic peak due to the smaller frequency of the plasmon resonance, which is a result of the increased size of these aggregates, when compared to their non-aggregated counterparts [47]. The interparticle distance is often the most important parameter in assays that utilize AuNPs. As seen in Figure 1.7, when aggregation occurs, the characteristic red colour of the Au colloid changes to blue and the band previously centred near 520 nm, changes to a broader band centred near 600 nm for 15 nm NPs [48], due to the coupling of the NPs plasmons.

This colour shift is the basis of many colorimetric detection assays, which often make use of other molecules to protect/induce NP aggregation and obtain a colorimetric response. An example of this is colorimetric DNA sensors, that allow the screening of a target DNA through controlled NP aggregation [49].

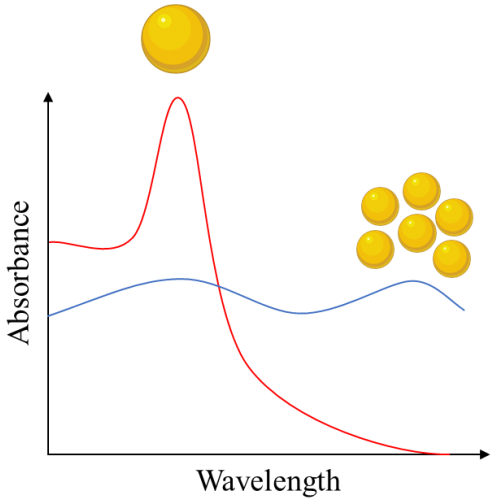

Figure 1.7 – Effect of AuNP aggregation on their UV-Vis spectrum. NP aggregation leads to a red shift of the absorption peak and a red to blue colloid colour change. Assets for the image were taken from Biorender.

(4) Extrinsic factors

The main factors considered in this category are tied to changes in the refraction index of the NPs caused by several factors: temperature, pressure, density and functionalization.

An example of this occurrence is when NPs are functionalized with biomolecules, which results in a raise of the refraction index and leads to a red shift of the absorption peak [50]. This is particularly interesting in assays that utilize DNA hybridization as a detection mechanism since when the oligonucleotide (OL) at the surface of the AuNPs hybridizes with a complementary single strand DNA (ssDNA) a slight red shift of the LSPR band can be seen. Nevertheless, this shift is usually quite small and, as such, other methodologies are commonly applied.

1.2.2. AuNPs synthesis

The synthesis of AuNPs has been widely explored in the last decades and several methods have been developed, which allow the synthesis of different types of NPs for specific applications [51]. Even though laser deposition and ablation represent useful techniques for the synthesis of AuNPs, chemical methods are the most used. These allow the formation of a wide range of sizes and shapes, depending on the synthesis parameters and materials used, making it possible to achieve a very small size dispersion through fine-tuning of the process. This manipulation is encouraged not only to control the size and shape of the obtained NPs, but also to attempt the utilization of more environmental-friendly reagents, which is also an increasing concern in the developed world.

1.2.2.1. Chemical methods

The chemical synthesis of AuNPs relies on the reduction of a Au precursor to atomic Au to allow the formation of NPs [52]. It makes use of 3 distinct elements: an Au salt, a reducing agent and a coating agent. The Au salt provides Au atoms to the synthesis, while the reducing agent leads to the formation of AuNPs through the reduction of Au to its atomic form. Lastly, the coating agent is essential for NP stabilisation, playing a vital role in determining their size, shape and avoiding NP aggregation. There are several distinct chemical methods commonly used, the most relevant being direct reduction and seed-mediated growth, which are based on the same concepts.

Each synthesis has two phases: nucleation, where seeds are formed, and growth, where seeds are grown [53], as illustrated in Figure 1.8. Initially, the concentration of Au in the solution must be raised above the C_{min} threshold. When this condition is met, the forces that lead to the dispersion of aggregates are weaker than the forces that lead to their formation, which results in the formation of several small aggregates, also called seeds, that will pave the way for the synthesis of AuNPs. As these seeds form, the concentration of Au in the solution will diminish below the C_{min} level. In this instance, there will not be enough Au to cause the formation of new aggregates and, instead, the remaining Au is going to accrete to the surface of those already formed, leading to their growth, since the Au concentration is still above the solubility point C_s.

In this process, the type of reducing agent used is extremely important, since it directly impacts the outcome of the synthesis [54]. For example, weaker reducing agents, such as sodium citrate, lead to longer nucleation phases, resulting in larger NPs with a less pronounced size deviation. On the other hand, stronger reducing agents, such as sodium borohydride, have the opposite impact, resulting in a shorter nucleation phase due to fast precipitation of Au. In this case, more nuclei are formed but less growth occurs.

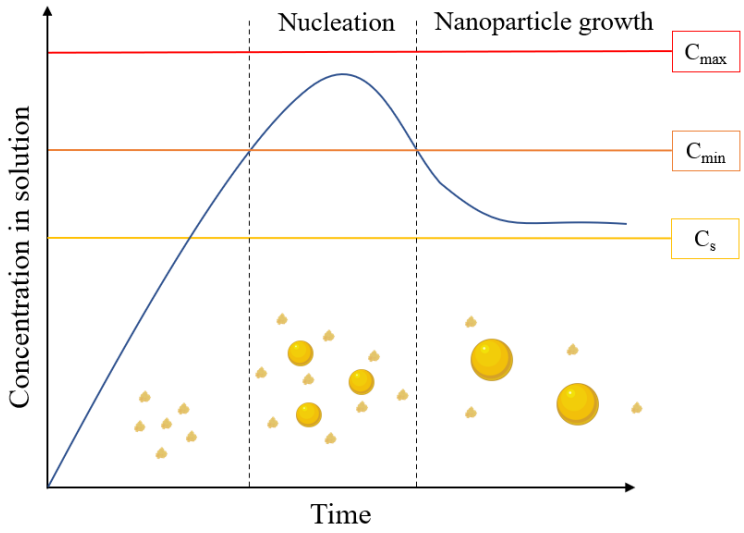

Figure 1.8 – Graphical scheme of the synthesis process of AuNPs. C_{max} – Au concentration at which total precipitation occurs; C_{min} – Au concentration at which partial precipitation occurs, allowing the formation of small aggregates; Cs – Threshold for Au solubility. Assets for the image were taken from Biorender.

(1) Direct reduction

The direct reduction method makes use of an Au salt and a reducing agent for AuNP synthesis. Since the majority of NPs' investigation focuses on 15 nm NPs, the most popularised direct reduction is the citrate method [55]. It makes use of sodium citrate, a weak reducing agent, capable of reducing the Au salt under high temperature and acidic conditions. In this method, citrate also acts as a coating agent, conferring negative charges to the NPs, lessening their aggregation. Through this method, spherical NPs from 9 to 120 nm can be synthesised, depending on the conditions used, as illustrated in Figure 1.9.

Apart from the citrate method, others allow the synthesis of NPs with distinct sizes, e.g., using boron sodium hydrate, a stronger reducing agent, to obtain smaller NPs (5 nm) [56].

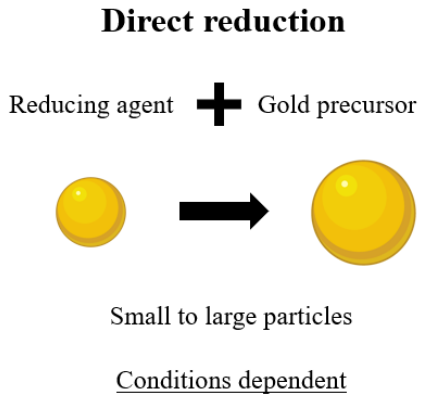

Figure 1.9 – Illustrative representation of the direct reduction chemical synthesis method. Assets for the image were taken from Biorender.

(2) Seed-mediated growth

In seed-mediated growth, the syntheses are usually conducted using distinct reacting conditions. This method is commonly used to obtain larger NPs with a smaller size deviation [57], which is quite substantial using direct reduction. On top of this, it can also be used to obtain NPs with a specific shape [58].

When the goal is to synthesise similar-sized NPs, the seeds must first be formed, using either a strong or weak reducing agent [59]. Following this step, their media is changed, with the addition of more Au precursor and a weak reducing agent. This will induce a slow growth of the aggregates, leading to a more uniform enlargement of the NPs and a smaller size deviation, due to limited-diffusion growth.

Regarding the manipulation of the NPs' shape, it is important to have in mind that, in a synthesis process, the shape and crystallographic structure of the resulting NPs is profoundly linked to their crystalline facets [60]. The growth of specific crystalline facets can be modulated by the introduction of certain components, usually denominated stabilisers, which can have a preference for particular crystalline facets. When these stabilisers are added, the facet they interact with becomes less available to interact with other materials in the solution, resulting in a less pronounced growth of that specific facet. Therefore, using a different set of stabilisers, it is possible to modulate the growth of certain crystalline facets of NPs and acquire distinct shapes. A summary of the size and shape manipulation can be seen in Figure 1.10.

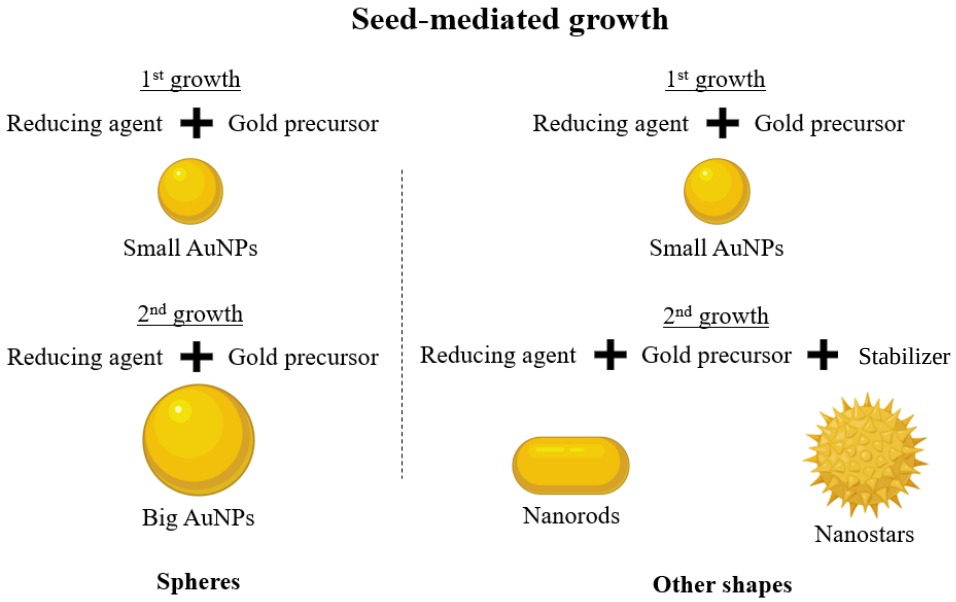

Figure 1.10 – Illustrative representation of the seed-mediated growth chemical synthesis method. This method is usually utilized to obtain larger NPs with a small size deviation, but through the addition of stabilizers, the shape of the resulting NPs can be modulated. Assets for the image were taken from Biorender.

1.2.3. Functionalisation

AuNPs have the ability to interact with several molecules, e.g. proteins [61], DNA [62], among others. This phenomenon allows for an extensive repertoire of applications that range from drug delivery to molecular detection. Despite this, a greater focus will be given to interactions with DNA.

When AuNPs come in contact with DNA, electrostatic and Van der Waals interactions between the two can occur [63], but these interactions are not that robust. Throughout the years, ways to strengthen these interactions and obtain stable NPs functionalized with DNA (Au-nanoprobes) have been attempted. By modifying the 3' or 5' end of an OL with a thiol group, a covalent-like interaction with AuNPs can be achieved, due to the high affinity of Au towards sulphur atoms [64].

The amount of thiol-modified oligonucleotide (SH-OL) that can adhere to the surface of AuNPs is tightly bound to their size and shape [64]. When using small spherical NPs, more interactions per area can be achieved due to their pronounced curvature, which prevents interactions between adjacent SH-OLs. When using larger NPs that have smaller curvature, less interactions per area can be achieved. Despite this, due to their larger superficial area, more SH-OLs can be loaded.

Even though the utilization of SH-OL allows a stronger interaction between AuNPs and DNA, some problems persist. After the synthesis process, the resulting AuNPs possess negative charge due to the citrate capping agent. Since DNA also possesses negative charge, only a small fraction adheres to the surface of AuNPs even when the thiol modification is used, due to repulsive charge effects. In order to overcome this problem and increase the rate of adsorption of SH-OLs, two methods were developed: (1) Salt-aging (SA) and (2) pH method.

(1) Salt-aging method

The SA method, firstly introduced by Mirkin et al., focuses in the slow raise of the ionic strength of the solution, through the addition of a salt [65]. This salt addition will add charged molecules to the solution and "mask" the negative SH-OL charges, as illustrated in Figure 1.11. This masking effect allows a closer proximity between SH-OL and AuNPs that were previously being repulsed due to their negative charge. The increased proximity will prompt an interaction between them, through the thiol group of the SH-OL.

The SA method is based on the equilibrium between the adsorption rate of SH-OLs and the aggregation rate of AuNPs. By raising the ionic strength in the solution, greater proximity between the two molecules is achieved, leading to a greater adsorption rate of SH-OLs and, consequently, a greater stabilization of the Au-nanoprobes towards ionic strength. Nevertheless, by raising the ionic strength of the solution, the aggregation rate of AuNPs also increases. As such, what determines if the functionalization is successful or aggregation occurs is the ratio between these rates. If the rate at which SH-OLs adsorbs to the surface of AuNPs is greater than the rate at which NPs aggregate, stable Au-nanoprobes can be achieved. On the other hand, if the ionic strength is raised too abruptly, the rate of aggregation will be higher than the adsorption rate and NP aggregation will be seen.

With this in mind, this method requires an extremely slow raise of the ionic strength of the solution, usually over the course of a few days, in order to avoid NP aggregation. Even though this method has been extensively applied to small NPs (15 nm), it has not seen extensive adoption when targeting larger NPs (40 nm and up) [66].

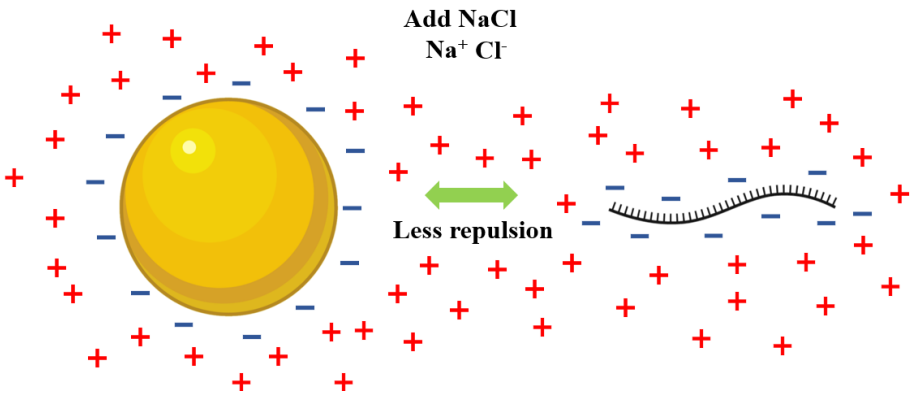

Figure 1.11 – Representative illustration of the SA method. Through the addition of NaCl, a screening of the negative charges of AuNPs and SH-OL is achieved, allowing a closer proximity between the two. Assets for the image were taken from Biorender.

(2) pH method

In the pH method, introduced by Zhang et al., instead of slowly raising the ionic strength of the solution, the functionalization is prompted by rapid pH lowering to a value of 3 [67]. As previously mentioned, SH-OLs have an inherent negative charge that hinders functionalization. The lowering of the pH allows the protonation of both adenosine and cytosine DNA residues, which have a pK_a value of 3.5 and 4.2 respectively. This effect partially neutralizes the negative charge of SH-OLs, facilitating the interactions between them and AuNPs, as illustrated in Figure 1.12. Even though the buffer used in this procedure raises the ionic strength of the solution, prompting NPs' aggregation, the SH-OLs rapidly start to adhere to the surface of AuNPs as the pH is lowered, effectively protecting them from the ionic strength raise.

This method has been described for both small (15 nm) and larger (40 nm and up) NPs [68]. It has two main advantages over the SA method: (1) it is described to have a better functionalization efficiency; (2) it can be performed over the course of several hours, instead of days.

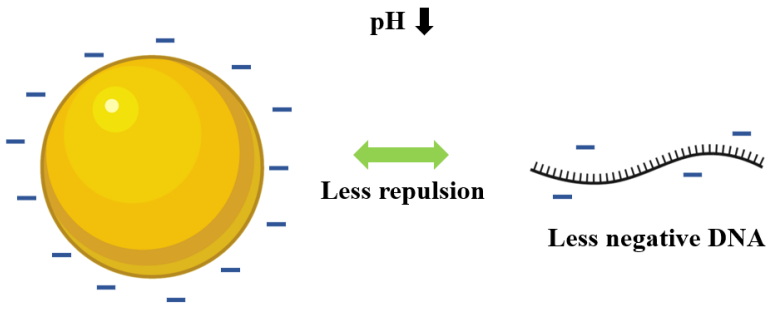

Figure 1.12 – Representative illustration of the pH method. Through pH lowering, adenosine and cytosine DNA residues are protonated, making SH-OLs less negative and allowing a closer proximity between them and AuNPs. Assets for the image were taken from Biorender.

1.2.4. DNA-AuNPs biosensors

A wide variety of developed assays make use of Au-nanoprobes, some utilizing them as a simple addon in the moment of recognition, while others make use of their transducer capabilities. In the latter case, NPs allow for the input signal, DNA hybridisation in this case, to have a strong correlation to their optical properties [69], such as the amplitude or the frequency of the visible radiation emitted.

Several mechanisms make use of Au-nanoprobes, but the most commonly seen in recent developed sensors are colorimetric based. These assays rely on changes to the environment's dielectric properties near AuNPs when hybridisation occurs, resulting in changes in the emitted radiation, and subsequently, the solution's colour.

1.2.4.1. Colorimetric detection mechanisms

Colorimetric detection conjugated with DNA hybridisation is one of the most promising types of sensors for point-of-care systems due to their low cost, simplicity and lack of necessity for specialised personnel [70].

In these types of systems, the main focus is a colorimetric change, from a red to a blue, when NPs aggregate. This colorimetric change is extremely sensitive and can be frequently detected by the naked eye. In some assays, aggregation occurs spontaneously, while others require the addition of salt to induce aggregation. In the latter's case, the increase of ionic strength through salt addition leads to the weakening of the electrostatic repulsions and, ultimately, to NP aggregation.

Even though there have been some colorimetric systems that relied on the hybridization of non-modified OLs, these types of assays have been associated with high variability. As such, a greater focus will be given to assays that utilize SH-OLs.

When referring to SH-OLs, there are two distinct approaches for direct colorimetric detection: (1) Cross-linking (CL); (2) Non-cross-linking (NCL).

(1) Cross-linking

In the CL assay, the main focus is the utilisation of two distinct Au-nanoprobes to detect a target ssDNA [65].

There are two approaches in this method: tail-to-tail and tail-to-head [71]. What differentiates them is the location of the thiol modification of the OLs. When both Au-nanoprobes use SH-OL with a modification at the same end, the Au-nanoprobes will hybridize in a tail-to-head conformation. When Au-nanoprobes use SH-OL modified at distinct ends, hybridisation will occur in a tail-to-tail conformation. A representation of these approaches is presented in Figure 1.13.

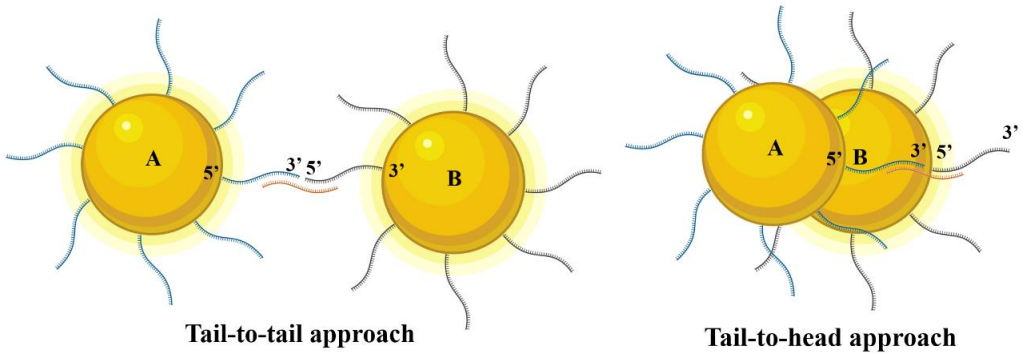

Figure 1.13 – Representation of the approaches used in the CL assay. In the tail-to-tail approach, the two SH-OLs are functionalized at opposing ends, while in the tail-to-head approach the two SH-OLs are functionalized at the same ends. Assets for the image were taken from Biorender.

The addition of a ssDNA target can lead to two responses. If the ssDNA target is complementary to both Au-nanoprobes, hybridization between the ssDNA and the SH-OLs at the surface of the AuNPs will occur. In this instance, the ssDNA will act as a linker between the Au-nanoprobes. This will cause the diminishing of the interparticle distance, which will result in the formation of aggregates and a colorimetric change from red to blue. These aggregates can be undone by raising the temperature of the sample above the melting point of the SH-OL – ssDNA complex.

On the other hand, if ssDNA is not complementary to both Au-nanoprobes, no linking will occur. In this instance, the interparticle distance remains high and no aggregation is seen, resulting in a red suspension of AuNPs. An illustration of the CL method can be seen in Figure 1.14.

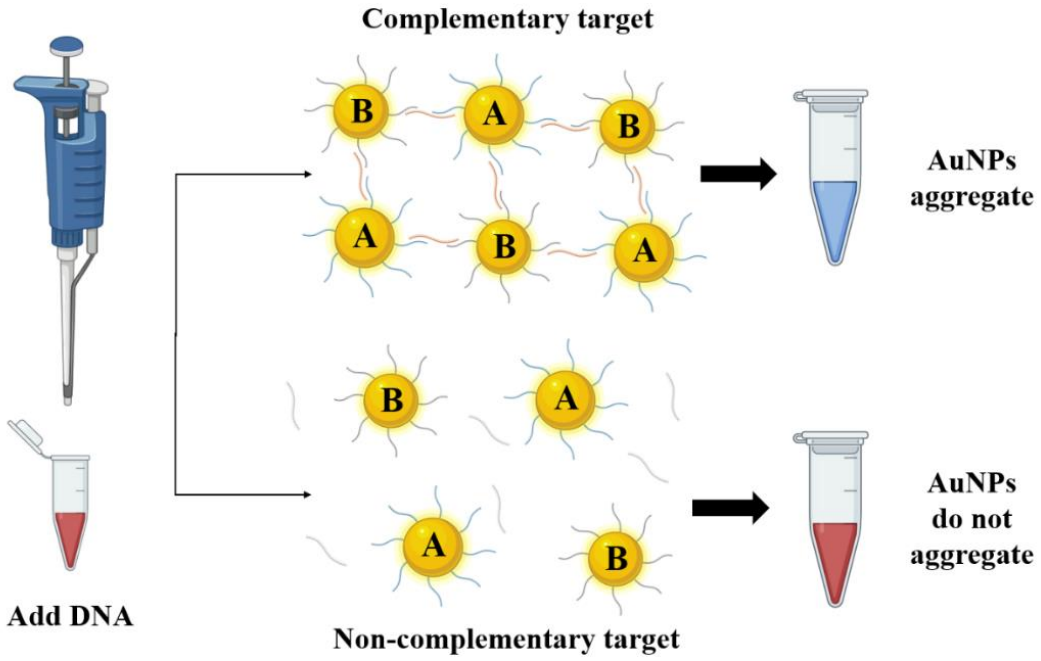

Figure 1.14 – Representation of the CL method. When the ssDNA target is added to the Au-nanoprobe solution two responses can occur: if complementarity is seen, the ssDNA target will hybridize with the SH-OLs at the surface of the AuNPs, acting as a linker, which results in NP aggregation and a blue coloration; if complementarity does not exist, the ssDNA will not hybridize and no aggregation is seen, resulting in a colloidal solution of red coloration. Assets for the image were taken from Biorender.

(2) Non-cross-linking

In the NCL assay, the main focus is the simplification of the system, using a single Au-nanoprobe to identify the presence of a target ssDNA [72].

The addition of ssDNA can lead to the following responses: if the added ssDNA is complementary to the Au-nanoprobes, hybridisation will occur. This hybridisation will grant a substantial shielding effect to AuNPs and avoid NP aggregation when ionic strength is raised in the system. This will result in a solution of red coloration, characteristic of a dispersed colloidal solution of AuNPs. On the other hand, when the added ssDNA is not complementary to the SH-OL at the surface of AuNPs, hybridisation will not occur. In this instance, the shielding effect will be weaker and will not be enough to avoid NP aggregation once the ionic strength is raised. This aggregation will result in a blue coloured solution. An illustration of the NCL method can be seen in Figure 1.15.

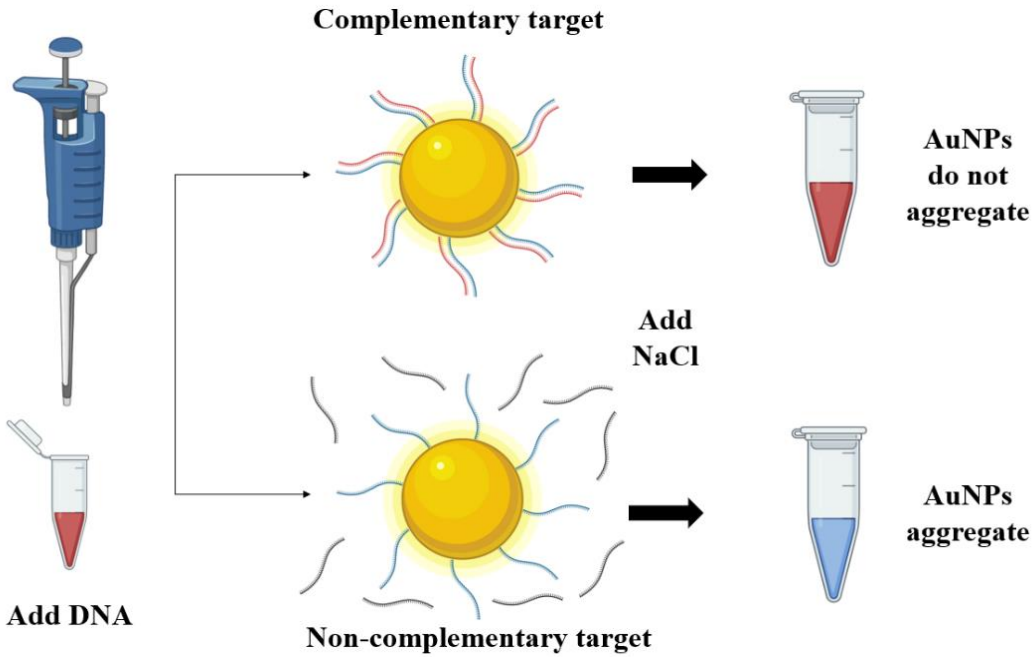

Figure 1.15 – Representation of the NCL method. When the ssDNA target is added to the Au-nanoprobe solution two responses can occur: if complementarity is seen, the ssDNA target will hybridize with the SH-OLs at the surface of the AuNPs, protecting them from aggregation upon ionic strength raise, resulting in a red colloid; if complementarity does not exist, the ssDNA will not hybridize and aggregation is seen, resulting in a blue coloration. Assets for the image were taken from Biorender.

1.2.4.2. Key differences between cross-linking and non-cross-linking

On top of the opposite colorimetric response seen for CL and NCL methodologies, other properties have been evaluated to compare the two [73]. One of the most important properties of these assays is the time required to obtain a response. For a long time, it was generally accepted that NCL allowed the acquisition of results much faster than CL, usually requiring minutes instead of hours, but this was proven to be a much more complicated matter.

Upon further evaluation, it was discovered that the amount of ssDNA target added to the sample was crucial for determining which assay had a better response time. Even though NCL was indeed faster when a lot of ssDNA was added to perform the assay, the opposing response was seen when less DNA was added, making CL more useful in the latter scenario.

Another key feature of these types of assays is their sensitivity. Here, the CL method is more capable since it can make use of less ssDNA to induce a measurable response.

When evaluating the complexity of both methods, the NCL assay presents itself as a simpler alternative to the CL method, due to the use of a single type of Au-nanoprobe.

The reproducibility of these methods is also an interesting point of discussion. While the CL method only requires ssDNA to be added, the NCL method also needs a salt to increase the ionic strength of the solution and induce NP aggregation. The stability of the Au-nanoprobes upon addition of salt has been proven to be variable, which could affect the reproducibility of this method.

Even though these properties are important to consider when designing an assay for a specific application, the introduction of SNPs adds another layer of required optimizations.

1.2.4.3. Single nucleotide polymorphisms detection

The beforementioned sensors induced a positive or negative response due to the presence or absence of a ssDNA target. In the last two decades, more complex assays have been developed in an attempt to scrutinise small mutations present in the ssDNA target that may be responsible for specific phenotypes, such as LI.

When it comes to SNPs, the design of the SH-OL is of extreme importance since not only has it been proved that the location of the SNP directly affects the capability of the ssDNA target to hybridise with the SH-OL [71], but also the spacer used [74], DNA length, etc. On a general basis, the smaller the number of SNPs that separate the complementary from the mutated ssDNA target sequences, the less the signal distinction between them. On the other hand, if the SNPs are located towards the edges of the SH-OL, a higher signal divergence can be achieved.

This signal difference can be manifested in different ways, depending on the type of assay. As evidenced in Figure 1.16, in the CL assay, two distinctions can be seen by introducing SNPs to the system [71]: (1) the aggregation induced by the hybridisation of the ssDNA with the SH-OL may be of lower intensity; (2) the melting point of the formed SH-OL – ssDNA complex may be significantly affected. On the other hand, as evidenced by Figure 1.17, in the NCL assay, the signal difference arises from the lower ionic strength protection granted by the complex, which results in more aggregation when compared to those formed with complementary ssDNA [75].

Although theoretically simple, achieving an assay capable of correctly scrutinising between a perfect complementary ssDNA and an almost perfect one, where SNPs are present, requires extreme optimisation, regardless of the type of assay chosen.

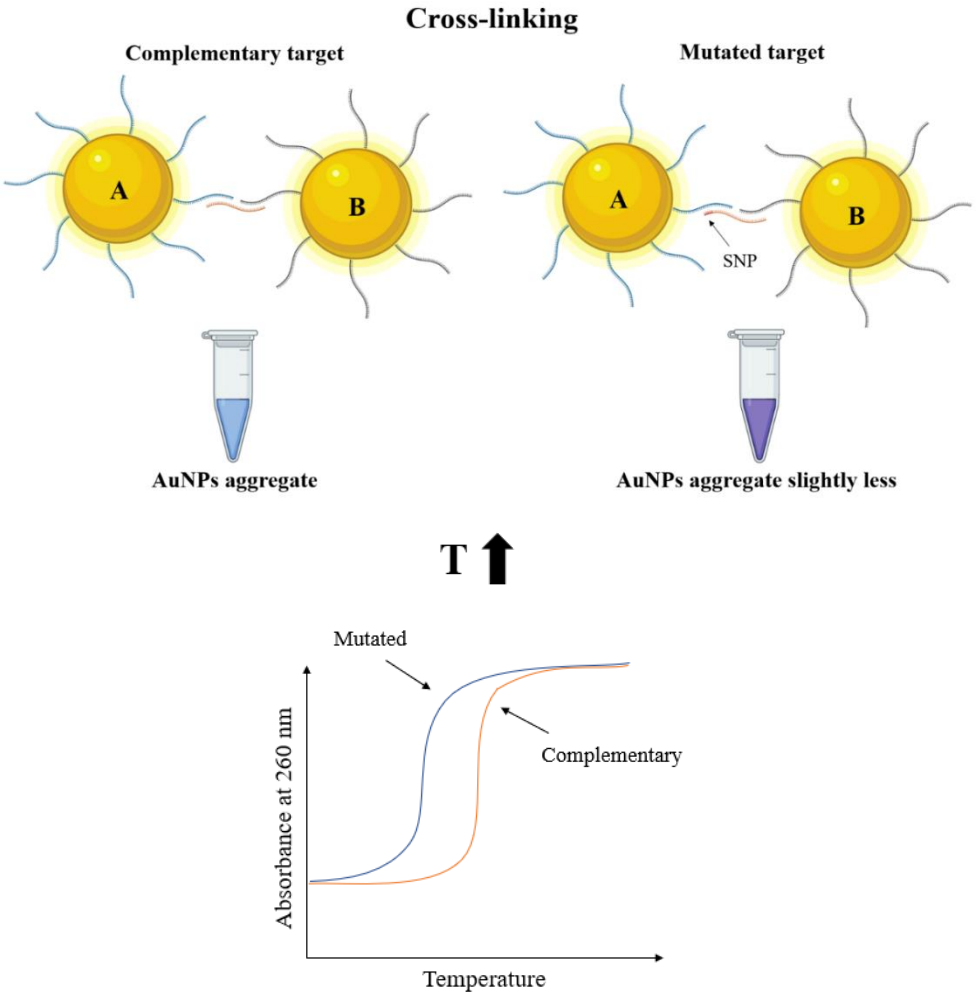

Figure 1.16 – Representation of SNP detection using the CL method. When the mutated ssDNA is added to the Au-nanoprobe solution a partial complementarity is seen, which results in slight NP aggregation and a purple coloration. The formed aggregates can be undone by raising the temperature, which can be used to identify if mutations are present, in case coloration alone does not provide a good indication. Assets for the image were taken from Biorender.

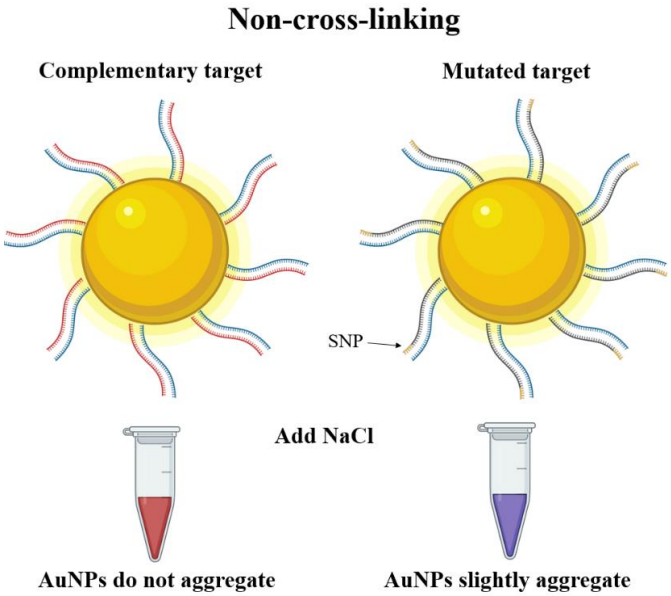

Figure 1.17 – Representation of SNP detection using the NCL method. When the mutated ssDNA is added to the Au-nanoprobe solution a partial complementarity is seen, which results in slight NP aggregation and a purple coloration upon the addition of a salt. Assets for the image were taken from Biorender.

Chapter 2

Objectives

The main objective of this thesis is the production of a fast and inexpensive colorimetric assay capable of detecting the presence of a SNP related to LI. To achieve this, Au-nanoprobes were developed for detection of synthetic ssDNA targets using the CL and NCL methodologies. For this purpose, several intermediate goals were set.

Initially, 15 and 40 nm AuNPs were synthetised and characterized to assess their size and concentration. This was followed by the optimization of their functionalization with SH-OLs using either the SA or pH method to determine the best functionalization method for each NP size and the amount of SH-OL necessary to produce stable Au-nanoprobes. Au-nanoprobe stability was then evaluated through induced aggregation with a salt solution to identify the salt concentration required for the desired level of aggregation. Their hybridization with distinct ssDNA targets was optimized by testing different ssDNA targets varying in size. Following this, CL and NCL methodologies were performed for both sizes of AuNPs and two mathematical methods for the calculation of the aggregation state of the samples were compared to verify the difference between the complementary and mutated ssDNA targets and assess the best AuNP size for colorimetric detection.

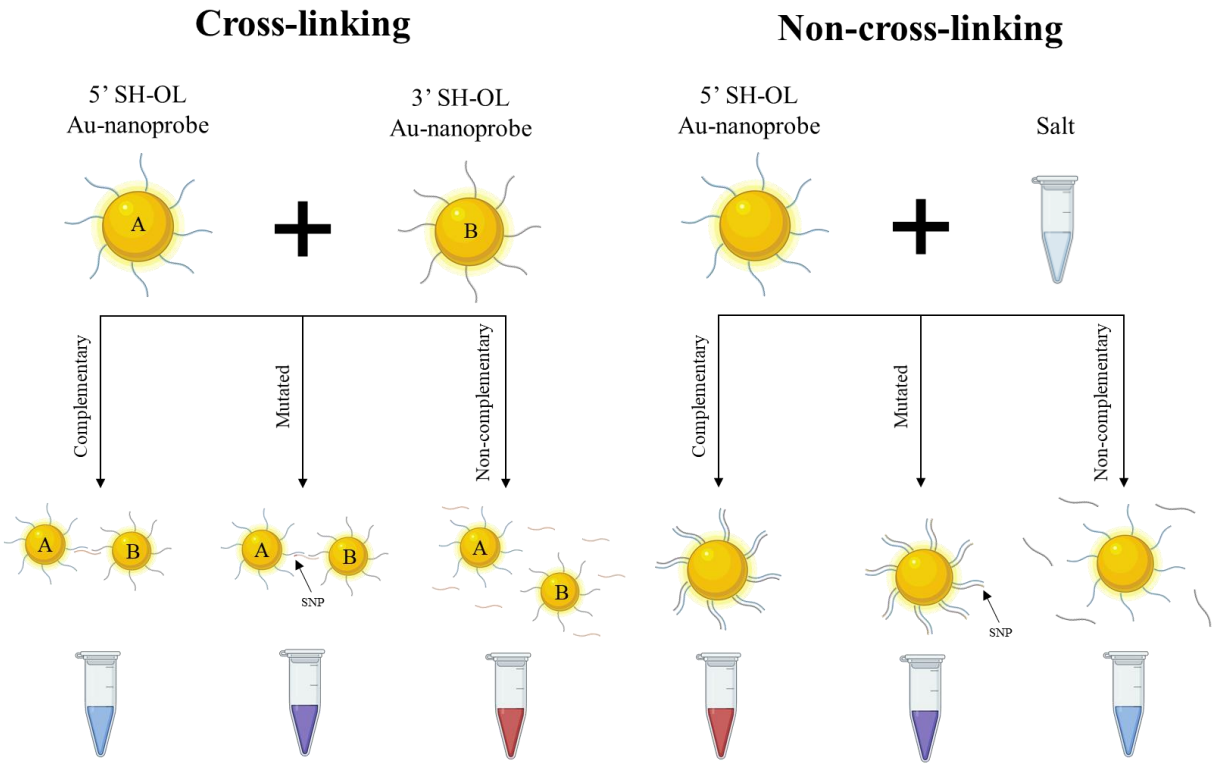

Figure 2.1 – Illustrative image of the CL and NCL methodologies for SNP detection. Assets for the image were taken from Biorender.

Chapter 3

Methods and Materials

3.1. Materials

3.1.1. Reagents

Table 3.1 – Reagents used, their brand and purity.

Reagent	Purity	Brand
Agarose	Certified Molecular Biology	Bio-rad
Sodium citrate tribasic dihydrate	> 99 %	Sigma-Aldrich
Sodium phosphate dibasic	> 99 %	Sigma-Aldrich
Sodium chloride	> 95 %	Scharlau
Sodium dodecyl sulphate	> 99 %	PanReac
Nitric acid (65% w/v)	> 99 %	PanReac
Gold chloride solution (30% w/w)	> 99.99 %	Sigma-Aldrich
Tris(hydroxymethyl)amino-methane	> 99.8 %	Sigma-Aldrich
Glacial acetic acid	> 99 %	Carlo Erba
Hydrochloric acid (37% w/v)	> 99 %	Fluka

3.1.2. General material

Table 3.2 – General material used and their brand.

Material	Brand
220 nm Filters	GVS
pH indicator strips	Macherey-Nagek

3.1.3. Equipment

Table 3.3 – Equipment used, their model and brand.

Equipment	Model	Brand
Analytical balance	AS 220/C/2	Radwag
Ultraviolet-visible spectrophotometer	Cary 50	Varian
Dynamic and electrophoretic light scattering analyser	Zetasizer Nano ZS	Malvern
Nanodrop	ND-1000	Thermo Fisher
Centrifuge	K2015R	Centurion Scientific
Microcentrifuge	Ministar Silverline	VWR
Thermo-shaker	TS-100	Biosan
Water bath		Bioblock Scientific
Sonicator	Ultrasonic 3000683	J.P. Selecta
Electrophoresis equipment		Bio-rad
Electrophoresis power supply	300 V	Labnet

3.1.4. Spectroscopy cuvettes

Table 3.4 – Cuvettes used, their optical path, sample volume and brand.

Cuvette	Material	Optical path (mm)	Sample volume (µL)	Brand
Semi-micro / micro cells	Quartz	10	100 1000	Hellma Analytics
Disposable folded capillary cells	Plastic	10	1000	Malvern

3.1.5. Oligonucleotides and purification columns

SH-OLs were ordered from both Eurofins Genomics and STAB VIDA. With the exemption of the 120 b.p. ssDNA targets, which were bought from Eurofins Genomics, all the other ssDNA targets were purchased from STAB VIDA. The sequence of each OL is presented in Table 3.5.

Table 3.5 – OLs used, their length in base pairs (b.p.) and sequence

Oligonucleotide		Length (b.p.)	Sequence
5’ thiol-modified OL		20	5’ (SH-C_6) AGT TCC TTT GAG GCC AGG GG 3’
3’ thiol-modified OL		20	5’ CTA CAT TAT CTT ATC TGT AT (C_3-SH) 3’
Complementary ssDNA	Parallel	40	5’ TCA AGG AAA CTC CGG TCC CCG ATG TAA TAG AAT AGA CAT A 3’
		50	5’ TCA AGG AAA CTC CGG TCC CCT TCC CAT CAA GCC CTA GGG CTC CTC GTG GC 3’
	Anti-parallel	40	5’ ATA CAG ATA AGA TAA TGT AGC CCC TGG CCT CAA AGG AAC T 3’
		120	5’ CTT AGA CCC TAC AAT GTA CTA GTA GGC CTC TGC GCT GGC AAT ACA GAT AAG ATA ATG TAG CCC CTG GCC TCA AAG GAA CTC TCC TCC TTA GGT TGC ATT TGT ATA ATG TTT GAT TTT TAG 3’
Mutated ssDNA	Parallel	40	5’ TCA AGG AAA CTC CGG TCC CTG ATG TAA TAG AAT AGA CAT A 3’
		50	5’ TCA AGG AAA CTC CGG TCC CTT TCC CAT CAA GCC CTA GGG CTC CTC GTG GC 3’
	Anti-parallel	40	5’ ATA CAG ATA AGA TAA TGT AGT CCC TGG CCT CAA AGG AAC T 3’
		120	5’ CTT AGA CCC TAC AAT GTA CTA GTA GGC CTC TGC GCT GGC AAT ACA GAT AAG ATA ATG TAG TCC CTG GCC TCA AAG GAA CTC TCC TCC TTA GGT TGC ATT TGT ATA ATG TTT GAT TTT TAG 3’
Non-complementary ssDNA		40	5’ TCC CGA GTT TCT TGT TAG ATT TTT AGT TTG TAA TAT GTT T 3’
		50	5’ TTC CCA TCA AGC CCT AGG GCT CCT CGT GGC TGC TGG GAG TTG TAG TCT GA 3’

For the purification of the beforementioned SH-OLs, NAP-5 columns from Illustra (GE Healthcare) were used. Typically, only one purification per column was applied. The lyophilized ssDNA targets were dissolved in water, while the SH-OLs required a pre-treatment, followed by a purification step.

3.2. Methods

Before and after contact with AuNPs, all glassware was washed with aqua regia, a mixture of 3:1 hydrochloric and nitric acid, to ensure that no contamination with AuNPs occurred. Upon washing, the glassware was rinsed with water until a pH value of 7 was reached, measured through the utilization of pH strips.

3.2.1. Thiol modified oligonucleotide pre-treatment and purification

Pre-treatment

The lyophilized SH-OLs were dissolved in 200 µL of 10 mM Tris(2-carboxyethyl) phosphine (TCEP) solution and left incubating under agitation for 60 minutes.

Purification

The NAP-5 column was washed with 10 mL of 10 mM phosphate buffer (PB) pH 8. Following this, 100 µL of SH-OL were added to the column until all volume was incorporated. Next, 400 µL of 10 mM PB pH 8 were added. An additional 500 µL of 10 mM PB pH 8 were used to elute the SH-OL through the column and 500 µL of sample were collected. To finalize, the column was once again washed with 10 mL of 10 mM PB pH 8 and 2 mL were added to properly store the column until further use.

To evaluate the success of the purification process, the 500 µL of SH-OL were analysed through UV-Vis, using a Nanodrop Analyzer. For each purification, a minimum of three replicates were obtained, using a 2 µL sample volume.

3.2.2. Gold nanoparticles synthesis

3.2.2.1. 15 nm AuNPs

The syntheses were made according to the revised Turkevich method developed by Kimling et al. [55]. Initially, 2 mL of sodium citrate tribasic dihydrate at 343 mM were mixed with 98 mL of milli-Q water and heated until boiling in a round-bottom flask under stirring (600 rpm), while kept from direct sunlight. Upon reaching the boiling temperature, 69.4 µL of Au chloride solution (30% w/w) at 1.445 M were added for a final concentration of 1 mM. The solution was left reacting for 5 minutes after which the reaction was stopped by ceasing heating and stirring. The solution was then left to cool to room temperature.

Once the solution had cooled down, it was filtered using 220 nm filters to a 250 mL flask, wrapped with foil to avoid direct sunlight and stored at 4 ºC until further use.

3.2.2.2. 40 nm AuNPs

The synthesis process was performed according to the method developed by Bastús et al. [76].

Seed formation

Initially, 97.05 mg of sodium citrate tribasic dihydrate were added to 150 mL of milli-Q water and the solution was heated until boiling under stirring (600 rpm). Afterwards, 1 mL of 25 mM Au chloride solution (30 % w/w) was added and left reacting for 10 minutes. Once the time had elapsed, the solution was cooled to 90 ºC to allow the growth of the seeds.

Seed growth

Upon reaching 90 ºC, another millilitre of 25 mM Au chloride solution was added and left to react for 30 minutes. This process was repeated once again and then the reaction was stopped and the solution was left to cool to room temperature.

After the two growth phases, the solution was diluted by extracting 55 mL and mixing with 53 mL of milli-Q water. The diluted solution was then heated to 90 ºC and 2 mL of 60 mM sodium citrate tribasic dihydrate were added, followed by the addition of 1 mL of 25 mM Au chloride solution. The solution was left reacting for 30 minutes after which the process was repeated up to two times, for a maximum of five growth phases.

After the fourth or fifth growth phase, the solution was left to cool down to room temperature and was then filtered using 220 nm filters to a 200 mL flask, wrapped in foil and stored at 4 ºC until further use.

3.2.3. Gold nanoparticles characterization

3.2.3.1. UV-Vis characterization

To estimate the size and concentration of the synthetized AuNPs, an UV-Vis spectrum of a 1:4 dilution in water of the AuNPs was acquired. With this spectrum it became possible to make beforementioned estimations through the work of Haiss et al. [77].

Firstly, a ratio of the maximum absorbance divided by the absorbance at 450 nm was calculated through equation 1:

$$R = \frac{Abs_{max}}{Abs_{450\ nm}} \quad (1)$$

Following this, the diameter, in nanometres, of the AuNPs was estimated using equation 2:

$$d = 0.112 \times e^{2.998 \times R} \quad (2)$$

With the size of the AuNPs, it was possible to assess their extinction coefficient at 450 nm through equation 3:

$$\varepsilon_{450\,nm} = e^{3.0869 \times \ln(d) + 10.869} \quad (3)$$

Once the extinction coefficient had been established, the concentration of the AuNPs was estimated using equation 4:

$$Concentration\ (nM) = \frac{Abs_{450\,nm} \times dilution\ factor}{optical\ path \times \varepsilon_{450\,nm}} \times 10^9 \quad (4)$$

3.2.3.2. Dynamic light scattering and electrophoretic light scattering measurements

DLS (Dynamic Light Scattering) and ELS (Electrophoretic Light Scattering) were performed in a Malvern Zetasizer Nano ZS (Malvern, Worcestershire, UK), at 25 °C, with light detection at 17° (ELS) and at 173° using the backscatter mode (DLS). All Au-nanoprobes were previously diluted 1:5 with 10 mM PB pH 8. The 15 and 40 nm AuNPs were measured at their stock concentrations. Each sample was measured at least 3 times; The measurements were taken as the average of a minimum three runs, and the results are presented as mean Z-Average and Polydispersity Index (PDI) for DLS and Zeta potential (mV) for ELS.

3.2.4. Gold nanoparticles functionalization

3.2.4.1. 15 nm gold nanoparticles

3.2.4.1.1. Salt-aging method

The functionalization method was adapted from Mirkin et al. [65]. A defined volume of AuNPs was mixed with a specific volume of SH-OL to ensure that the pretended ratio (between 50 and 250) of OLs per NP was applied. The solution was then left incubating for 2 hours, after which AGE II (2 % (w/v) Sodium Dodecyl Sulphate (SDS) with 10 mM PB pH 8) was added, for a final SDS concentration of 0.01 % (w/v), followed by sonication for 10 seconds and a 20-minute rest. Once the time had elapsed, AGE III (0.01 % (w/v) SDS with 10 mM PB pH 8 and 1.5 M NaCl) was added, for a final NaCl concentration of 0.05 M. After the addition, 10 more seconds of sonication were applied, as well as a 20-minute rest. A final addition of AGE III was then done, to raise the final concentration of NaCl to 0.1 M, followed by the same 10-second sonication period. The solution was then let to rest at room temperature without direct light contact for 16 hours.

After 16 hours, the functionalized AuNPs were centrifuged at 13000 g for 25 minutes. Following this, the supernatant was discarded and the Au-nanoprobes were redispersed in the same total volume with 10 mM PB pH 8. The concentration of the Au-nanoprobes was estimated from the initial concentration of the AuNPs, adjusted to the final sample volume.

3.2.4.1.2. pH method

This functionalization method was adapted from Zhang et al. [67]. Similarly to the SA method, a defined volume of AuNPs was mixed with a specific volume of SH-OL to ensure that the pretended ratio (between 50 and 250) of OLs per NP was applied. The solution was then left incubating for 2 hours. Afterwards, citrate-HCl buffer pH 3 was added for a final concentration of 8 mM and the solution was left resting at room temperature for 16 hours kept from direct sunlight.

After 16 hours, the procedure was identical to the SA method, requiring a 13000 g centrifugation for 25 minutes, followed by redispersion in 10 mM PB pH 8. Once again, the final concentration of the Au-nanoprobes was estimated from the initial concentration of the AuNPs.

3.2.4.2. 40 nm gold nanoparticles

3.2.4.1.1. Salt-aging method

For the SA functionalization of 40 nm AuNPs, the procedure was identical to the 15 nm AuNPs. The only difference was seen in the last centrifugation step where the 40 nm Au-nanoprobes were centrifuged at 800 g for 15 minutes and redispersed in half of the total volume with 10 mM PB pH 8.

3.2.4.1.2. pH method

Functionalization with gold nanoparticles at stock concentration

The 40 nm AuNPs were initially functionalized using their stock concentration by performing a pH method identical to the one used for the 15 nm AuNPs, with the exception of the last centrifugation step (800 g for 10 minutes) and redispersion in half of the initial volume.

Functionalization with concentrated gold nanoparticles

A second pH functionalization method was performed which required NP centrifugation to concentrate the AuNPs. This method was adjusted from Zhang et al. [78]. Firstly, 500 µL of AuNPs were centrifuged at 800 g for 15 minutes and 474 µL of the supernatant were discarded. The resulting concentrated AuNPs were then mixed with 36 µL of SH-OL adjusted to a determined concentration, to ensure the desired ratio (between 200 and 2500) of OLs per NP was applied. The mixture was let to rest at room temperature for 2 hours, after which 2 µL of 500 mM citrate-HCl buffer pH 3 were added. Following a 10-minute rest, the addition was repeated 3 more times, with the same resting period in-between, for a final citrate concentration of 57 mM. Once the 4 additions were complete, the solution was left to rest for 1 hour at room temperature. To finalize, the colloid was centrifuged at 800 g for 15 minutes and redispersed in half of the initial total volume with 10 mM PB pH 8.

Functionalization with concentrated gold nanoparticles and intercalating agent

To evaluate the possibility of utilizing 6-mercapto-1-hexanol as an intercalating agent, an addition of 4 µL of mercapto-hexanol was made at a determined concentration to ensure that a ratio of 100 molecules of intercalating agent per NP was applied. This addition was made after the four additions of citrate and was followed by the 1-hour rest of the functionalization protocol, centrifugation at 800 g and redispersion in half of the initial volume.

3.2.5. Agarose gel electrophoresis

All agarose gels were made using agarose 0.5 % and were run at 120 V for 20 minutes. Generally, no sample dilution was applied, and each well was loaded with a volume of 20 to 30 µL of AuNP/Au-nanoprobe solution, depending on the size of the well utilized. The exact volume utilized is stated in each obtained gel.

3.2.6. Stability assays

3.2.6.1. 15 nm gold nanoparticles

AuNPs/Au-nanoprobes' stability was assessed using either NaCl, ranging from 10 to 1600 mM, or $MgCl_2$, ranging from 1 to 100 mM. Typically, for a stability assay, seven distinct salt concentrations were chosen to be tested. Afterwards, for each salt concentration, the necessary volume of AuNPs/Au-nanoprobes for a final concentration of 2.5 nM were mixed with 10 mM PB pH 8 and heated at 95 ºC for 10 minutes, considering a final sample volume of 100 µL. Once the time had elapsed, the samples were left resting at room temperature for another 10 minutes. Following this, the desired salt concentration was added to each sample with 1- or 2-minutes interval. After 15 minutes, an UV-Vis spectrum of each sample was taken, respecting the time interval applied in the salt addition step.

3.2.6.2. 40 nm gold nanoparticles

The stability assays using 40 nm AuNPs/Au-nanoprobes were identical to the ones applied to the 15 nm ones, with the exception that the final AuNPs/Au-nanoprobes concentration was 0.15 or 0.25 nM (mentioned in each assay).

3.2.7. Colorimetric assays

3.2.7.1. 15 nm gold nanoparticles

Colorimetric assays were similar to the stability assays but varied on two key aspects: (1) only one salt concentration was chosen to be added to the samples; (2) ssDNA was initially added to the mixture of Au-nanoprobes and 10 mM PB pH 8 buffer in a concentration ranging from 0.25 to 100 ng/µL. A total of 3 to 5 samples were usually tested: the control sample, where no salt and no ssDNA were added; a salt sample, where salt was added but not ssDNA; ssDNA samples, where a specific ssDNA (complementary, mutated or non-complementary) was added alongside the defined salt concentration. The incubation time applied in these assays was also varied from 3 to 15 min.

3.2.7.2. 40 nm gold nanoparticles

The colorimetric assays for 40 nm Au-nanoprobes followed the same principle of the 15 nm ones, but the final concentration of Au-nanoprobes was changed from 2.5 nM to 0.25/0.15 nM.

3.2.8. Cross-linking assays

Cross-linking assays were performed through the mixing of 50 µL of Au-nanoprobe obtained using SH-OL with the thiol group at 5' (5' SH-OL) and 50 µL of Au-nanoprobe obtained using SH-OL with the thiol group at 3' (3' SH-OL). The mixing of the two was performed using the Au-nanoprobes at the concentration they were obtained after the functionalization step. Following this, 60 pmol of the desired ssDNA targets were added. The solutions were then heated at 75 ºC for 15 minutes and left to rest for two or three hours at room temperature, after which UV-Vis spectra were taken.

3.2.9. Ratios calculation

For the evaluation of the aggregation state of the AuNPs/Au-nanoprobes in the stability and colorimetric assays, two distinct methodologies were applied: ratio method; subtraction method.

3.2.9.1. Ratio method

For the ratio calculation in stability assays, the spectrum of the control sample (with no added salt) was used to decide the wavelength of the AuNPs/Au-nanoprobes in their dispersed state. On the other hand, the spectrum of the sample with the most salt, where more aggregation is seen, was utilized to determine the wavelength of the AuNPs/Au-nanoprobes in their aggregated state (when no aggregation was seen the ratios were not calculated).

With defined wavelengths for the dispersed and the aggregated states, a ratio was calculated for every sample of the assay by dividing the absorbance at the wavelength defined for the dispersed state with the absorbance at the wavelength defined for the aggregated state, as stated in equation 5.

$$Ratio = \frac{Abs_{nm(dispersed)}}{Abs_{nm(aggregated)}} \quad (5)$$

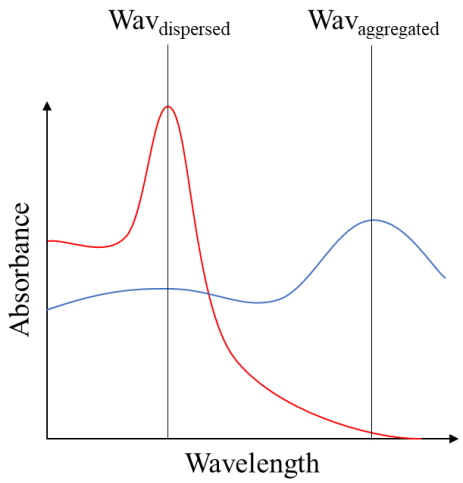

Figure 3.1 – Representation of the defined wavelengths for the dispersed and the aggregated state in the ratio method, allowing the calculation of an aggregation ratio for every sample in the assays. In red: dispersed AuNPs spectrum; in blue: aggregated AuNPs spectrum.

For the ratio calculation in colorimetric assays, a similar approach was utilized, but the wavelength of the aggregated state was defined using the salt sample (where only Au-nanoprobe and salt are present). The ratios were then calculated for the tested samples: control; salt; complementary ssDNA; mutated ssDNA; non-complementary ssDNA.

3.2.9.2. Subtraction method

In the subtraction method, the spectrum of the sample with the highest salt concentration was subtracted from the control sample (with no added salt). From this subtracted spectrum, the wavelength corresponding to the maximum absorbance was attributed to the dispersed state of the AuNPs/Au-nanoprobes, while the wavelength corresponding to the minimum absorbance is attributed to their aggregated state. A ratio was then calculated for each sample by dividing the absorbance at the wavelength defined for the dispersed state with the absorbance at the wavelength defined for the aggregated state.

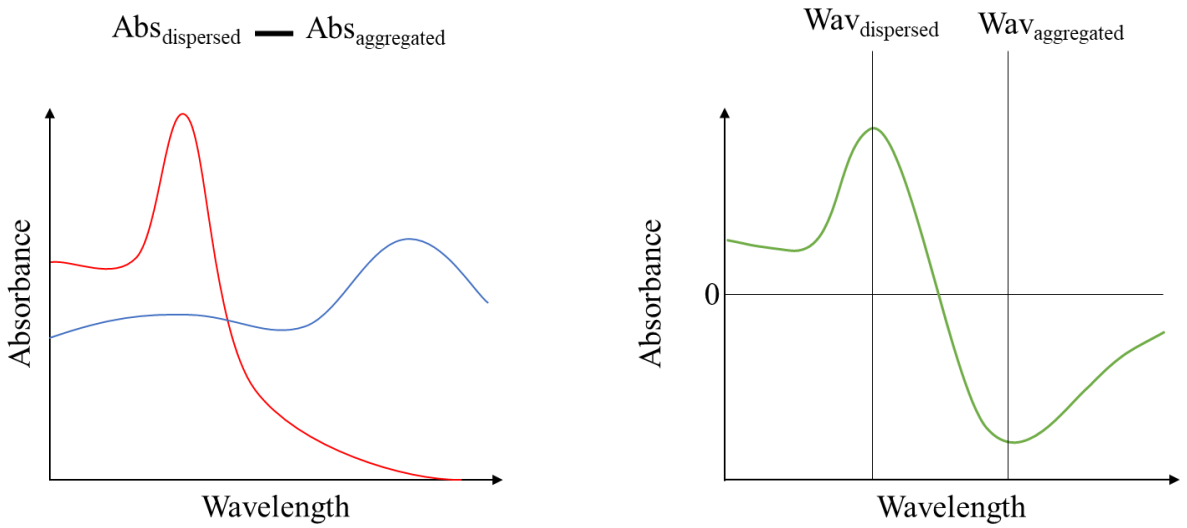

Figure 3.2 – Representation of the defined wavelengths for the dispersed and the aggregated state in the subtraction method, allowing the calculation of an aggregation ratio for every sample in the assays. In red: dispersed AuNPs spectrum; in blue: aggregated AuNPs spectrum; in green: subtracted spectrum (dispersed – aggregated).

For the colorimetric assays a similar approach to the ratio method was applied. Instead of using the sample with the highest salt concentration for spectra subtraction, the salt sample was used in its place (where only nanoprobe and salt are present). The ratios were then calculated for the tested samples: control; salt; complementary ssDNA; mutated ssDNA; non-complementary ssDNA.

3.2.10. Aggregation ratios percentual difference calculation

Independently of the method used to calculate the aggregation ratios of the samples, the percentual difference between the aggregation ratio of the complementary and mutated ssDNA samples was calculated using the following equation 6:

$$\%\, difference = \frac{Aggregation\ ratio_{\,complementary} - Aggregation\ ratio_{\,mutated}}{Aggregation\ ratio_{\,complementary}} \times 100 \quad (6)$$

3.2.11. Statistical analysis

Statistical analysis was performed for specific colorimetric assays using anti-parallel ssDNA targets (40 and 120 b.p.) and both AuNPs (15 and 40 nm). The following ssDNA concentrations were tested: 6, 18 and 36 ng/µL. A two sample t-Test at a 0.05 level was performed using the aggregation ratio of the complementary and mutated samples. A total of three replicates were used to perform the analysis at each ssDNA concentration and NP size. The analysis was done using OriginPro.

Chapter 4

Results and Discussion

4.1. Thiol-modified oligonucleotide purification and DNA characterization

The pre-treatment and purification of SH-OLs are critical in order to ensure that thiol groups are in their reduced form, capable of interacting with Au, and to eliminate any undesirable components, including the TCEP required in the previous treatment, together with any possible impurities. The data obtained from Nanodrop measurements is presented in Table 4.1.

Table 4.1 – Characterization of all utilized OLs. The concentration of each OL is presented, as well as contamination indicative ratios. All samples were characterized using a 2 µL sample volume. The presented error corresponds to the standard deviation.

Oligonucleotide		Length (b.p.)	Batch	Concentration (ng/µL)	Ratio 260/280 nm	Ratio 260/230 nm
5' SH-OL		20	1	122 ± 1	1.84 ± 0.01	2.37 ± 0.02
			2	160 ± 2	1.82 ± 0.00	2.32 ± 0.00
			3	161 ± 2	1.81 ± 0.01	2.34 ± 0.01
			4	198 ± 5	1.77 ± 0.00	1.71 ± 0.02
			5	169 ± 2	1.81 ± 0.01	2.26 ± 0.01
			6	228 ± 2	1.83 ± 0.00	2.29 ± 0.03
			7	70 ± 1	1.88 ± 0.01	2.43 ± 0.13
			8	98 ± 1	1.80 ± 0.02	2.33 ± 0.02
			9	99 ± 1	1.80 ± 0.01	2.25 ± 0.01
3' SH-OL		20	1	125 ± 0	1.87 ± 0.00	2.39 ± 0.02
Complementary ssDNA	Parallel	40	1	1702 ± 9	1.87 ± 0.00	2.32 ± 0.00
			2	1400 ± 10	1.89 ± 0.00	2.25 ± 0.00
		50	1	1124 ± 8	1.64 ± 0.01	1.87 ± 0.01
	Anti-parallel	40	1	1356 ± 4	2.12 ± 0.00	2.38 ± 0.00
			2	1360 ± 10	1.94 ± 0.00	2.41 ± 0.01
			3	520 ± 1	2.16 ± 0.01	2.38 ± 0.02
		120	1	1667 ± 5	1.90 ± 0.00	2.13 ± 0.00
Mutated ssDNA	Parallel	40	1	1835 ± 6	1.93 ± 0.01	2.39 ± 0.01
			2	1255 ± 4	1.93 ± 0.00	2.31 ± 0.00
		50	1	1213 ± 5	1.60 ± 0.00	1.94 ± 0.01
	Anti-parallel	40	1	1288 ± 7	1.96 ± 0.00	2.46 ± 0.01
			2	1206 ± 3	2.10 ± 0.00	2.37 ± 0.01
			3	551 ± 1	2.13 ± 0.01	2.38 ± 0.01
		120	1	1802 ± 7	1.86 ± 0.00	2.30 ± 0.00
Non-complementary ssDNA		40	1	1842 ± 35	1.73 ± 0.00	2.68 ± 0.00
			2	1222 ± 9	1.81 ± 0.00	2.53 ± 0.03
			3	532 ± 1	1.84 ± 0.00	2.58 ± 0.00
		50	1	1280 ± 3	1.43 ± 0.00	2.25 ± 0.00

The purity of the samples can be evaluated through the 260/280 nm ratio, indicative of protein contamination if below 1.8, and the 260/230 nm ratio, indicative of contamination with organic compounds, chaotropic salts or detergents if below 2.2 [79]. The results presented in Table 4.1 show that, for all the SH-OLs, only batch number four of the 5' SH-OL had ratios indicative of slight contamination (1.77 for 260/280 ratio and 1.71 for 260/230 ratio). Apart from this batch, all the others had ratios within the desirable limits and were used in the upcoming work.

The purity of the synthetic ssDNA targets was also evaluated. Since ssDNA targets were not previously purified, an increase in the contamination ratios was expected, when compared to the SH-OL samples. Despite this, near 72 % of the samples of ssDNA target tested had ratios above the set thresholds. For the samples that showed slight signs of contamination, the minimum ratios recorded were 1.43 for the 260/280 nm ratio and 1.87 for the 260/230 nm ratio. Since biological samples would be used as extracted, without any purification step, high purity of these samples is not mandatory to conduct a proof-of-concept of this colorimetric system. As such, all the tested batches were utilized in the colorimetric assays.

4.2. Gold nanoparticles synthesis and characterization

4.2.1. 15 nm AuNPs

The determination of the size and concentration of the AuNPs is an important step in evaluating the success of the synthesis process and can provide insight on the size dispersion of the colloidal sample. A good indication of a successful synthesis lies in a colorimetric change during the synthesis process. Typically, if NP formation occurs, the clear citrate solution turns red upon the addition of Au chloride, which is the colour emitted by AuNPs. This effect is illustrated in Figure 4.1.

Figure 4.1 – Illustrative image of the colour change that occurs upon the addition of Au chloride.

A more in-depth characterization of AuNPs can be made using the UV-Vis spectra. The spectra obtained during one of the syntheses is presented in Figure 4.2.

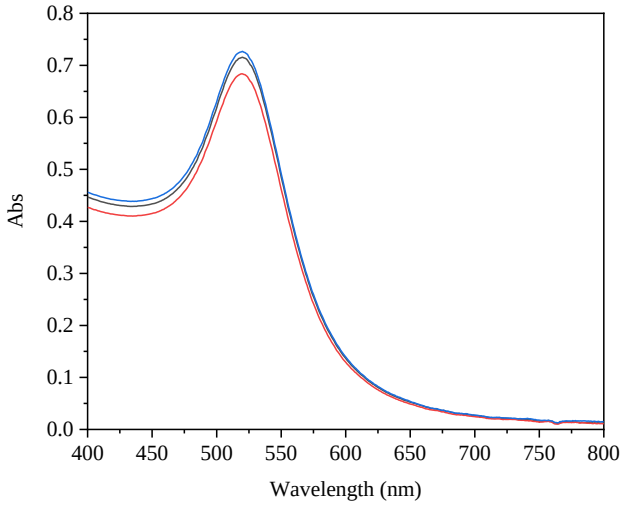

Figure 4.2 – Spectra of three replicates of one synthesis of AuNPs. All samples were diluted 1:4 with milli-Q water.

The UV-Vis spectra presented in Figure 4.2 are indicative of a successful synthesis of AuNPs. The formation of a single LSPR peak is associated with spherical AuNPs, due to their high symmetricity. This single peak is also a sign of a dispersed colloidal solution, and its narrow shape is suggestive of NP size monodispersion. These spectra also allow the estimation of the size and concentration of the synthetized AuNPs, through the use of the equations developed by Haiss et al. [77]. The estimations obtained are presented in Table 4.2.

Table 4.2 – Size and concentration of the different batches of synthetized 15 nm AuNPs.

Batch	Size (nm)	Concentration (nM)	LSPR peak (nm)
1	13.5	9.4	519
2	14.5	8.0	519
3	15.5	6.9	520

The results obtained in Table 4.2 reveal some variation in NP size and concentration across distinct batches of AuNPs. This effect could be attributed to slight differences that occur during the synthesis process, in particular with the temperature of the solution, which is critical in the Au chloride addition step. Kimling et al., from whom the synthesis method was adapted, described a size dispersion of 13 to 16 % for syntheses of NPs under 40 nm [55]. In the presented work, the size of the obtained AuNPs did not vary more than 1.5 nm from the ideal 15 nm, which corresponds to a 10 % deviation and is within the size dispersion described.

Another important data that should be evaluated after the synthesis of AuNPs is their LSPR band peak, since it directly correlates to their size. The wavelength of the peaks obtained for these syntheses varied from 519 to 520 nm. These values are in congruence to what other authors have obtained for 15 nm AuNPs [33].

4.2.2. 40 nm AuNPs

Compared to the synthesis of 15 nm AuNPs, the synthesis of 40 nm AuNPs is more complex since it includes distinct growth phases. The UV-Vis spectra of these growth phases, as well as pictures of the colloidal solution at each phase can be seen in Figure 4.3.

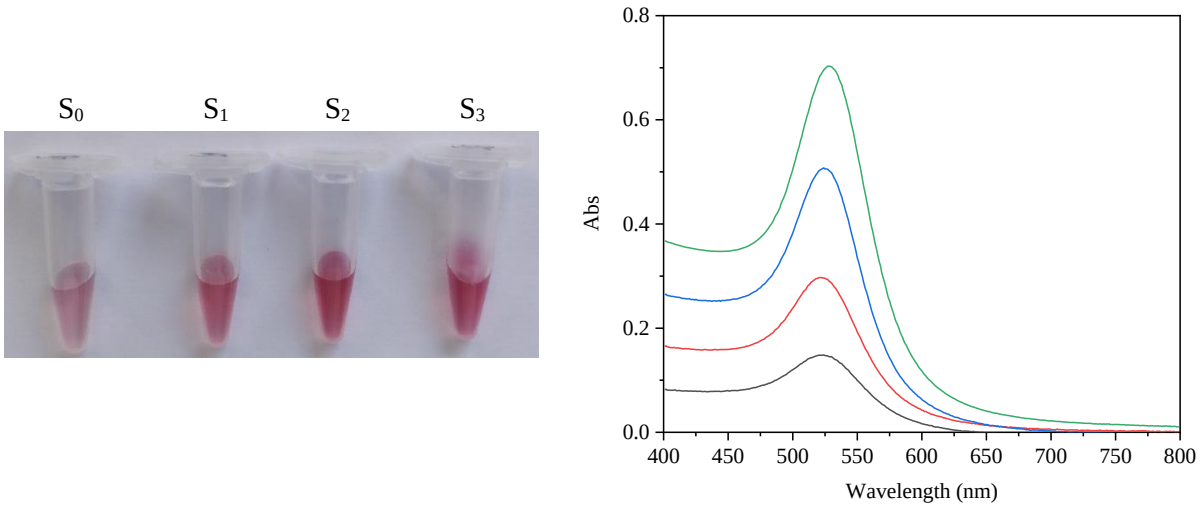

Figure 4.3 – Pictures of the several growth phases of a synthesis of 40 nm AuNPs and their respective spectra. Black – S_0 in a 1:4 dilution; Red – S_1 in a 1:4 dilution; Blue – S_2 in a 1:4 dilution; Green – S_3 in a 1:3 dilution. All dilutions were made with mili-Q water.

From Figure 4.3, it is possible to verify that an increase in the intensity of the colour of the colloid is seen when more growth phases are applied, which is accompanied by a more intense peak in the UV-Vis spectra. The LSPR peak also suffers a red shift, which is a known occurring phenomenon of increasing the size of the AuNPs [36]. The increase in the maximum absorbance seen is also indicative of the growing extinction coefficient that occurs when larger NPs are present.

Generally, after the fourth growth phase (S_3 sample), the AuNPs present a diameter close to 40 nm. The UV-Vis spectrum of this growth phase is indicative of a successful synthesis of AuNPs: the single peak visualized indicates that the synthetised NPs are dispersed, and the narrowness of the peak suggests NP monodispersion.

The spectra obtained from this sample can also be utilized to estimate the size and concentration of the obtained AuNPs, through the equations developed by Haiss et al. [55]. The estimations obtained are presented in Table 4.3.

Table 4.3 – Size and concentration of the different batches of synthetized 40 nm AuNPs.

Batch	Size (nm)	Concentration (nM)	LSPR peak (nm)
1	41.0	0.20	528
2	36.9	0.34	527
3	40.0	0.19	528

The results obtained in Table 4.3 show some variation in the size and concentration of the obtained AuNPs across several batches. Once again, this can be attributed to variability during the synthesis process. For the 40 nm AuNPs, the recorded size did not vary more than 3.1 nm from the desired 40 nm. This corresponds to an approximate deviation of 8 %. Bastús et al., from whom the synthesis method was adapted, described a focusing of the size distribution from 11.9 % to 5.9 % when the size of the resulting AuNPs was increased from 8.4 to 180.5 nm [55]. As such, the deviation obtained in this synthesis is within the error of this method.

The wavelength of the LSPR peaks obtained varied between 527 and 528 nm. This values are in congruence with the values described in the literature for 40 nm AuNPs [80].

4.3. Gold nanoparticles functionalization

4.3.1. 5' thiol-modified oligonucleotide

4.3.1.1. 15 nm gold nanoparticles

The optimization of the functionalization process of AuNPs is extremely important to ensure the production of stable Au-nanoprobes. A comparison between the SA and pH functionalization methods was conducted through the utilization of several ratios of 5' SH-OL per NP. The initial comparison, made through UV-Vis, is presented in Figure 4.4.

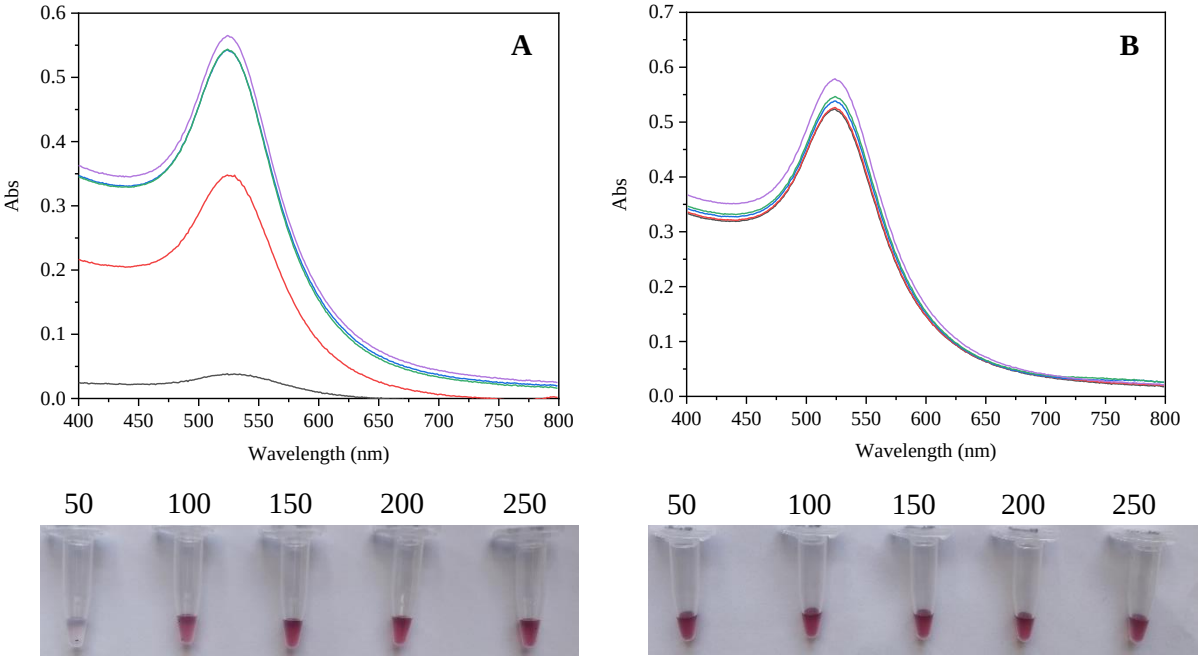

Figure 4.4 – Spectra and photos of several ratios of 5' SH-OL per NP using the SA method (graph A) and the pH method (graph B) for 15 nm AuNPs. Legend: Black – Ratio of 50; Red – Ratio of 100; Dark blue – Ratio of 150; Green – Ratio of 200; Purple – Ratio of 250. All spectra were obtained using a 1:4 dilution in 10 mM PB pH 8 and 100 µL of sample volume.

The results presented in Figure 4.4 reveal clear differences between the SA and pH method. As seen in graph A, the SA method required a ratio of 150 SH-OL per AuNP to ensure that a major loss of Au-nanoprobes did not occur during the functionalization step, evidenced by the lowered absorbance of the smaller ratios. On the other hand, using the pH method, a ratio of 50 was enough to obtain stable Au-nanoprobes. This could indicate a greater functionalization efficiency for the pH method, as described in the literature [55].

Mirkin et al. produced stable Au-nanoprobes using a ratio of 68 SH-OL per NP for 13 nm AuNPs with the SA method [55]. The difference seen between the results obtained here and the ones obtained by Mirkin et al. could be related to the increased AuNP concentration used by Mirkin (17 nM), around double of the one used in these assays (between 7 and 9 nM). Another possibility may lie in the distinct SH-OL used by Mirkin, which may influence the functionalization process. Despite this, other authors have reported the utilization of higher ratios for the SA functionalization of 15 nm AuNPs [72].

Zhang et al. produced stable Au-nanoprobes using a ratio of 20 SH-OL per NP for 13 nm AuNPs with the pH method [55]. It is possible that the pH method employed in this work would also result in stable Au-nanoprobes using a ratio of 20, but the minimum ratio tested was 50. As such, it is not possible to confirm if differences between the results obtained by Zhang et al. and the results obtained here exist.

When the spectrum of the obtained Au-nanoprobes is compared to the spectrum of AuNPs, another indication regarding the success of the functionalization process is seen. A comparison of both spectra can be seen in Figure 4.5.

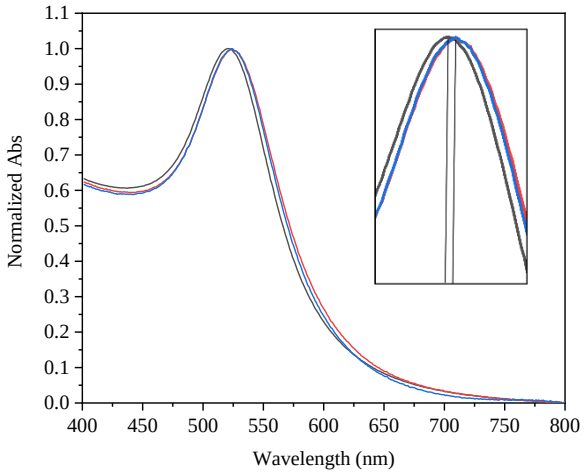

Figure 4.5 – Normalized spectra of 15 nm AuNPs and Au-nanoprobes, obtain using the SA method and the pH method. Black – AuNPs; Red – Au-nanoprobes obtained using the SA method; Blue – Au-nanoprobes obtained using the pH method. Both functionalization methods applied a ratio of 150 5' SH-OL per NP. All spectra were obtained using a 1:4 dilution with 10 mM PB pH 8 and 100 µL sample volume.

As evidenced by Figure 4.5, the LSPR peak of the obtained Au-nanoprobes suffers a slight red shift of a few nanometres, from 520 to 524 nm, which could be related to slight changes in the refractive index of the AuNPs that occurs when SH-OLs attach to their surface.

To complement the results obtained through UV-Vis, agarose gel electrophoresis was performed. This technique has been used by other authors to distinguish between AuNPs and Au-nanoprobes [81]. The agarose gels obtained are presented in Figure 4.6.

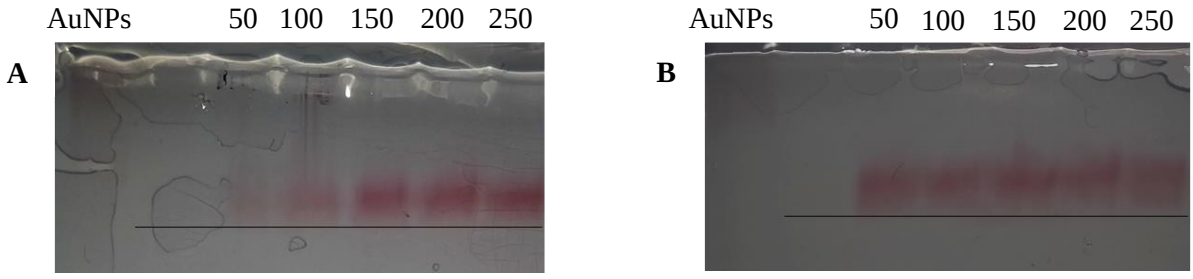

Figure 4.6 – Agarose gels of the several ratios of 5' SH-OL per NP obtained using the SA method (image A) and the pH method (image B) for 15 nm AuNPs. The gels were obtained using 0.5% agarose and the sample volume was 20 µL.

The agarose gels presented in Figure 4.7 confirm what was seen through UV-Vis, regarding the ratios required for successful functionalization for each method.

The control sample, where only AuNPs were added, had a small gel migration. When analysing the Au-nanoprobes, it is possible to verify that increased migration is seen when AuNPs are functionalized with SH-OLs. Theoretically, the adherence of SH-OLs to the surface of AuNPs should increase the size of the conjugate (relative to the citrate-capped AuNPs), but should also increase its negative charge, due to the negative charge of DNA. In agarose gels, the charge and size of the molecule dictates the migration. An increase in size leads to less migration, while an increase in charge leads to more migration. As such, in order to explain the enhanced migration of the Au-nanoprobes, the effect of the charge has to be more considerable than the effect of the size. Despite this, some authors suggest that size has a more significant effect on migration, as opposed to charge. This was evidenced by Pellegrino et al., as their results demonstrated that AuNPs had increased migration, when compared to the Au-nanoprobes, due to the size increase upon introduction of SH-OLs [81]. The distinct migration behaviour of the AuNPs may be tied to the capping-agent of the AuNPs used by Pellegrino et al. In their studies, the capping-agent was replaced from citrate to a phosphine to enhance NP stability. Regarding the studies conducted here, if citrate capped AuNPs aggregate in the agarose gel running buffer TAE, an increase in NP size would occur, due to the formation of large aggregates, explaining the reduced migration. This option was tested by diluting AuNPs in TAE buffer and NP aggregation was seen.

Another interesting visible result lies in the slightly reduced migration for bigger ratios seen in both functionalization methods. This occurrence may be related to the addition of more SH-OLs per NP, which may raise the overall size of the Au-nanoprobes and lead to decreased gel migration. This is a plausible effect if the surface of the AuNPs has not been fully covered with the ratios applied. This was also visualized by Pellegrino et al., where the introduction of more SH-OLs resulted in an increase of the diameter of the Au-nanoprobes and, ultimately, less gel migration [81].

Lastly, by comparing the two functionalization methods, it becomes apparent that the SA method leads to more compact bands, while the pH method seems to lead to bands with more intense band smearing. This could be indicative of a less homogenous functionalization process, where the AuNPs are not equally functionalized, which could affect the colorimetric response.

This comparison was further elaborated through the use of DLS and ELS. These techniques allow the estimation of the hydrodynamic size, polydispersity index and zeta potential of the AuNPs and Au-nanoprobes, which may justify some of the results obtained. The data obtained from these techniques is presented in Table 4.4.

Table 4.4 – Hydrodynamic size, polydispersity index and zeta potential measurements obtained for 15 nm AuNPs and Au-nanoprobes using both functionalization methods. All Au-nanoprobe samples were measured using a 1:4 dilution in 10 mM PB pH 8. The diluted control was diluted 1:4 in mili-Q water. The control sample was obtained without dilution. The presented error corresponds to the standard deviation.

Sample	Ratio	Hydrodynamic size (nm)	Polydispersity index	Zeta potential (mV)
Control	0	21 ± 0	0.30 ± 0.04	- 37.0 ± 2.2
Diluted control	0	32 ± 1	0.44 ± 0.01	- 30.7 ± 0.3
Salt-aging	50	100 ± 3	0.50 ± 0.07	- 31.8 ± 3.1
	100	53 ± 1	0.44 ± 0.01	- 31.7 ± 0.6
	150	34 ± 0	0.36 ± 0.01	- 18.6 ± 0.7
	200	56 ± 1	0.46 ± 0.01	- 27.5 ± 0.9
	250	54 ± 2	0.51 ± 0.10	- 21.8 ± 1.5
pH	50	33 ± 0	0.43 ± 0.01	- 27.6 ± 1.2
	100	58 ± 1	0.50 ± 0.03	- 30.7 ± 0.9
	150	27 ± 0	0.32 ± 0.04	- 27.3 ± 1.7
	200	29 ± 1	0.38 ± 0.01	- 23.2 ± 1.3
	250	28 ± 1	0.35 ± 0.01	- 25.1 ± 1.3

As evidenced by the results presented in Table 4.4, the hydrodynamic size of the control sample is considerably higher than the size estimation made using UV-Vis (21.4 vs 15.5 nm). This discrepancy can be attributed to the fact that the UV-Vis's size estimation, developed by Haiss et al., is correlated with transmission electron microscopy, which focuses on the NP metallic core [77]. On the other hand, dynamic light scattering focuses on the hydrodynamic size of the AuNPs, which includes components at their surface, such as the citrate capping agent [82]. In this scenario, the citrate capping agent is considered for the overall NP size and leads to its increase. The polydispersity index of the control sample is acceptable, since a value below or equal to 0.3 is usually attributed to monodisperse samples [83]. Lastly, the zeta potential value obtained for the control sample (-37.0 mV) is on par with those described in the literature for 15 nm AuNPs [84]. When comparing the control sample to its diluted counterpart, a raise in the hydrodynamic size, polydispersity index and zeta potential can be seen.

Regarding the SA method, it can be concluded that a ratio of 50 SH-OLs per NP leads to extensive aggregation, which is corroborated by the extremely high hydrodynamic size of that sample. With the exception of the 150 ratio, a constant hydrodynamic size can be seen across the remaining ratios. DLS measurements show that using the ratio of 100 does not result in NP aggregation. Despite this, both UV-Vis and agarose gel electrophoresis revealed that this ratio was not adequate for the obtention of stable nanoprobes, due to intense Au-nanoprobe loss. This loss may be attributed to the formation of aggregates large enough to precipitate, that will not interfere in the spectra due to sedimentation, which could also explain the DLS measurements seen.

The size increase seen between the control and stable Au-nanoprobes is also an important point of discussion. In the literature it is described that each DNA b.p. measures about 0.34 nm [85]. When accounting for 20 b.p., the theoretical size of the full sequence should be around 6.8 nm. Another important element of the SH-OL is the spacer located between the thiol-group and the sequence, a chain of six carbons in this case, which also contributes to the overall size of the SH-OL. With this in mind, when comparing the difference in hydrodynamic size between the control sample and the stable Au-nanoprobes, the difference seen (around 30 nm) is higher than expected, even when accounting for twice the size of the SH-OLs that characterizes a successfully functionalized Au-nanoprobe. Even though it could be attributed to NP aggregation, the results obtained from the other techniques suggest this is not the case. As such, the reason behind this steep increase is not fully understood.

Also apparent, regardless of the ratio used, is the fact that the polydispersity index increases after the functionalization process. This is indicative of the presence of several populations of differently sized AuNPs. The formation of these distinct populations in ratios where aggregation was seen could be attributed to NP aggregation. In ratios capable of producing stable Au-nanoprobes this effect can be related to the non-homogenous functionalization of the AuNPs, where some NPs are functionalized with more SH-OL than others.

Lastly, there also seems to exist a correlation between the zeta potential of the AuNPs and the ratio applied in the functionalization. As seen by the results obtained, the higher the ratio, the higher the zeta potential of the Au-nanoprobes. In the functionalization process, the citrate capping agent, which is negatively charged at the working pH, is substituted by the SH-OLs. Since DNA is also negatively charged, a decrease in the zeta potential of the AuNPs would be expected, as the number of SH-OLs per NP is increased. The tendency seen in these results is the opposite. A possible explanation for this phenomenon may be that the negative charges of the DNA are being stabilized by ions in solution.

Regarding the pH method, aggregation is seen for the ratio of 100. This measurement seems to be an outlier, since neither smaller nor larger ratios led to this level of aggregation. For the smallest ratio of 50, the hydrodynamic size seems to be slightly higher than the other ratios, which may be related to NP aggregation. For the other ratios, the hydrodynamic size is extremely similar. Comparing the hydrodynamic size of the samples obtained using the pH method versus the SA method, a prominent difference is seen between them. The Au-nanoprobes produced using the pH method have a hydrodynamic size of approximately 28 nm, compared to the 54 nm seen for the SA method. These Au-nanoprobes have a smaller than expected hydrodynamic size, since successfully functionalizing AuNPs should lead to an increase in the hydrodynamic size around two times the theoretical size of the SH-OL (around 16 nm). A possible explanation for this phenomenon may lie in distinct orientations of the SH-OL at the surface of AuNPs, which could lead to the differences in hydrodynamic size seen, if the adopted conformation is not straight.

The polydispersity indexes, although higher than the beforementioned threshold, are also smaller than the ones obtained using the SA method, which is preferred and may be indicative of less aggregation or a more homogenous functionalization. These results contradict what was obtained in the agarose gel electrophoresis, where the pH method seemed to produce less homogenous Au-nanoprobes, evidenced by more intense band smearing. This could be correlated to variability of the functionalization process. The zeta potential of these Au-nanoprobes also seems to be more stable, with no clear tendency when the ratio is increased. Despite not diminishing with the increase of the functionalization ratio, the zeta potential obtained for the ratio of 50 using the pH method is similar to the zeta potential of the ratio of 200/250 using the SA method. This may be correlated to the distinct functionalization efficiencies between the pH and SA method. It is possible that a ratio of 50 using the pH method results in as much SH-OL density at the surface of AuNPs as a ratio of 200 using the SA method.

The same correlations between AuNP functionalization and their hydrodynamic size and zeta potential was seen by Park et al. using phosphine capped AuNPs [86]. Similarly to the results obtained here, Park et al. saw an increase in the hydrodynamic size and decrease in zeta potential of the AuNPs, upon functionalization with SH-OLs.

The introduction of SH-OLs at the surface of AuNPs should lead to an increase in the stability of the obtained Au-nanoprobes. As such, to assess the success of the functionalization process, stability assays were performed for AuNPs and Au-nanoprobes. These assays would also allow a comparison between the stability of the Au-nanoprobes obtained using the distinct functionalization methods. The stability assays of the AuNPs are presented in Figure 4.7.

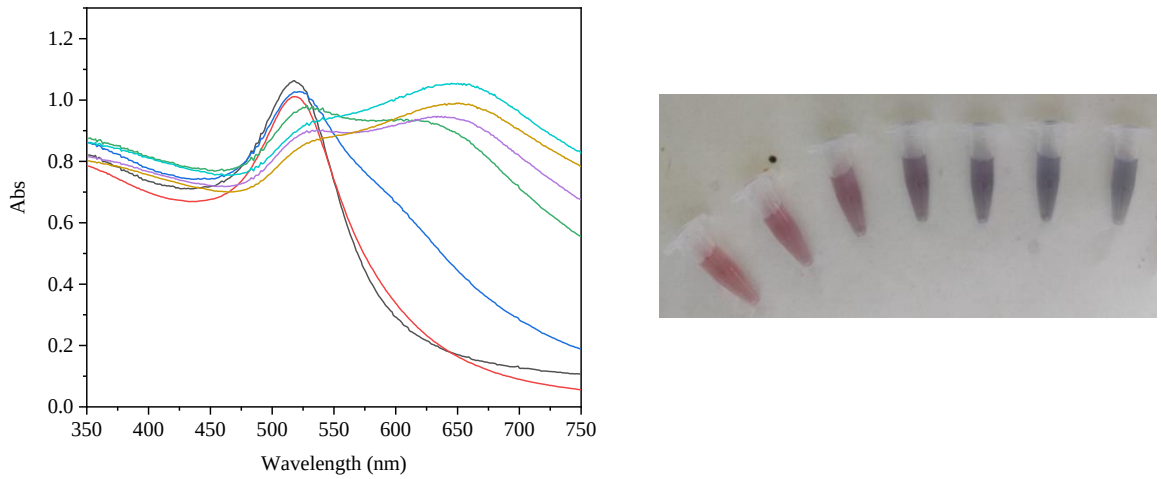

Figure 4.7 – 15 nm AuNPs stability evaluation by UV-Vis and respective colorimetric response. Black – 0 mM NaCl; Red – 40 mM NaCl; Dark blue – 50 mM NaCl; Green – 60 mM NaCl; Purple – 70 mM NaCl; Gold – 80 mM NaCl; Light blue – 90 mM NaCl. The colorimetric response is ordered from smallest to highest NaCl concentration. All spectra were obtained using a 1:4 dilution with 10 mM PB pH 8 and 100 µL sample volume.

As evidenced by Figure 4.7, the stability of the citrate capped AuNPs towards salt is extremely low. After the addition of 50 mM of NaCl, extensive aggregation of the colloid sample can be seen in the UV-Vis spectra. The formation of aggregates is evidenced by the surging of another LSPR peak at less energetic wavelengths, characteristic of clusters of NPs. This phenomenon can also be detected by eyesight, due to the intense colorimetric change that occurs from red to blue, indicative of the formation of the new LSPR peak. As more NaCl is added, the characteristic LSPR peak of the 15 nm AuNPs at 519 nm diminishes, while the new LSPR peak near 600 nm intensifies, indicative of the growing population of aggregates in solution.

The results obtained here are on par with the results obtained by Zimbone et al., which verified that a concentration of 60 mM of NaCl was enough to induce intense AuNP aggregation, although their NPs were slightly larger, with an LSPR peak around 522 nm [86].

Following this, stability assays using Au-nanoprobes obtained through the two functionalization methods were performed. The results obtained are presented in Figure 4.8.

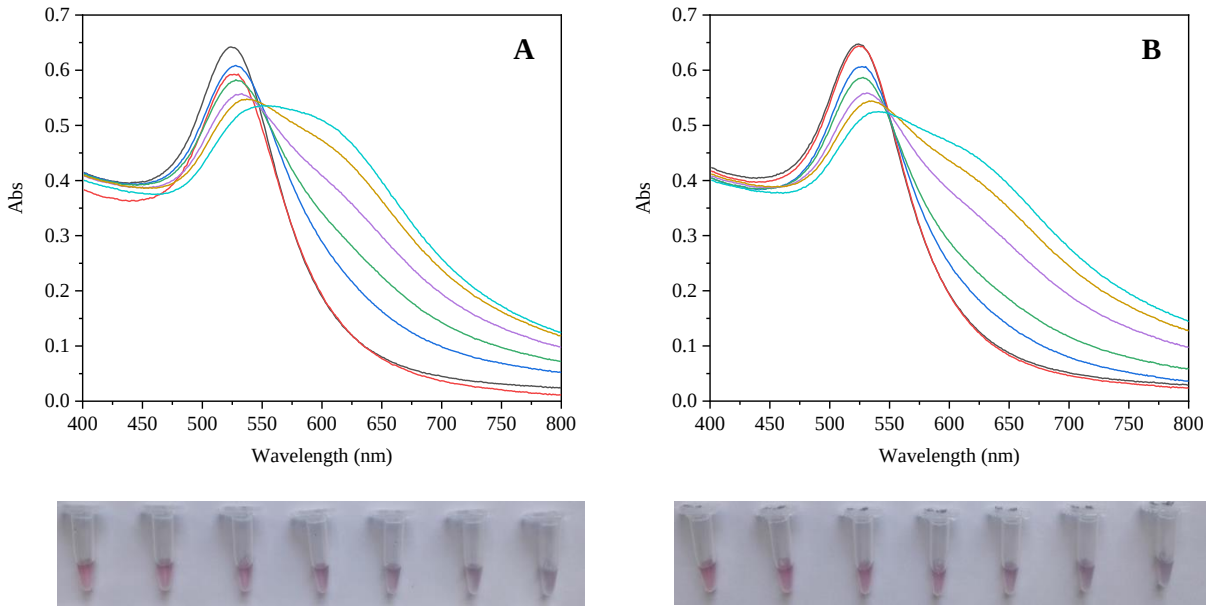

Figure 4.8 – 15 nm Au-nanoprobes stability evaluation through UV-Vis and respective colorimetric response. Graph A corresponds to the SA method and graph B to the pH method. A ratio of 150 5' SH-OLs per NP was applied for both functionalization methods. For both spectra: Black – 0 mM NaCl; Red – 300 mM NaCl; Dark blue – 400 mM NaCl; Green – 500 mM NaCl; Purple – 600 mM NaCl; Gold – 700 mM NaCl; Light blue – 800 mM NaCl. The colorimetric response is ordered from smallest to highest NaCl concentration. All spectra were obtained using a final Au-nanoprobe concentration of 2.5 nM and 100 µL sample volume.

Figure 4.8 confirms that the stability of the Au-nanoprobes is substantially higher than the stability of the NPs. Unlike AuNPs, which start to aggregate with less than 50 mM of NaCl, these Au-nanoprobes only see a similar level of aggregation with 500 mM of NaCl. This increased stability seen for Au-nanoprobes is an indication that the functionalization was successful as the SH-OLs at the surface of the AuNPs are conferring greater protection against aggregation. It is also important to note that, independently of the functionalization method applied, the stability of the Au-nanoprobes is extremely similar.

Stakenborg et al. also evaluated the increased stability of 30 nm AuNPs upon functionalization with 5' mercaptohexanol modified OLs [87]. Their results demonstrated an increase in the stability of the Au-nanoprobes of one order of magnitude (from 20 mM to 200 mM), which is on par with the results obtained here. The differences in stability seen in the results obtained here may be attributed to the different size of AuNPs used or due to the distinct modification applied to the functionalization OL.

Even though no significant differences between the two functionalization methods were seen in the stability assays, they were useful in establishing the NaCl concentration necessary to induce a desirable Au-nanoprobe aggregation (upwards of 700 mM). NCL colorimetric assays were then performed to evaluate the colorimetric distinction between ssDNA targets. The results obtained are presented in Figure 4.9.

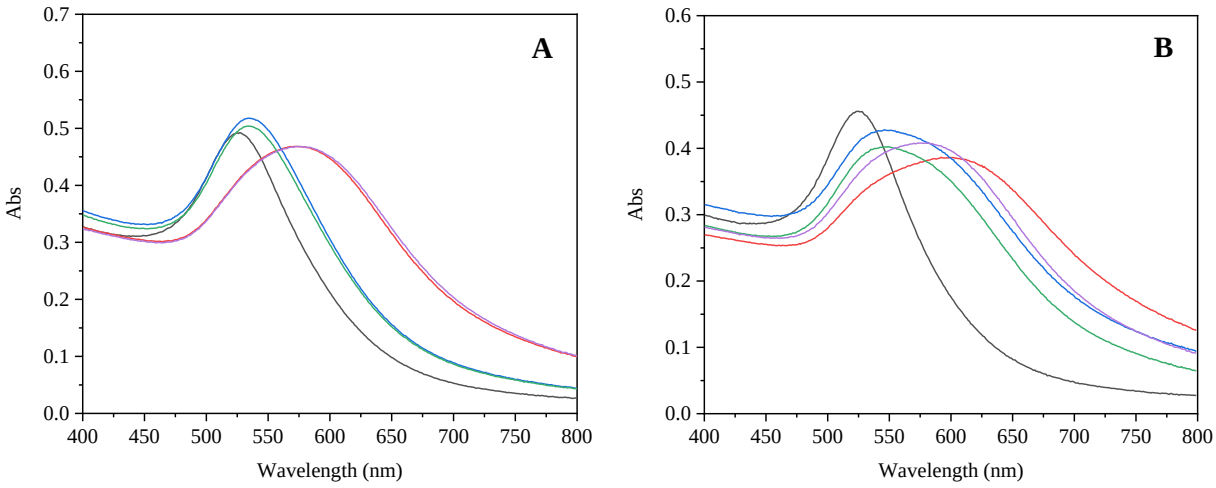

Figure 4.9 – 15 nm Au-nanoprobes colorimetric evaluation through UV-Vis. Graph A corresponds to the SA method and graph B to the pH method. A ratio of 150 5' SH-OLs per NP was applied for both functionalization methods and the colorimetric assay was performed using 800 mM NaCl and 40 b.p. anti-parallel ssDNA. For both spectra: Black – Control sample; Red – Salt sample; Dark blue – Complementary ssDNA sample; Green – Mutated ssDNA sample; Purple – Non-complementary ssDNA sample; All spectra were obtained using a final Au-nanoprobe concentration of 2.5 nM, a ssDNA concentration of 18 ng/µL and 100 µL sample volume.

From the spectra presented in Figure 4.9, clear differences between the two functionalization methods can be seen. For the SA method both the complementary and mutated ssDNA samples show an intense stabilization of the Au-nanoprobes. On the other hand, these same samples do not provide a prominent increase in stabilization when the pH method was applied. Another important aspect is that for the SA Au-nanoprobes the non-complementary ssDNA target does not provide any additional stabilization effect, while for the pH method Au-nanoprobe stabilization does occur. This could indicate a worse or unsuccessful hybridization when the pH functionalization method is applied.

These results indicate that the SA method should be preferred for the functionalization of 15 nm AuNPs, due to the higher hybridization efficiency and stabilization effect seen, comparatively to the pH method.

4.3.1.2. 40 nm gold nanoparticles

The functionalization of 40 nm AuNPs may prove to be more complex due to their inherent reduced stability. Initially, several ratios of 5' SH-OL per NP were tested. This revealed that the SA method was not capable of producing stable Au-nanoprobes, while the pH method produced overall stable Au-nanoprobes associated to some degree of variability. Improvements to the pH method, such as preconcentration of the stock AuNPs, were done. The results obtained for the revised pH method are presented in Figure 4.10.

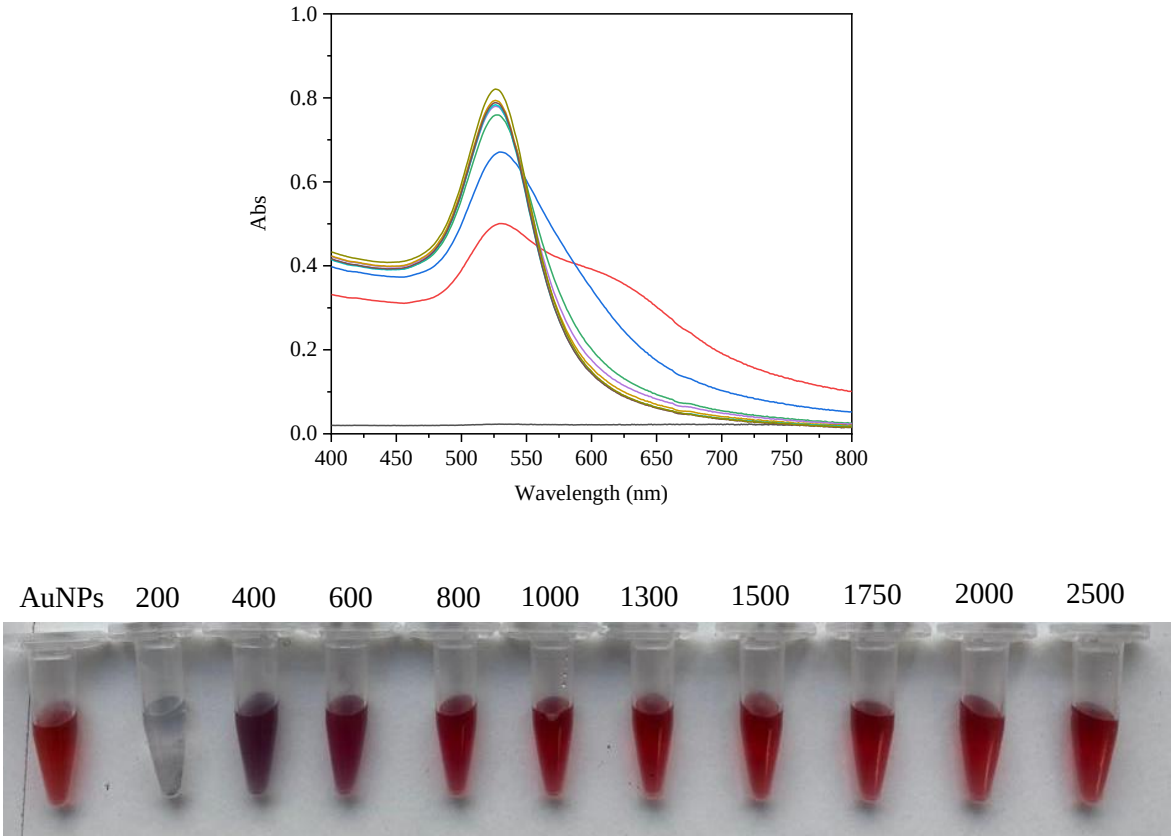

Figure 4.10 – Spectra and photos of several ratios of 5' SH-OL per NP using the revised pH method for 40 nm AuNPs. Black – Ratio of 200; Red – Ratio of 400; Dark blue – Ratio of 600; Green – Ratio of 800; Purple – Ratio of 1000; Gold – Ratio of 1300; Light blue – Ratio of 1500; Brown – Ratio of 1750; Yellowed green – Ratio of 2000; Greyed blue – Ratio of 2500. All spectra were obtained using a 1:4 dilution with 10 mM PB pH 8 and 100 µL of sample volume.

In Figure 4.10 it can be seen that promising Au-nanoprobes can be obtained starting with a ratio of 800 5' SH-OLs per NP, as indicated by the position and band width of the corresponding LSPR peaks. Nevertheless, as 800 and 1000 ratios still resulted in slight Au-nanoprobe aggregation in different replicates, a higher ratio (1300) was considered as the smallest ratio capable of producing stable Au-nanoprobes.

The results obtained by Zhang et al. confirm the critical role of AuNPs concentration during functionalization [68]. Initially, Zhang et al. verified that a ratio of 6400 SH-OLs per NP was necessary for the functionalization of 50 nm AuNPs at 0.1 nM using the regular pH method. After concentrating the 50 nm AuNPs 100 times, the required ratio saw a decrease to 666 SH-OLs per NP in their tested conditions. When compared to the values obtained in this work, Zhang et al. was capable of producing stable Au-nanoprobes using less SH-OLs per NP. The difference seen may be tied to the overall concentration of the AuNPs used. In this work, the AuNPs were only concentrated 20 times, for a final concentration around 4 nM, while Zhang et al. concentrated their AuNPs 100 times, for a final concentration around 10 nM.

Comparing the 40 nm AuNPs with de 15 nm ones, a higher ratio of SH-OLs per NP is needed to obtain stable Au-nanoprobes. This phenomenon may be tied not only to the larger surface of the 40 nm AuNPs, which requires more SH-OL to reach equal density at its surface, but also to the inherent lessened stability of these larger AuNPs.

Following this, agarose gel electrophoresis was performed. The gels obtained are presented in Figure 4.11.

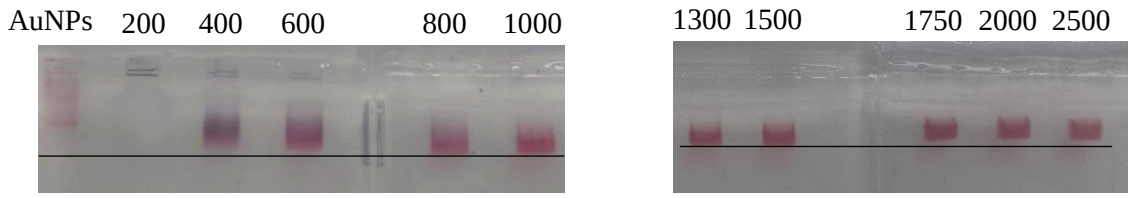

Figure 4.11 – Agarose gels of the several ratios of 5' SH-OL per NP obtained using the revised pH method for 40 nm AuNPs. The gels were obtained using 0.5% agarose and the sample volume was 20 µL.

The gels presented in Figure 4.11 show diminished distinction between promising Au-nanoprobes (ratio of 800 SH-OLs per NP and up) and Au-nanoprobes where intense signs of aggregation were seen in UV-Vis, as is the case of the 400 and 600 ratios.

Similarly to 15 nm AuNPs, slight migration is seen for the control sample of the 40 nm AuNPs. The Au-nanoprobes also show increased migration, when compared to the citrate capped AuNPs. For the ratios capable of producing stable Au-nanoprobes (1300 and up), a tendency of less band migration is seen with the increase of the ratio of 5' SH-OLs per NP. This also occurred with the 15 nm Au-nanoprobes and may be tied to the density of SH-OLs at the surface of the AuNPs or even the diminishing of the zeta potential of the Au-nanoprobes, when larger ratios are applied.

To further explore the functionalization process, DLS and ELS measurements were obtained. The data obtained is presented in Table 4.5.

Table 4.5 – Hydrodynamic size, polydispersity index and zeta potential measurements obtained for 40 nm AuNPs and Au-nanoprobes using the revised pH method. All the samples were measured using a 1:4 dilution in mili-Q water (control) or 10 mM PB pH 8 (Au-nanoprobes). The presented error corresponds to the standard deviation.

Sample	Ratio	Hydrodynamic size (nm)	Polydispersity index	Zeta potential (mV)
Control	0	43 ± 1	0.31 ± 0.04	- 27.2 ± 2.2
pH	200	-	-	-
	400	95 ± 1	0.29 ± 0.02	- 40.1 ± 2.2
	600	86 ± 0	0.28 ± 0.01	- 36.3 ± 3.1
	800	63 ± 1	0.26 ± 0.00	- 29.4 ± 1.8
	1000	57 ± 1	0.24 ± 0.01	- 27.2 ± 2.9
	1300	52 ± 1	0.20 ± 0.01	- 25.6 ± 1.7
	1500	49 ± 1	0.17 ± 0.00	- 23.6 ± 1.5
	1750	49 ± 0	0.17 ± 0.00	- 23.7 ± 0.3
	2000	51 ± 0	0.21 ± 0.01	- 26.2 ± 1.2
	2500	51 ± 0	0.20 ± 0.00	- 22.7 ± 1.2

The results presented in Table 4.5 reveal that the control sample displays a hydrodynamic size slightly larger than the estimated size using the UV-Vis technique. Like previously mentioned, this occurrence is related to differences between the size of metallic core and hydrodynamic size. The polydispersity index of the control sample is on the threshold for a monodisperse solution. This may be tied to the centrifugation steps applied, which has already been proven to be capable of inducing NP aggregation. The zeta potential of this sample is on par with the reported values [88].

When comparing the control sample with the Au-nanoprobes, an increase in the hydrodynamic size can be seen. Regarding the functionalized samples, it is possible to verify that the Au-nanoprobes' hydrodynamic size tends to diminish with the increase of the ratio of 5' SH-OLs per NP, up until de 1300 ratio, after which it seems to stabilize. This corroborates the results obtained through UV-Vis, where this was the smallest ratio capable of consistently producing stable Au-nanoprobes. When compared to the control sample, the difference is about 7 to 8 nm, which is in agreeance with the theoretical calculations of the size of the SH-OL. These results are also similar to the ones obtained for the 15 nm AuNPs when the pH method was applied. The polydispersity index of these samples follows the same trend as the hydrodynamic size, but all the samples are below the monodispersion threshold. While desirable, it was expected that the samples with the smaller ratios, where aggregation is seen, would have a polydispersity index above that value. As such, although the hydrodynamic size increase and sample coloration suggests the presence of aggregates, these can not be confirmed by the polydispersity index, indicating a possible limitation of this technique.

The indexes obtained for the 40 nm AuNPs are objectively better than the ones obtained for the 15 nm AuNPs. This may be related to the lower size dispersion seen during the synthesis process or may be justified by a bad batch of 15 nm AuNPs. Regarding the zeta potential measurements, two main conclusions can be taken. Firstly, for the lower ratios, the potential is substantially lower than the ones obtained for the control sample. Secondly, as the ratios get bigger, the zeta potential tends to increase, until it becomes higher than the potential of the control samples, similarly to the 15 nm AuNPs using the pH method. For the first case, even if the potential of the control samples is arguably lower than it should be, due to slight aggregation, the samples of the lower ratios saw considerably more aggregation, justifying a higher potential, not a lower. As such, further studying of these samples using other techniques, such as Nanoparticle Tracking Analysis, would be beneficial to understand the occurrences seen and confirm the presence of aggregates. A possible explanation for the second case was already explored for the 15 nm AuNPs, where the same situation applies.

To assess the success of the functionalization process, stability assays were performed to compare the ionic strength stabilization of the AuNPs versus Au-nanoprobes. The results obtained are presented in Figure 4.12.

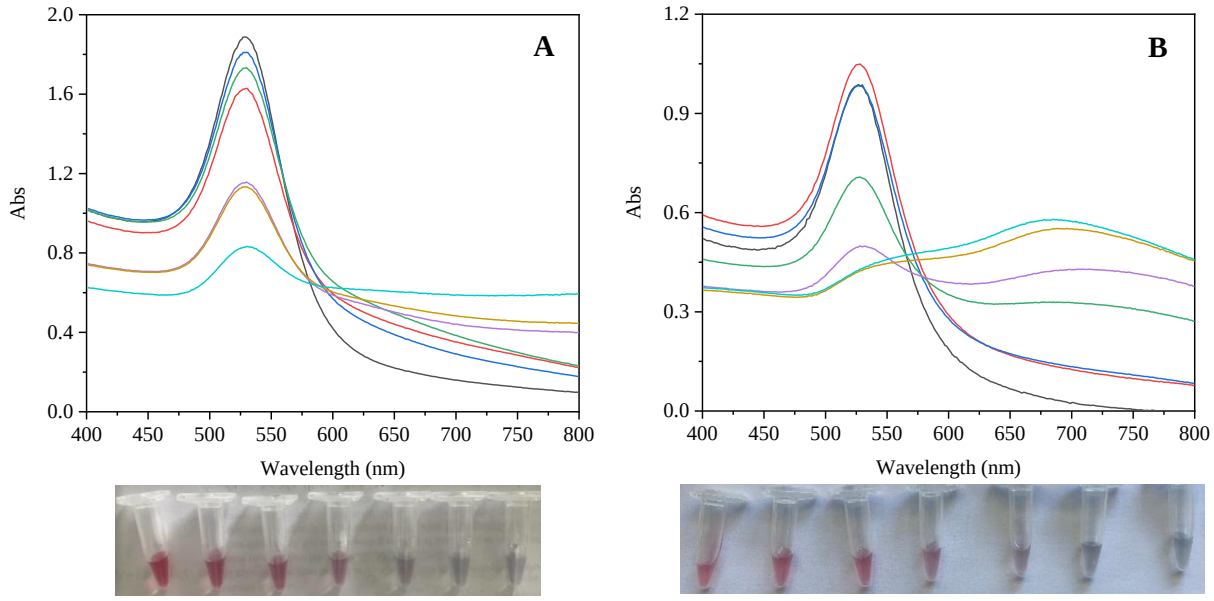

Figure 4.12 – 40 nm AuNPs (graph A) and Au-nanoprobes (graph B) stability evaluation through UV-Vis and their colorimetric response. Au-nanoprobes were obtained using the revised pH method with a ratio of 1300 5' SH-OL per NP. Graph A: Black – 0 mM NaCl; Red – 60 mM NaCl; Dark blue – 70 mM NaCl; Green – 80 mM NaCl; Purple – 90 mM NaCl; Gold – 100 mM NaCl; Light blue – 110 mM NaCl. Graph B: Black – 0 mM NaCl; Red – 200 mM NaCl; Dark blue – 250 mM NaCl; Green – 300 mM NaCl; Purple – 350 mM NaCl; Gold – 400 mM NaCl; Light blue – 450 mM NaCl. The colorimetric response is ordered from smallest to highest NaCl concentration. All AuNP spectra were obtained using a final NP concentration of 0.25 nM and 100 µL sample volume. Au-nanoprobe spectra were obtained using a final Au-nanoprobe concentration of 0.15 nM.

From the conducted stability assays, it is possible to conclude that the NaCl concentration required to induce intense NP aggregation (90 mM) is much smaller than the concentration required to induce Au-nanoprobe aggregation (300 mM). As previously mentioned, the increased stability verified through the introduction of SH-OLs is related to the negative charge of these molecules, highlighting the repulsion effect seen between molecules, which results in enhanced NaCl stability. The results obtained support the correct functionalization of the 40 nm AuNPs and is in agreeance with the results obtained for the 15 nm AuNPs. As such, it is possible to conclude that the revised pH method is capable of producing stable 40 nm Au-nanoprobes.

4.3.2. 3' thiol-modified oligonucleotide

4.3.2.1. 15 nm gold nanoparticles

The second SH-OL used in this project was designed with the thiol group at the 3' end in order to apply a head-to-tail approach in the CL assays, as the first one had the thiol group at 5'.

The initial UV-Vis ratio testing results obtained for the SA and pH functionalization methods using the 3´ SH-OL are presented in Figure 4.13.

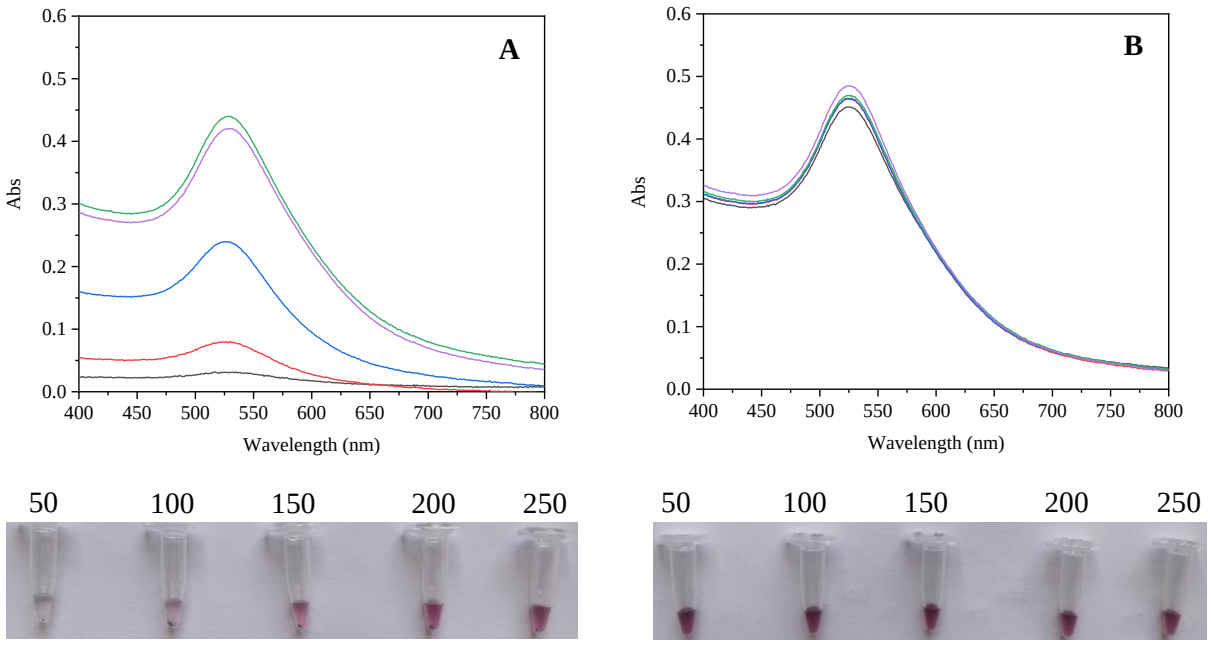

Figure 4.13 – Spectra and photos of several ratios of 3' SH-OL per NP using the SA method (graph A) and the pH method (graph B) for 15 nm AuNPs. Legend for both spectra: Black – 50 mM NaCl; Red – 100 mM NaCl; Blue – 150 mM NaCl; Green – 200 mM NaCl; Purple – 250 mM NaCl. All spectra were obtained using a 1:4 dilution with 10 mM PB pH 8 and 100 µL of sample volume.

From the results presented in Figure 4.13, it is possible to verify that the pH method allows the utilization of smaller ratios to obtain stable Au-nanoprobes, comparatively to the SA method. Regarding the SA method, a ratio of 200 is necessary to produce stable Au-nanoprobes. When compared to the 5' SH-OL, it can be verified that the SA method required a higher ratio to produce stable Au-nanoprobes when the 3' SH-OL is used. This phenomenon could be associated to the lower G/C content of this SH-OL, which would consequently lower its stability [89]. Even for the ratios that seem to produce stable Au-nanoprobes, a substantial loss of Au-nanoprobes is seen during the process, as a smaller absorbance peak is registered when using 3' SH-OL comparatively to the 5' SH-OL (0.6 a.u. for 5' SH-OL vs 0.45/0.5 a.u. for the 3' SH-OL). Another important aspect is the shape of the spectra of the obtained Au-nanoprobes. When compared to the spectra of the Au-nanoprobes obtained with the 5' SH-OL, slight signs of aggregation are present in the spectra obtained using the 3' SH-OL. This is evidenced by the slight sulk that can be seen near 580 nm for either functionalization method.

The differences seen could also be attributed to the smaller spacer used in the 3' SH-OLs, which use a 3-carbon spacer instead of a 6-carbon spacer, or in the distinct conditions that the thiol modification is inserted. Unlike the 5' thiol, which is added after OL synthesis, the introduction of a 3' thiol requires the use of a specific support, which could affect the amount of modified OL obtained [90].

Despite this, both methods showed the capability of producing stable Au-nanoprobes. 3' SH-OL attachment was also supported by the slight red shift of the LSPR peak by a few nanometres, as had occurred for the 5' SH-OL.

To further compare the two methods, agarose gel electrophoresis was performed. The gels obtained can be seen in Figure 4.14.

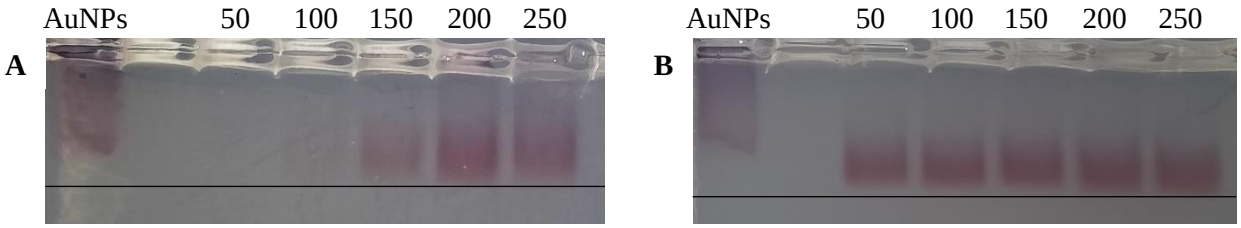

Figure 4.14 – Agarose gels of the several ratios of 3' SH-OL per NP obtained using the SA method (image A) and the pH method (image B) for 15 nm AuNPs. The gels were obtained using 0.5% agarose and the sample volume was 30 µL.

The results obtained in the agarose gel electrophoresis reenforce the ones obtained through UV-Vis. The agarose gel is able to discern the ratios capable of producing stable Au-nanoprobes. The bands obtained using the pH method appear to be more intense and focused, without as much band smearing, when compared to the SA samples. The intensity of the band could be an indication of a more uniform functionalization but could also be tied to a slightly higher absorbance of the samples in the pH method.

When compared to the agarose gels of the 5' SH-OL, it is also possible to conclude that considerably less migration is seen in the samples using the 3' SH-OL. This may be indicative of an overall less effective functionalization, which introduces slight Au-nanoprobe aggregation, resulting in less band migration. Another difference between the two SH-OLs is the behaviour of the migration when larger ratios are applied. Unlike the 5' SH-OL, where band migration saw a decrease with the increase of the ratio applied in the functionalization step, the same is not as prevalent here.

The results obtained until this point seem to indicate that the Au-nanoprobes obtained using the 3' SH-OL are not as robust as the ones obtained using the 5' SH-OL. Since for the 5' SH-OL the SA method allowed better Au-nanoprobe stabilization in the colorimetric assays, presumably due to higher hybridization efficiency, the SA method, using a ratio of 200 was also chosen for the 3' SH-OL.

4.3.2.2. 40 nm gold nanoparticles

The functionalization process of the 3' SH-OL was also evaluated for 40 nm AuNPs using the revised pH method that used concentrated AuNPs. The initial UV-Vis results obtained for several ratios of 3' SH-OL per NP are presented in Figure 4.15.

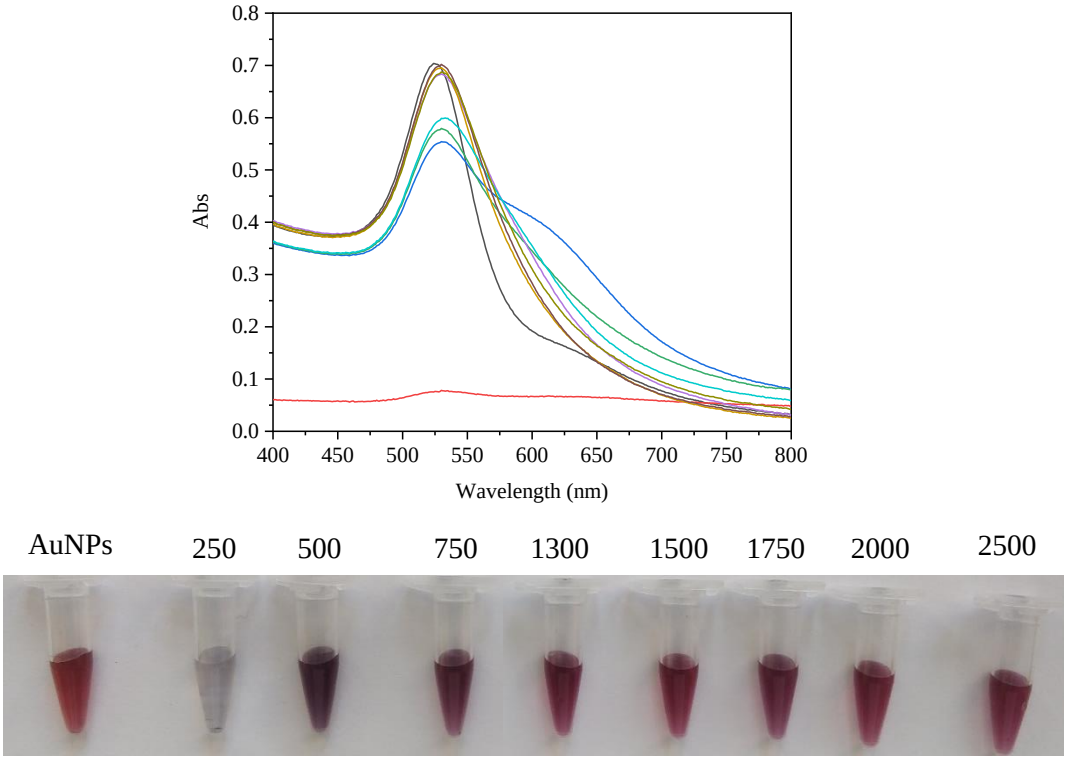

Figure 4.15 – Spectra and photos of several ratios of 3' SH-OL per NP using the revised pH method for 40 nm AuNPs. Black – Control sample after centrifugations; Red – Ratio of 250; Dark blue – Ratio of 500; Green – Ratio of 750; Purple – Ratio of 1300; Gold – Ratio of 1500; Light blue – Ratio of 1750; Brown – Ratio of 2000; Yellowed green – Ratio of 2500. All spectra were obtained using a 1:4 dilution with 10 mM PB pH 8 and 100 µL of sample volume.

The ratio testing results, presented in Figure 4.17, indicate similarities with the functionalization of the 15 nm AuNPs using the 3' SH-OL. A higher requirement for the functionalization ratio is seen when compared to the 5' SH-OL, since the ratio of 1300 still displayed some aggregation, evidenced by the colour of the Au-nanoprobes solution and the UV-Vis spectra. Another recurring phenomenon is the overall more aggregated state of the resulting Au-nanoprobes, evidenced by the sulk that occurs near 600 nm.

Despite this, the Au-nanoprobes still displayed a red shift of the LSPR peak, indicative of SH-OL attachment. For 40 nm Au-nanoprobes, the ratio of 1500 3' SH-OL per NP was the smallest capable of producing stable Au-nanoprobes. Ideally, since the ratio of 1750 still resulted in slight Au-nanoprobe aggregation, the ratio of 2000 should be used, but due to volume constraints, the 1500 ratio was chosen.

To compare the mobility of the Au-nanoprobes with the citrate capped AuNPs and the Au-nanoprobes obtained using the 5' SH-OL, agarose gel electrophoresis was performed. The gels obtained are presented in Figure 4.16.

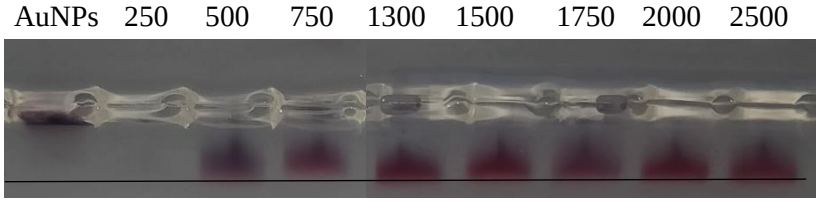

Figure 4.16 – Agarose gel of the several ratios of 3' SH-OL per NP obtained using the revised pH method for 40 nm AuNPs. The gel was obtained using 0.5% agarose and the sample volume was 30 µL.

From the agarose gel, presented in Figure 4.16, it is possible to assess that the distinction between ratios that resulted in NP aggregation and ratios capable of producing stable Au-nanoprobes is not ideal. The major factor that allows differentiation is the colour of the band and the migration pattern to a lesser degree. This is in agreeance with the agarose gel obtained for the 40 nm Au-nanoprobes obtained with the 5' SH-OL. Similarly to the results obtained for the 15 nm AuNPs, the migration is smaller using the 3' SH-OL. The intensity of the band is comparable to those obtained using the 5' SH-OL, with slight changes being justified by the difference in absorbance at the LSPR peak between the two (0.7 for the 3' SH-OL and 0.8 for the 5' SH-OL). Unlike the results obtained using the 5' SH-OL, there does not seem to exist diminishing migration, as a larger ratio is applied.

Overall, the results indicate that the Au-nanoprobes obtained using the 3' SH-OL are worse than the ones obtained using the 5' SH-OL. This is similar to the results obtained for the 15 nm AuNPs.

Nevertheless, the nanoprobes obtained using a ratio of 1500 were further utilized in the forthcoming CL assays.

4.4. Hybridization optimization

4.4.1. Target DNA

The optimization of the ssDNA target to be utilized in the upcoming colorimetric assays is extremely important to verify if the designed colorimetric system is functioning correctly. Initially, 50 b.p. parallel ssDNA targets, capable of parallel hybridization with the Au-nanoprobes were utilized. These targets were used due to immediate availability and to obtain information on the capability of parallel hybridization. NCL colorimetric assays were performed using 40 nm Au-nanoprobes obtained with the 5' SH-OL and taking into account the stability assays presented in the previous chapter. The results obtained for these colorimetric assays are presented in Figure 4.17.

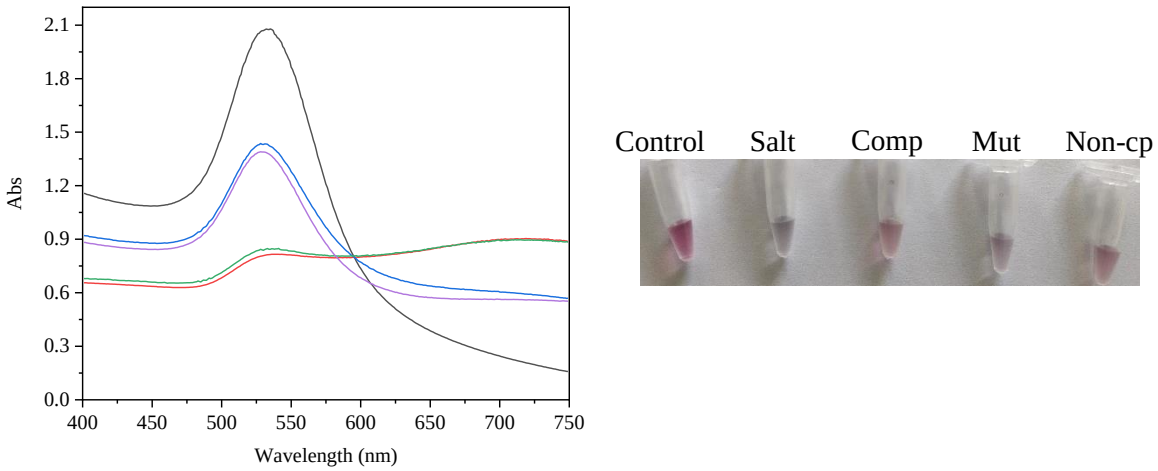

Figure 4.17 – Colorimetric assays of the 40 nm Au-nanoprobes obtained through the revised pH method with a ratio of 1300 5' SH-OL per NP, using 50 b.p. parallel ssDNA. These spectra were obtained using 300 mM NaCl. Black – Control sample; Red – Salt sample; Dark blue – Complementary ssDNA sample; Green – Mutated ssDNA sample; Purple – Non-complementary ssDNA sample; All spectra were obtained using a final Au-nanoprobe concentration of 0.25 nM, a ssDNA concentration of 21 ng/µL and 100 µL sample volume.

From the results presented in Figure 4.17, it is possible to identify that a clear difference between the complementary and mutated ssDNA samples exists, especially considering that a parallel ssDNA is being utilized. Despite this, the protection against aggregation conferred by the non-complementary ssDNA was higher than the mutated and on par with the complementary ssDNA, which at first glance is confusing and was not expected. Theoretically, both the complementary and mutated ssDNA targets should confer much better salt protection than the non-complementary ssDNA, which does not possess a complementary sequence to any portion of the SH-OL at the surface of the AuNPs. The results obtained contradict this and may be indicative of non-specific interactions between the Au-nanoprobes and the non-complementary ssDNA.

A possible explanation was achieved by Cárdenas et al., through the examination of the interactions between AuNPs and both SH-OL and regular OLs [91]. Their results showed that ssDNAs could adsorb to AuNPs pre-functionalized with SH-OLs. This occurrence would lead to a greater Au-nanoprobe surface coverage, which could increase the stability of the resulting Au-nanoprobes, explaining the results seen here.

To verify if the design and length of the ssDNA targets could influence the protection conferred by the non-complementary ssDNA, new 40 b.p. parallel ssDNAs were developed taking in consideration the exact sequence of the gene where the mutation is inserted. The results obtained from colorimetric assays using the newly designed 40 b.p. parallel ssDNA targets are presented in Figure 4.18.

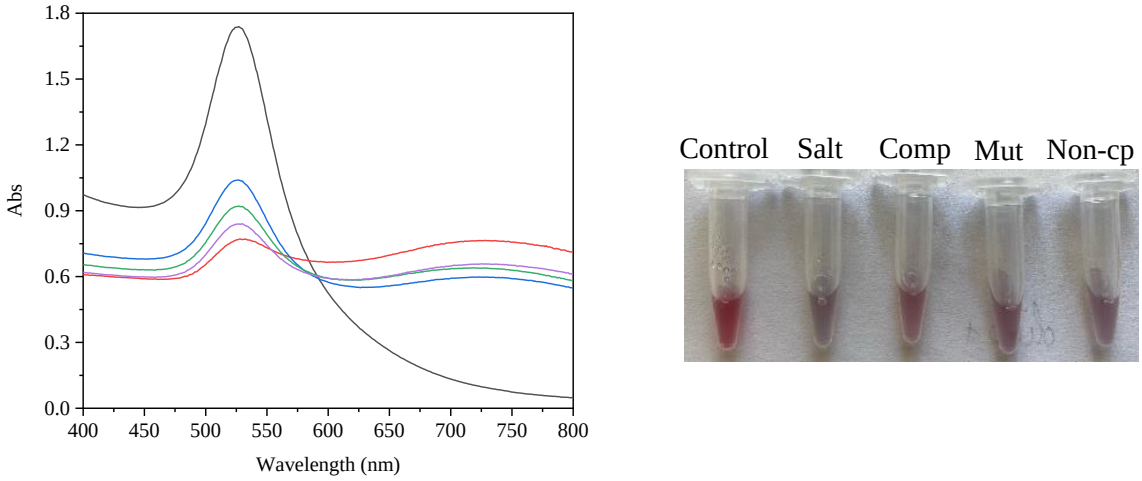

Figure 4.18 – Colorimetric assays of the 40 nm Au-nanoprobes obtained through the revised pH method with a ratio of 1300 5' SH-OL per NP, using 40 b.p. parallel ssDNA. These spectra were obtained using 400 mM NaCl. Legend: Black – Control sample; Red – Salt sample; Dark blue – Complementary ssDNA sample; Green – Mutated ssDNA sample; Purple – Non-complementary ssDNA sample; All spectra were obtained using a final Au-nanoprobe concentration of 0.25 nM, a ssDNA concentration of 18 ng/µL and 100 µL sample volume.

The alteration of the ssDNA sequence proved to have a significant impact on the colorimetric assays. As evidenced by the results in Figure 4.18, the non-complementary ssDNA Au-nanoprobe stabilization was diminished like intended. The aggregation of this sample was smaller than the aggregation seen for the mutated ssDNA sample, which is in congruence with the theoretical method and results obtained by other authors [72]. Despite this, the difference between the aggregation of the complementary and the mutated ssDNA samples diminished using 40 b.p. parallel ssDNA targets. A decrease of the stabilization provided by the complementary ssDNA was also seen. These results are indicative that the ssDNA length and/or composition severely affects the Au-nanoprobe stabilization.

Samuels verified that DNA sequences richer in G/C content had increased thermal stability, which increased their longevity [89]. The increased stability seen for higher G/C contents may explain the smaller stability effect provided by the complementary ssDNA target. The redesign from the 50 b.p. to 40 b.p. lowered the G/C content of the ssDNA, which led to a decrease of its melting temperature, from 95 to 75 ºC. As such, the resulting SH-OL – ssDNA complex could have a lessened stability, justifying the results obtained.

To evaluate the differences between parallel and anti-parallel hybridization, new 40 b.p. anti-parallel ssDNA targets were designed taking into consideration the gene sequence and tested. The colorimetric assays obtained using these ssDNA targets are presented in Figure 4.19.

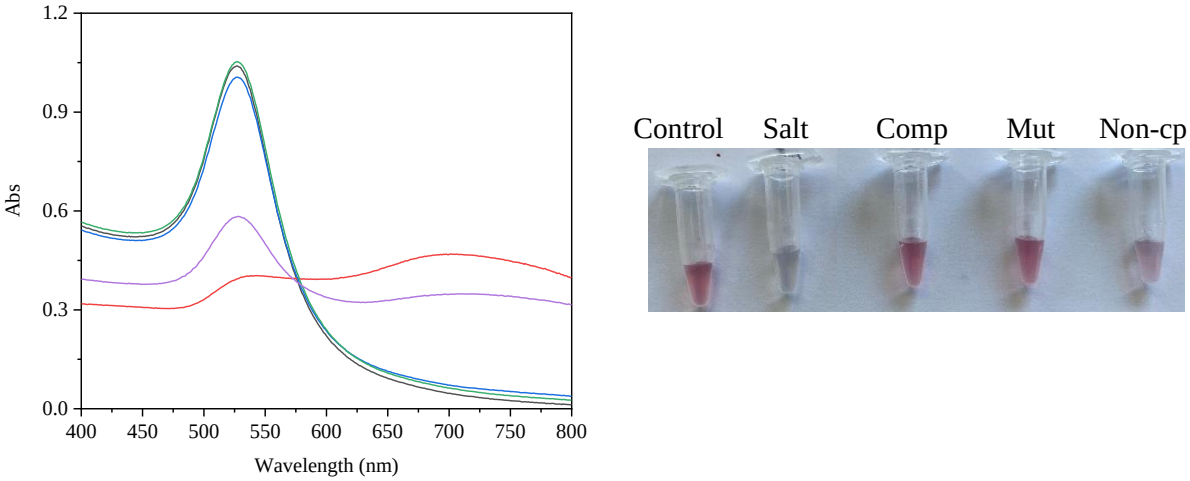

Figure 4.19 – Colorimetric assays of the 40 nm Au-nanoprobes obtained through the revised pH method with a ratio of 1300 5' SH-OL per NP, using 40 b.p. anti-parallel ssDNA. These spectra were obtained using 350 mM NaCl. Black – Control sample; Red – Salt sample; Dark blue – Complementary ssDNA sample; Green – Mutated ssDNA sample; Purple – Non-complementary ssDNA sample; All spectra were obtained using a final Au-nanoprobe concentration of 0.15 nM, a ssDNA concentration of 18 ng/µL and 100 µL sample volume.

The results presented in Figure 4.19 allowed the assessment that the anti-parallel ssDNA targets saw enhanced hybridization, which led to higher Au-nanoprobe stabilization. This is evidenced by the fact that both the complementary and mutated ssDNA samples do not show any signs of aggregation. In the previous assays, even though the complementary and mutated ssDNA targets generally presented some sort of Au-nanoprobe stabilization, the effect provided was very small, and often the difference between these samples was also small. Even the difference between these samples and the non-complementary ssDNA sample was not very significant. Using the anti-parallel 40 b.p. ssDNA targets, the difference between the complementary/mutated and the non-complementary ssDNA samples increased. This is indicative that the SH-OL – ssDNA complex formed using anti-parallel ssDNA is more stable.

Szabat et al. stated that the stabilization provided by parallel DNA hybridization is lower than their anti-parallel counterpart [92]. Parallel hybridization also depends on the sequence of the DNA and requires specific conditions, such as low pH and temperatures. Since distinct conditions were used in our assays, this could have affected the hybridization and, consequently, decreased the stabilization effect of the parallel ssDNA targets.

Although the complementary and mutated anti-parallel ssDNA samples do not show any difference in terms of Au-nanoprobe aggregation, this may be attributed to the fact that neither sample showed any signs of aggregation, requiring higher salt concentrations to induce it. As such, new colorimetric assays were performed with increased NaCl concentration.

The increased protection seen using anti-parallel ssDNA targets was so intense that no aggregation was attained even for NaCl concentrations upwards of 2.5 M. As such, new assays were developed using $MgCl_2$, a divalent salt, to increase the ionic strength [93]. Several new colorimetric assays were performed with varying $MgCl_2$ concentrations, and the optimal salt concentrations for each nanoparticle size were determined (30 mM for 15 nm AuNPs and 50 mM for 40 nm). An example of the developed colorimetric assays is presented in Figure 4.20.

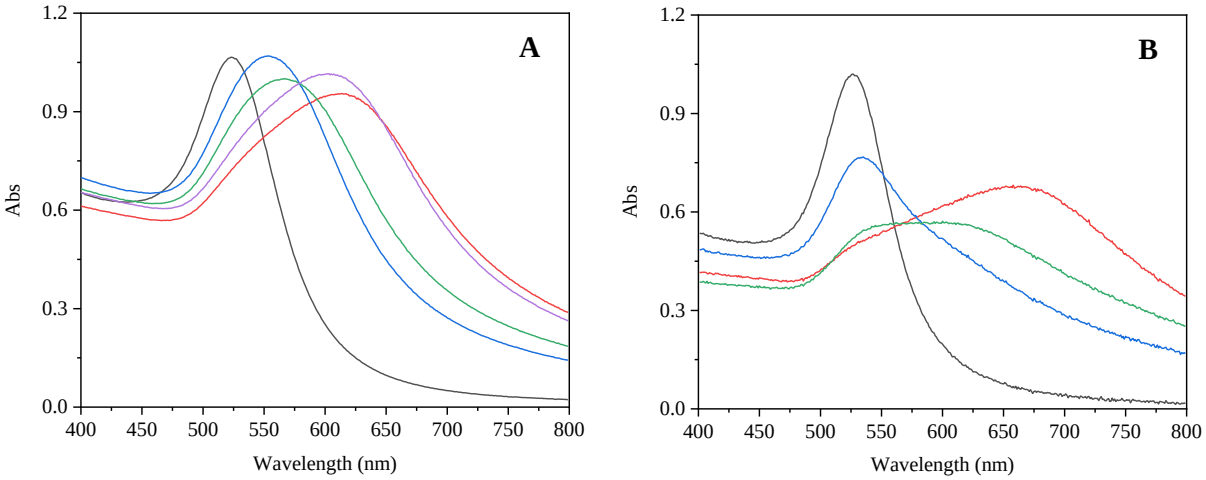

Figure 4.20 – Colorimetric assays of both sizes of Au-nanoprobes using 40 b.p. anti-parallel ssDNA. Graph A – Spectra of the 15 nm Au-nanoprobes, obtained through the SA method with a ratio of 150 5' SH-OL per NP and using 40 mM $MgCl_2$. Graph B – Spectra of the 40 nm Au-nanoprobes, obtained through the revised pH method with a ratio of 1300 5' SH-OL per NP and using 50 mM $MgCl_2$. Black – Control sample; Red – Salt sample; Dark blue – Complementary ssDNA sample; Green – Mutated ssDNA sample; Purple – Non-complementary ssDNA sample; All spectra were obtained using a final Au-nanoprobe concentration of 2.5 nM (15 nm) or 0.15 nM (40 nm), a ssDNA concentration of 18 ng/µL and 100 µL sample volume.

The results presented in Figure 4.20, obtained using a ssDNA target concentration of 18 ng/µL, reveal a good distinction between the complementary and mutated ssDNA samples. Another key aspect lies in the fact that no significant Au-nanoprobe stabilization was obtained using the non-complementary ssDNA, as evidenced by graph A. As such, it is possible to conclude that 40 b.p. anti-parallel ssDNA targets induced the best colorimetric response of the tested ssDNA targets.

It is important to note that the level of induced aggregation affected the colorimetric distinction obtained at distinct ssDNA concentrations. For instance, when smaller $MgCl_2$ concentrations were used, a greater colorimetric distinction between the complementary and mutated ssDNA samples occurred for smaller ssDNA concentrations. When the $MgCl_2$ concentration was increased, these smaller ssDNA concentrations resulted in small differences between samples due to intense aggregation. On the other hand, for larger ssDNA concentrations, the aggregation effect was almost non-existent when small $MgCl_2$ concentrations were applied, resulting in a small colorimetric distinction. If high $MgCl_2$ concentrations were applied, the aggregation effect increased, leading to greater colorimetric distinction.

4.4.2. Intercalating agent

Intercalating agents are molecules that can be added to the Au-nanoprobes to block the unoccupied spaces at their surface. The effect of 6-mercapto-1-hexanol, an intercalating agent, on the stability of the Au-nanoprobes and its colorimetric response was evaluated using 40 nm Au-nanoprobes obtained with 5' SH-OL. The stability assays obtained are presented in Figure 4.21.

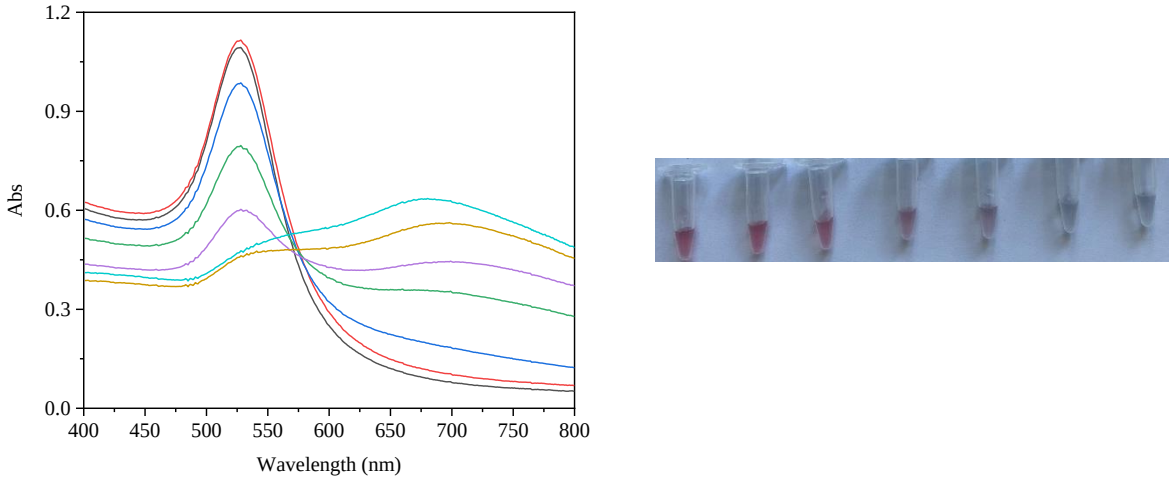

Figure 4.21 - Stability assays of the 40 nm Au-nanoprobes obtained through the revised pH method using a ratio of 1300 5' SH-OL per NP and 100 molecules of 6-mercapto-1-hexanol per NP. Black – 0 mM NaCl; Red – 200 mM NaCl; Dark blue – 250 mM NaCl; Green – 300 mM NaCl; Purple – 350 mM NaCl; Gold – 300 mM NaCl; Light Blue – 450 mM NaCl. The colorimetric response is ordered from smallest to highest NaCl concentration. All spectra were obtained using a final nanoprobe concentration of 0.15 nM and 100 µL sample volume.

The stability assays presented in Figure 4.21 reveal that the effect of the intercalating agent on the stability of the Au-nanoprobes is extremely small. Over several replicates, either the stability was unaffected or an increase between 25 and 50 mM of the NaCl concentration required to induce Au-nanoprobe aggregation was seen.

The increase in the Au-nanoprobe stability was lower than the ones reported in the literature for other intercalating agents. Stakenborg et al. obtained an Au-nanoprobe stability increase from 200 mM to 500 mM when 10 - 100 µM tri(ethylene glycol) was used as a backfilling molecule on Au-nanoprobes [87]. The addition of mercapto-hexanol was also evaluated by the authors but lower concentrations were used (1 µM), which did not have a significant effect on Au-nanoprobe stability. The mercapto-hexanol ratio applied in this work (100 molecules per NP) corresponds to an effective final concentration around 0.1 µM. When compared to the results obtained by Stakenborg et al., the unaffected stability of the Au-nanoprobes visualized here could be explained either by the small concentration/ratio of mercapto-hexanol used or by the use of mercapto-hexanol, since other agents seem to have a more prominent effect.

To evaluate if the introduction of mercapto-hexanol had an effect on the colorimetric response of the Au-nanoprobes upon addition of ssDNA targets, colorimetric assays were conducted. The results obtained are presented in Figure 4.22.

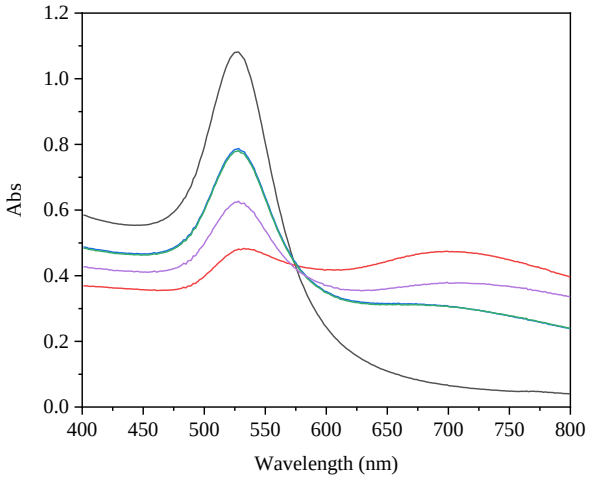

Figure 4.22 – Colorimetric assays of the 40 nm Au-nanoprobes obtained through the revised pH method with a ratio of 1300 5' SH-OL per NP and 100 molecules of 6-mercapto-1-hexanol per NP, using 40 b.p. parallel DNA and an NaCl concentration of 350 mM. Black – Control sample; Red – Salt sample; Dark blue – Complementary ssDNA sample; Green – Mutated ssDNA sample; Purple – Non-complementary ssDNA sample; All spectra were obtained using a final Au-nanoprobe concentration of 0.15 nM, a ssDNA concentration of 18 ng/µL and 100 µL sample volume.

The colorimetric assays obtained using mercapto-hexanol and 40 b.p. parallel ssDNA targets, presented in Figure 4.22, show that the introduction of the intercalating agent did not significantly impact the colorimetric response of the tested samples. The unaffected colorimetric response may be an indication that DNA hybridization was not hindered through the introduction of the intercalating agent. Nevertheless, the main benefices of using the intercalating agent were the expected increased Au-nanoprobe stability, which could be extremely helpful in guaranteeing a functioning assay for longer periods of time. Since this effect was not seen, the utilization of mercapto-hexanol during the functionalization step was not applied in the forthcoming assays.

4.5. Cross-linking

4.5.1. 15 nm gold nanoparticles

CL was one the methodologies utilized to discern the SNP related to LI. To verify if the developed 15 nm Au-nanoprobes were able to achieve a measurable difference between the complementary and mutated ssDNA targets, CL assays were performed. The results obtained are presented in Figure 4.23.

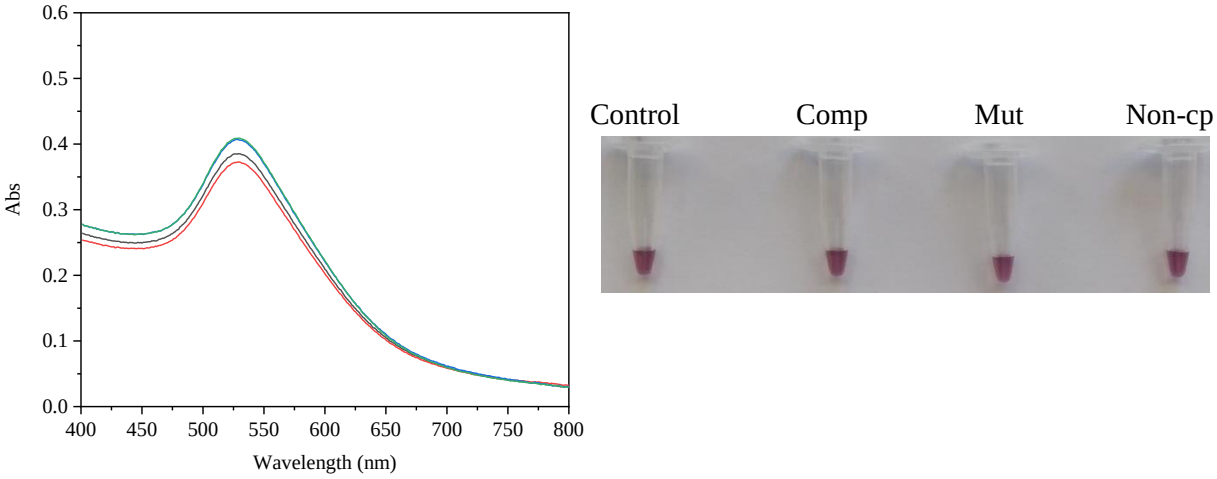

Figure 4.23 – CL assay and colorimetric response of the 15 nm Au-nanoprobes obtained through the SA method using a ratio of 150 for 5' SH-OL and a ratio of 200 for 3' SH-OL. These assays were conducted using 40 b.p. anti-parallel ssDNA. Black – Control sample; Red – Complementary ssDNA sample; Blue – Mutated ssDNA sample; Green – Non-complementary ssDNA sample; All spectra were obtained using 1:3 dilution with PB pH 8, a ssDNA concentration of 60 pmol and 100 µL sample volume.

The CL assays, presented in Figure 4.23, reveal that no aggregation was induced with the introduction of any type of ssDNA. This could indicate that neither the complementary nor the mutated ssDNA targets were capable of acting as a linker between the two Au-nanoprobes. If significant linking had occurred, a NP network would form, resulting in a very small interparticle distance, which would be discerned as aggregation. Since no new LSPR peaks or colour change were seen, it is possible to conclude that these agglomerates did not form. A possible explanation for this occurrence may be tied to incorrect DNA hybridization with one of the Au-nanoprobes in the solution. Since the Au-nanoprobes obtained using the 5' SH-OL had already been proven to be capable of inducing correct DNA hybridization, the cause was expected to lie in the Au-nanoprobes obtained using the 3' SH-OL. To test this possibility, a colorimetric assay was performed using only the latter Au-nanoprobes. The results obtained are presented in Figure 4.24.

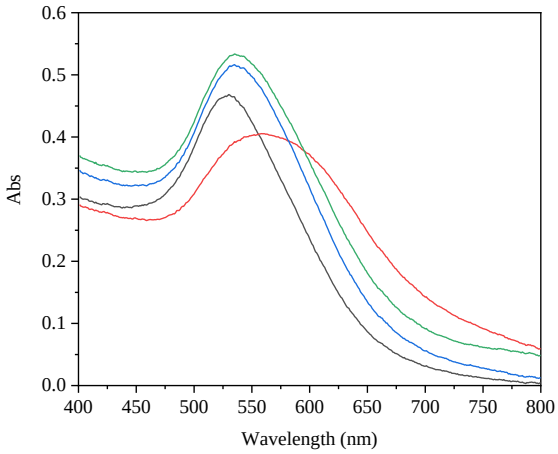

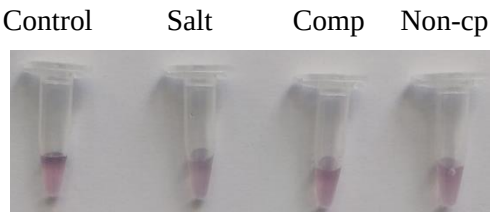

Figure 4.24 – Colorimetric assays and response of the 15 nm Au-nanoprobes obtained through the SA method with a ratio of 200 3' SH-OL per NP using 40 b.p. anti-parallel ssDNA. Black – Control sample; Red – Salt sample; Dark blue – Complementary ssDNA sample; Green – Non-complementary ssDNA sample. All spectra were obtained using a final Au-nanoprobe concentration of 2.5 nM, a ssDNA concentration of 18 ng/µL, NaCl concentration of 800 mM and 100 µL sample volume.

The colorimetric assays presented in Figure 4.24 show severe problems with DNA hybridization. These problems are highlighted in the intense aggregation protection provided by the non-complementary ssDNA. Since the non-complementary ssDNA does not possess any complementarity with the 3' SH-OL, no Au-nanoprobe stabilization should occur. Despite this, the data obtained shows the opposite effect. These results could be tied to non-specific interactions with the Au-nanoprobes as previously explored. Despite this, these assays were conducted at 800 mM of NaCl, which resulted in intense aggregation for the non-complementary ssDNA using 5' SH-OL Au-nanoprobes. The level of stabilization seen here is indication of non-specific hybridization.

4.5.2. 40 nm gold nanoparticles

CL assays were also performed using the 40 nm Au-nanoprobes. The results obtained are presented in Figure 4.25.

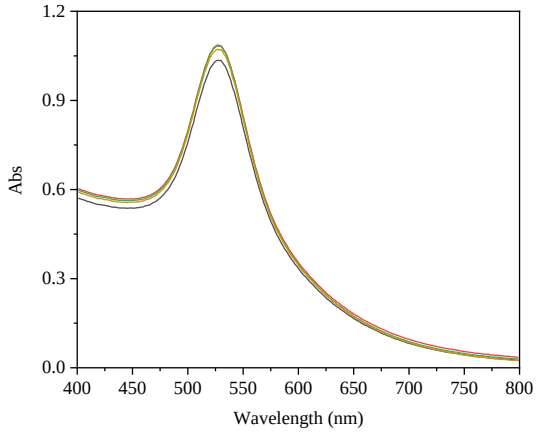

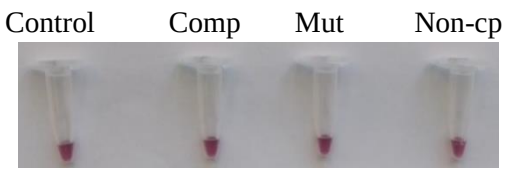

Figure 4.25 – CL assay and colorimetric response of the 40 nm Au-nanoprobes obtained through the revised pH method using a ratio of 1300 for 5' SH-OL and a ratio of 1500 for 3' SH-OL. These assays were conducted using 40 b.p. anti-parallel ssDNA. Black – Control sample; Red – Complementary ssDNA sample; Blue – Mutated ssDNA sample; Green – Non-complementary ssDNA sample; All spectra were obtained using 1:3 dilution with PB pH 8, a ssDNA concentration of 60 pmol and 100 µL sample volume.

The results presented in Figure 4.25 reveal that, for 40 nm Au-nanoprobes, no aggregation was seen for any of the added ssDNA targets. These results are identical to the ones obtained using the 15 nm Au-nanoprobes and are an indication of suboptimal hybridization. As such, the 3' SH-OL Au-nanoprobes were once again evaluated using a colorimetric assay. The results obtained can be seen in Figure 4.26.

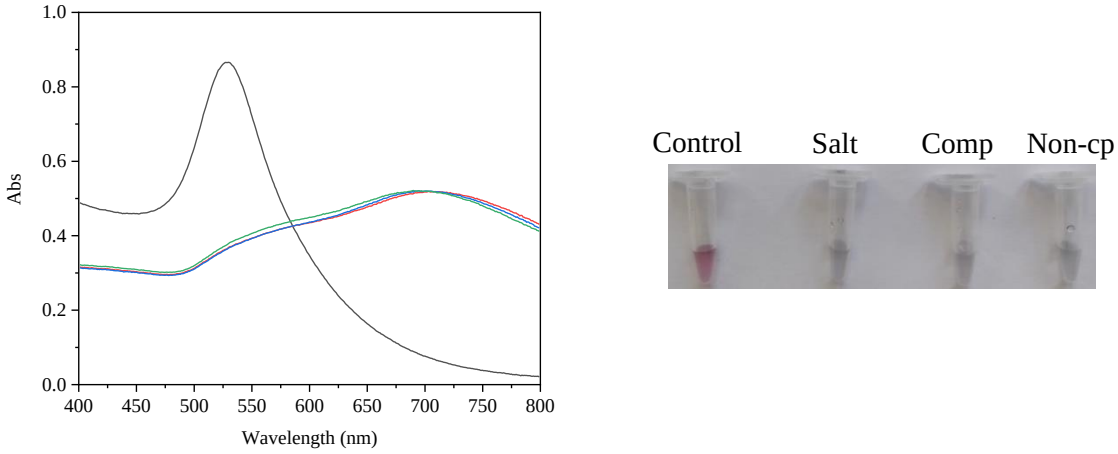

Figure 4.26 – Colorimetric assays and response of the 40 nm Au-nanoprobes obtained through the revised pH method with a ratio of 1500 3' SH-OL per NP using 40 b.p. anti-parallel ssDNA. Black – Control sample; Red – Salt sample; Dark blue – Complementary ssDNA sample; Green – Non-complementary ssDNA sample. All spectra were obtained using a final Au-nanoprobe concentration of 0.15 nM, a ssDNA concentration of 18 ng/µL, a NaCl concentration of 350 mM and 100 µL sample volume.

The colorimetric assays performed reveal that none of the tested ssDNA targets stabilize the 40 nm 3' SH-OL Au-nanoprobes. Although this was expected for the non-complementary ssDNA, the non-existent stabilization effect seen for the complementary ssDNA is indicative of severe hybridization hinderance. These results were opposite of the ones verified for 15 nm 3' SH-OL Au-nanoprobes, where both ssDNA targets provided a strong stabilization effect. This extreme variable behaviour and the lacking specificity towards ssDNA allow the conclusion that these Au-nanoprobes are not functional for ssDNA detection and a redesign should be considered.

4.6. Non-cross-linking

4.6.1. Anti-parallel DNA with 40 base pairs

4.6.1.1. 15 nm gold nanoparticles

The NCL assay was developed using only the 5' SH-OL Au-nanoprobes, which were previously proven to be effective for evaluating the differences between the complementary and mutated 40 b.p. anti-parallel ssDNA targets. As seen in Figure 4.27, the study was continued with a ssDNA target concentration curve that allowed the calculation of aggregation ratios through the ratio and subtraction method and assess the percentual differences between both samples.

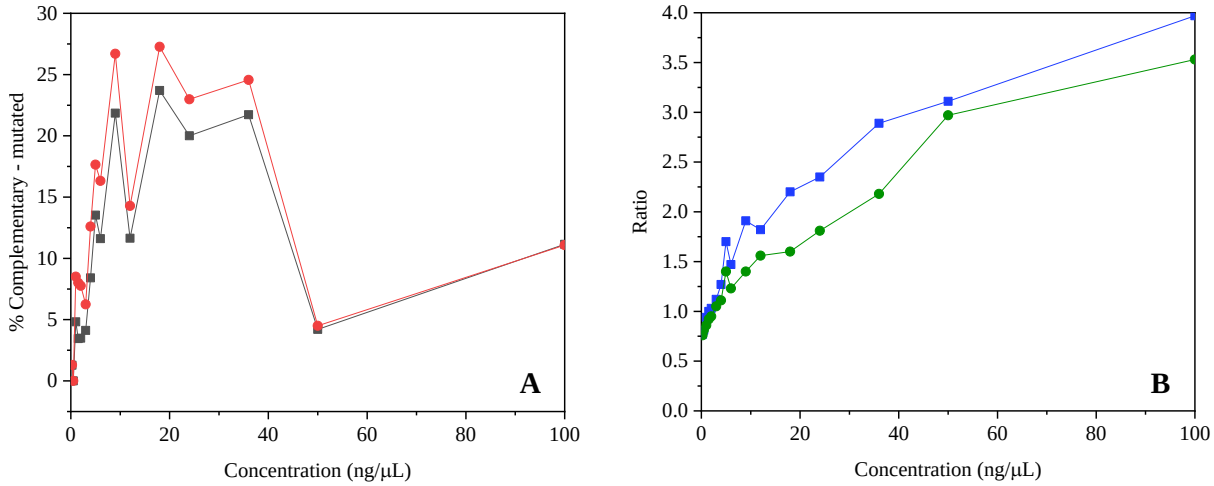

Figure 4.27 – Percentual difference calculated between the aggregation ratios of the complementary and mutated ssDNA samples (graph A) and aggregation ratios calculated for these samples using the subtraction method (graph B) for several ssDNA concentrations. These assays were performed using the 15 nm Au-nanoprobes obtained through the SA method using a ratio of 150 5' SH-OL per NP and the 40 b.p. anti-parallel ssDNA. Graph A: black – Percentual difference obtained using the ratio method; Red – Percentual difference obtained using the subtraction method. Graph B: blue – Complementary ssDNA samples aggregation ratios; Green – Mutated ssDNA samples aggregation ratios. All calculations were obtained using spectra with a final nanoprobe concentration of 2.5 nM and a 100 µL sample volume.

The concentration curves presented in Figure 4.27 are indicative that the ssDNA target concentration utilized in the colorimetric assays severely impacts the hybridization between Au-nanoprobes and ssDNA. This effect was seen for the aggregation ratios of the complementary and mutated ssDNA targets, as well as the differences between the two. As shown by graph A, when the ssDNA concentration is raised, the difference between the complementary and mutated ssDNA samples tends to widen. The mentioned effect seems to reach a plateau at 12 ng/µL that persists until 36 ng/µL, after which the difference seen decreases.

The concentrations curves of the aggregation ratios (graph B) may provide further insight over this phenomenon. The obtained data illustrates smaller increments of stability as the ssDNA concentration is increased. On top of this, when high ssDNA concentrations are applied, almost no aggregation of the Au-nanoprobes is seen, evidenced by their high aggregation ratios. These effects may result in smaller differences between the complementary and mutated ssDNA samples, since the maximum stability threshold is close to being reached for the salt concentration used.

Fine analysis of the difference between the aggregation ratios calculated for the complementary and mutated ssDNA targets reveals that a difference of 10 % is seen at 4 ng/µL, while a considerable difference of 20 % is reached at 9 ng/µL. Despite this considerable difference between the aggregation ratios of these samples, the colour of the colloid was not enough to discern them, independently of the concentration tested.

As seen in graph A of Figure 4.27, it is possible to conclude that the differences between the complementary and mutated ssDNA targets were enhanced using the subtraction method, therefore making it preferable over the ratio method. Generally, the subtraction method increased the percentual difference between the complementary and mutated ssDNA targets by about 3-5 %, independently of the ssDNA concentration used. Since the maximum percentual difference between samples verified is 25 %, a 3-5 % gain using the subtraction method results in a 1.12 to 1.2-fold increase in the distinction between samples, which is significant.

Compared to other studies in the literature, the difference between the complementary and mutated ssDNA targets found in our work seems to be on par. Carlos et al. studied the detection of an SNP in the Fat mass and obesity associated-gene using 14 nm AuNPs functionalized with 5' SH-OL [87]. In the mentioned work, colorimetric distinction between PCR products of the wild-type and mutated samples was evaluated through a NCL method using the ratio method. Carlos et al. demonstrated an increasing difference between samples from 5 ng/µL up until 30 ng/µL. The maximum percentual difference recorded between the aggregation ratios of the wild-type and mutated PCR products was around 21 %, using a concentration of 30 ng/µL. For the results obtained here, an identical percentual difference was seen between 12 and 36 ng/µL.

To verify the effect of the incubation time of the assay on the colorimetric response, a variation of this time between 3 and 15 minutes was evaluated. The resulting percentual differences for each incubation time tested are represented in Figure 4.28.

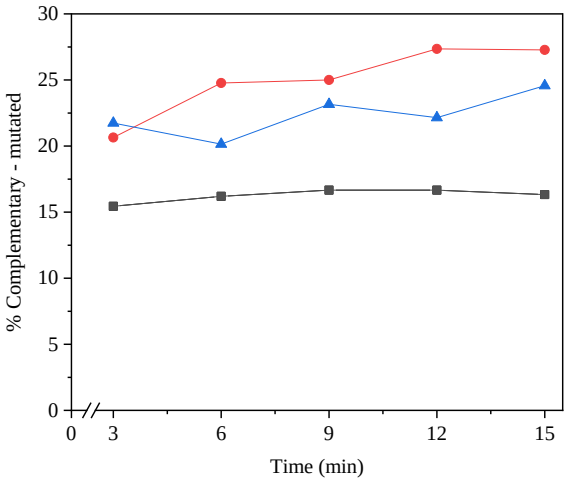

Figure 4.28 – Percentual difference calculated between the aggregation ratios of the complementary and mutated ssDNA samples at different incubation times for several ssDNA concentrations. These assays were performed using the 15 nm Au-nanoprobes obtained through the SA method with a ratio of 150 5' SH-OL per NP and the 40 b.p. anti-parallel ssDNA. Black – 6 ng/µL; Red – 18 ng/µL; Blue - 36 ng/µL. All calculations were obtained using spectra with a final Au-nanoprobe concentration of 2.5 nM and a 100 µL sample volume.

The time-dependent assays presented in Figure 4.28 reveal that, for the tested conditions, the percentual difference between the aggregation ratios of the complementary and mutated ssDNA samples does not tend to be affected by the incubation time applied. This is a result of stable aggregation ratios, which can be an indication of one of two possibilities: either the aggregation of the 15 nm Au-nanoprobes is not time-dependent or the aggregation is time-dependent but occurs at a very slow pace, after initial aggregation upon introduction of salt. The latter is supported by increased visual colorimetric distinction that was recorded several hours after performing the colorimetric assays.

This effect was visualized for all the concentrations tested, assuring that this independency from time is also unaffected by the ssDNA concentration used. Since this effect was observable even for the smaller ssDNA concentration tested (0.25 ng/µL), it is possible to postulate that this effect is inherent to these smaller Au-nanoprobes, not requiring ssDNA supplementation and hybridization to occur. This characteristic is interesting and desirable from a point-of-care perspective, since the time incubation time of the assay could be tailored to the end consumer's needs.

To evaluated if the differences seen were statistically significant, several replicates were performed at specific ssDNA concentrations (6, 18 and 36 ng/µL). The aggregation ratios, percentual difference and the results of the t-Test can be seen in Table 4.6. The spectra and colorimetric response for a replicate of each ssDNA concentration is also presented in Figure 4.29.

Table 4.6 – Statistical significance of several replicates obtained for 6, 18 and 36 ng/µL of 40 b.p. anti-parallel ssDNA targets, using a t-Test at a 0.05 level, for the 15 nm Au-nanoprobes. Ratios were calculated according to the subtraction method.

DNA concentration (ng/µL)	Ratio Comp	Ratio Mut	Difference (%)	t-Test at 0.05 level	
				Equal variance assumed	Equal variance not assumed
6	1.47	1.22	17.0	0.0674	0.1192
	1.27	1.22	3.9		
	1.42	1.26	11.3		
18	1.72	1.50	12.8	0.6812	0.7005
	1.79	1.78	0.6		
	1.71	2.22	-29.8		
36	4.45	2.24	49.7	0.1626	0.2186
	2.38	1.89	20.6		
	2.54	1.75	31.1		

Statistical analysis of selected concentrations (6, 18 and 36 ng/µL) revealed that the differences between the complementary and mutated ssDNA samples are not statistically significant, as observed in Table 4.6. The high variability among assays could be responsible for this. The observed variability is undesirable and may be indicative that the aggregation of the Au-nanoprobes is not reproducible. Despite this, statistically significant detection of SNPs using Au-nanoprobes has already been described in the literature [87]. As such, further optimization of both the functionalization process and the colorimetric assays could lead to a more reproducible test.

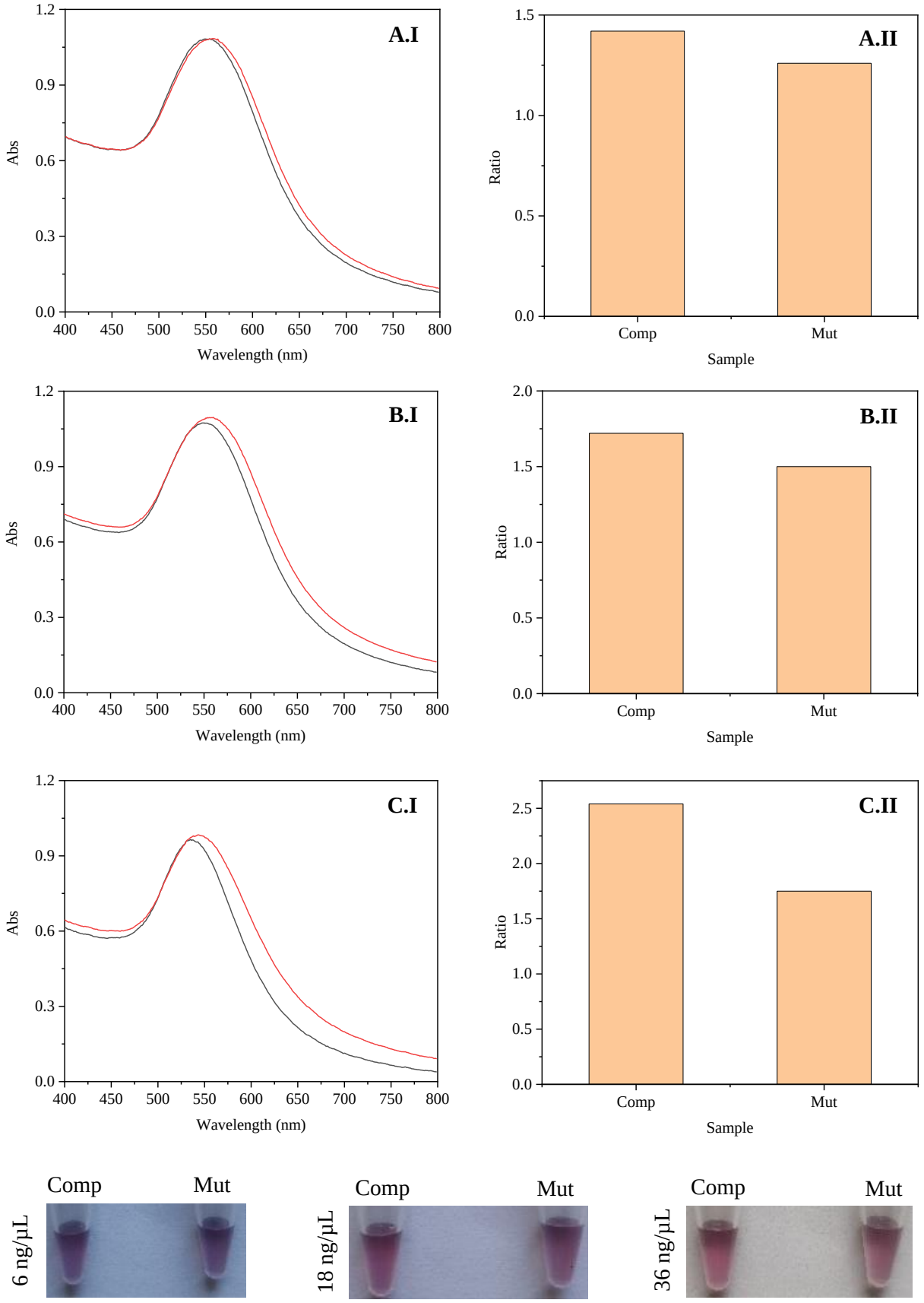

Figure 4.29 – Colorimetric assays and response of the 15 nm Au-nanoprobes obtained through the SA method with a ratio of 150 5' SH-OL per NP using several concentrations of 40 b.p.anti-parallel ssDNA. Graph A – 6 ng/µL; Graph B – 18 ng/µL; Graph C – 36 ng/µL. Graphs .I – UV-Vis spectra of the obtained samples. Black – Complementary ssDNA sample; Red – Mutated ssDNA sample. All spectra were obtained using a final Au-nanoprobe concentration of 2.5 nM and a 100 µL sample volume. Graphs .II – Aggregation ratios calculated using the subtraction method for each sample.

The incubation temperature of the colorimetric assay is important for hybridization between the ssDNA and the 5' SH-OL at the surface of the Au-nanoprobes. A variation of this temperature, between 75 and 95 ºC was studied, to verify its effect on the colorimetric response. The results obtained are presented in Figure 4.30.

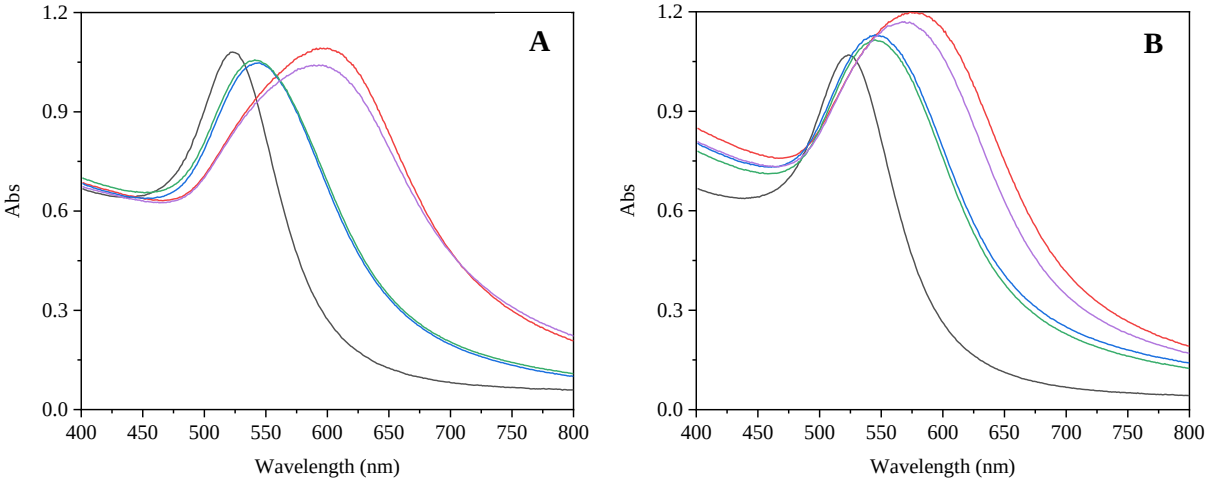

Figure 4.30 – Colorimetric assays of the 15 nm Au-nanoprobes obtained through the SA method with a ratio of 150 5' SH-OL per NP using 40 b.p. anti-parallel ssDNA at different incubation temperatures. Graph A – 75 ºC; Graph B – 95 ºC. Black – Control sample; Red – Salt sample; Blue – Complementary ssDNA sample; Green – Mutated ssDNA sample; Purple – Non-complementary ssDNA sample. All spectra were obtained using a final Au-nanoprobe concentration of 2.5 nM, a ssDNA concentration of 18 ng/µL and a 100 µL sample volume.

Temperature testing results show that, for the tested conditions, the increase of the incubation temperature from 75 ºC up to 95 ºC did not affect the stabilization of the Au-nanoprobes, when incubated with 40 b.p. anti-parallel ssDNA. Since the melting temperature of the ssDNA – 5' SH-OL complex formed after hybridization is around 75 ºC, it was expected that an increase in the incubation temperature would have a negative impact on hybridization and, consequently, lead to a loss of protection against aggregation. In the tested conditions, this effect was not visualized for the complementary and mutated ssDNA samples, and is indicative that hybridization is not jeopardized, even when these higher temperatures are applied. Despite this, slight differences in the aggregation profile of the samples without ssDNA or incubated with non-complementary ssDNA were seen, evidenced by the blue shift of the LSPR peak. This may be an indication that the Au-nanoprobes show a temperature-dependent stabilization effect that is not present when hybridization occurs, arguably due to the higher stability of these samples.

Nevertheless, the ability to utilize higher incubation temperatures is extremely desirable for the application of real patient samples. Since these samples would come in a double stranded DNA conformation, a denaturation of the sequence would have to be employed to allow hybridization with the 5' SH-OL at the surface of the Au-nanoprobes. This denaturation step is usually a heating step at 95 ºC [94]. As such, the temperature-independent behaviour seen for the Au-nanoprobes is desirable for this application.

4.6.1.2. 40 nm gold nanoparticles

NCL assays were performed using the 40 nm 5' SH-OL Au-nanoprobes to assess the impact of NP size on the colorimetric system. The initial concentration curves, where the aggregation ratios and percentual difference are represented, can be seen in Figure 4.31.

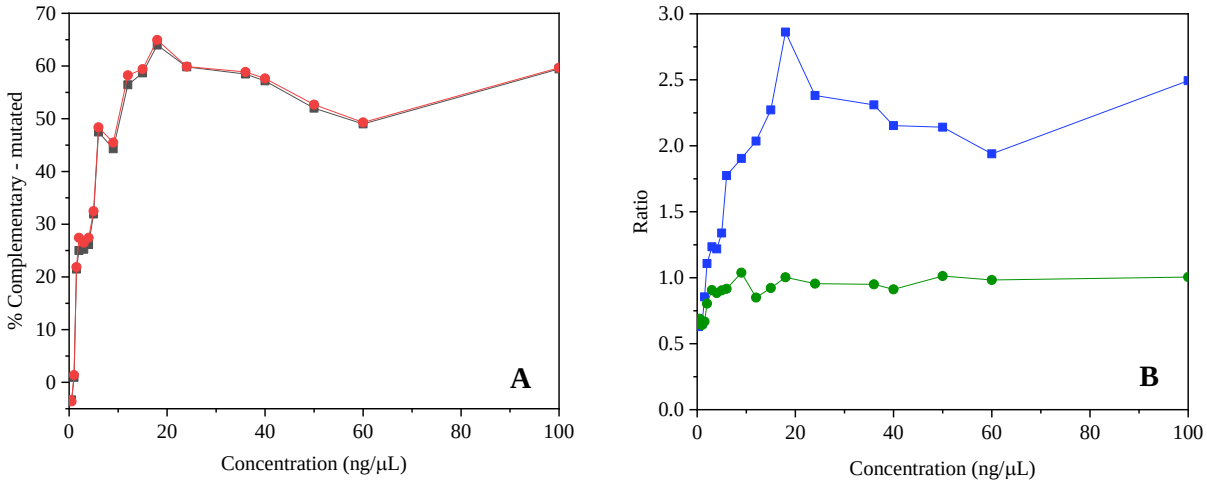

Figure 4.31 – Percentual difference calculated between the aggregation ratios of the complementary and mutated ssDNA samples (graph A) and aggregation ratios calculated for these samples using the subtraction method (graph B) for several ssDNA concentrations. These assays were performed using the 40 nm Au-nanoprobes obtained through the revised pH method with a ratio of 1300 5' SH-OL per NP and 40 b.p. anti-parallel ssDNA. Graph A: black – Percentual difference obtained using the ratio method; Red – Percentual difference obtained using the subtraction method. Graph B: blue – Complementary ssDNA samples aggregation ratios; Green – Mutated ssDNA samples aggregation ratios. All calculations were obtained using spectra with a final Au-nanoprobe concentration of 0.15 nM and a 100 µL sample volume. The results presented were obtained using an incubation time of 3 minutes instead of the usual 15 minutes.

The concentration curve obtained using the 40 nm Au-nanoprobes reveals a distinct behaviour compared their 15 nm counterpart. As evidenced by graph A of Figure 4.31, the concentration of the ssDNA target also has a great impact on the percentual difference between the aggregation ratios of the complementary and mutated ssDNA samples. When the concentration is raised, the difference between the two samples tends to increase, until a plateau is reached. Contrarily to the 15 nm Au-nanoprobes, which saw a reduction of this difference for concentrations above 36 ng/µL, the same phenomenon does not occur using the 40 nm Au-nanoprobes, where a stabilization of the difference is seen for all tested concentrations. A remarkable improvement of the colorimetric response was also attained using the 40 nm Au-nanoprobes. While the 15 nm Au-nanoprobes resulted in a maximum percentual difference near 25 %, the maximum obtained for the 40 nm Au-nanoprobes nears 65 %. This massive improvement leads to the ability to discern complementary and mutated ssDNA samples by eyesight, which is extremely desirable for a point-of-care test. The aggregation ratios of each respective sample, presented in graph B, reveal that the main difference between both sizes of Au-nanoprobes lies within the stabilization effect of the mutated ssDNA target. Unlike the 15 nm Au-nanoprobes, where the stabilization effect was high with the mutated ssDNA, the contrary is seen for 40 nm Au-nanoprobes.

As seen in graph B, when using the 40 nm AuNPs, the mutated ssDNA provides almost no stabilization to the Au-nanoprobes, whereas the complementary ssDNA tends to provide comparable stabilization to what was obtained for the 15 nm Au-nanoprobes.

An analysis of the percentual differences between complementary and mutated ssDNA samples reveals that a concentration of 1.5 ng/µL is the smallest concentration where a difference between the two samples is seen, but this difference is already at the 20 % mark, which was only obtained when using 9 ng/µL with the 15 nm Au-nanoprobes. For DNA concentrations equal or higher to 12 ng/µL the percentual difference stabilized near 60 %, resulting in increased sample distinction. The samples were able to be discerned by eyesight starting at 9 ng/µL, since the complementary sample remained red, while the mutated sample turned blue.

The differences between the aggregation ratio calculation methods are extremely small. Unlike 15 nm Au-nanoprobes, which saw a 5 % increase of the percentual difference between samples when the subtraction method was applied, the same is not seen using the 40 nm Au-nanoprobes. The difference between the two methods is non-existent for most concentrations tested, as evidenced by graph A. This may be related to the broader aggregated peaks formed, which result in small differences in the absorbance obtained for two slightly deviated wavelengths that typically occurs when using both methods.

The effect of the incubation time was also evaluated for the 40 nm Au-nanoprobes. The results obtained are presented in Figure 4.32.

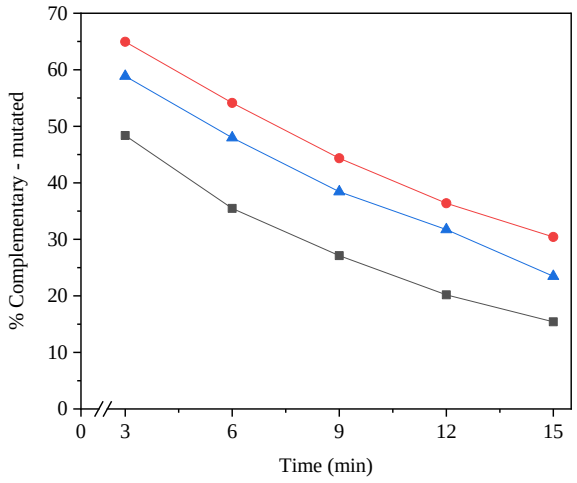

Figure 4.32 – Percentual difference calculated between the aggregation ratios of the complementary and mutated ssDNA samples at different incubation times for several ssDNA concentrations. These assays were performed using the 40 nm Au-nanoprobes obtained through the revised pH method with a ratio of 1300 5' SH-OL per NP and 40 b.p. anti-parallel ssDNAs. Black – 6 ng/µL; Red – 18 ng/µL; Blue - 36 ng/µL. All calculations were obtained using spectra with a final Au-nanoprobe concentration of 0.15 nM and a 100 µL sample volume.

The results obtained at distinct incubation times reveal a direct correlation between the increase of the incubation time and the decrease of the percentual difference. From a percentual difference of 60 %, at 3 minutes of incubation time, a decrease to 25 % is seen, if the incubation time applied is 15 min. This is accompanied by a lack of visual distinction between the complementary and mutated ssDNA samples. The continued aggregation of the Au-nanoprobes occurs for both the complementary and the mutated ssDNA targets, but since the mutated ssDNA sample already displays intense aggregation, the steep increase of the aggregation seen for the complementary ssDNA sample is more impactful. This leads to the decrease of the percentual difference between the aggregation ratios seen. Contrarily to the 15 nm Au-nanoprobes, whose aggregation ratios and percentual differences remained constant, independently of the incubation time, the 40 nm Au-nanoprobes display intense time-dependent aggregation.

A statistical analysis of the beforementioned ssDNA concentrations was also performed using the 40 nm Au-nanoprobes. The results are presented in Table 4.7. A colorimetric assay of each ssDNA concentration can also be seen in Figure 4.33.

Table 4.7 – Statistical significance of several replicates obtained for 6, 18 and 36 ng/μL of 40 b.p. anti-parallel ssDNA targets, using a t-Test at a 0.05 level, for the 40 nm Au-nanoprobes. Ratios were calculated according to the subtraction method. The results presented were obtained using an incubation time of 3 minutes instead of the usual 15 minutes.

DNA concentration (ng/μL)	Ratio Comp	Ratio Mut	Difference (%)	t-Test at 0.05 level	
				Equal variance assumed	Equal variance not assumed
6	1.18	0.98	16.9	0.0360	0.0774
	1.56	0.89	42.9		
	1.20	0.88	26.7		
18	2.21	1.09	50.9	0.0661	0.1190
	1.51	0.98	35.2		
	1.42	1.15	18.9		
36	2.74	1.01	63.1	0.0053	0.0111
	2.05	1.00	51.3		
	2.32	1.33	42.8		

Statistical analysis of several replicates obtained for 6, 18 and 36 ng/μL reveal that there is a statistically significant difference between the complementary and mutated ssDNA samples, when using a t-Test at a 0.05 level for 6 and 36 ng/μL. A greater number of replicates could also benefit the 18 ng/μL ssDNA concentration since the difference between samples was always present, even for this concentration. The obtained results may be tied to either the increased percentual difference obtained between the samples or may be related to higher reproducibility of the assays, when using the 40 nm Au-nanoprobes.

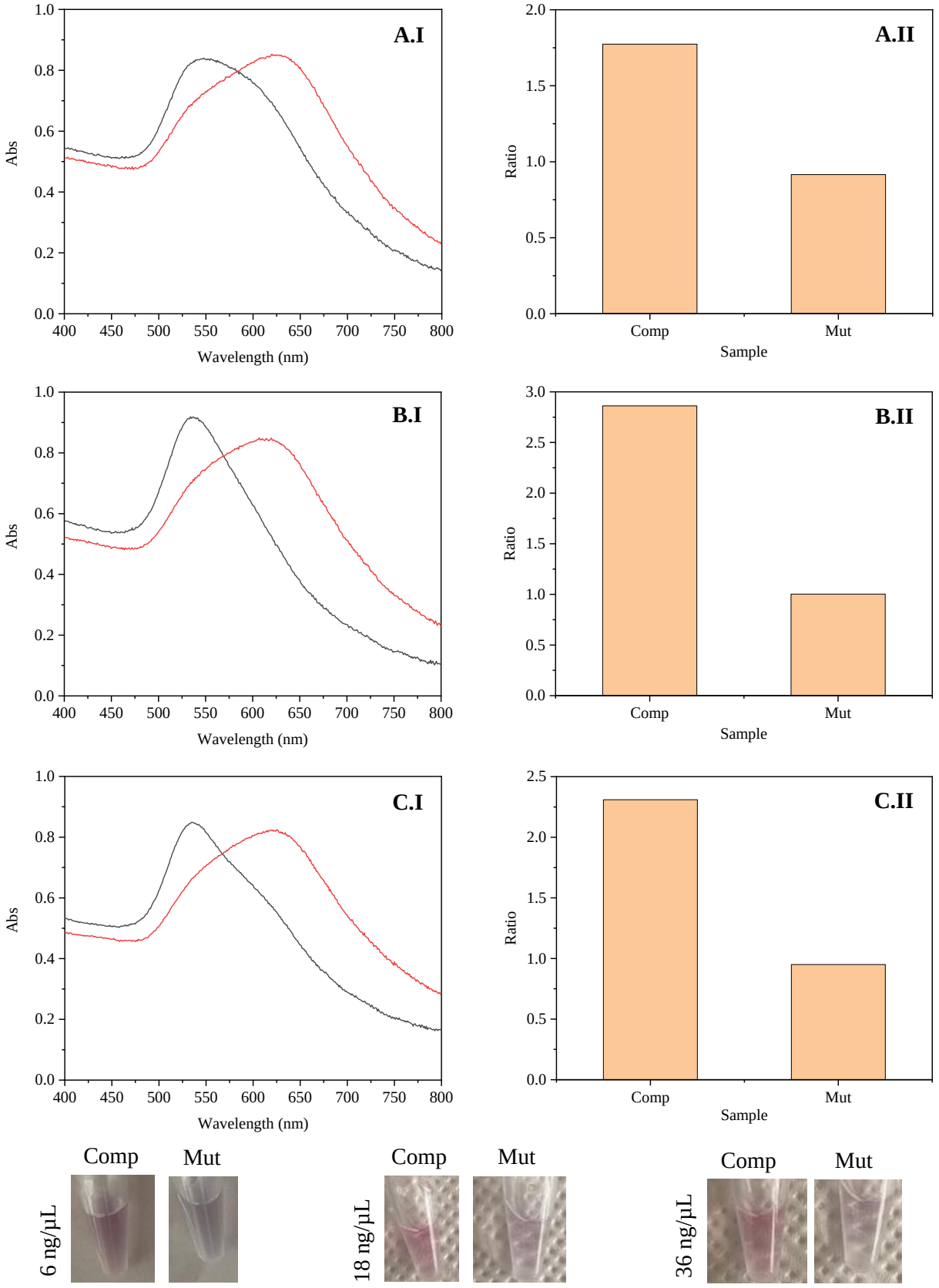

Figure 4.33 – Colorimetric assays and response of the 40 nm Au-nanoprobes obtained through the revised pH method with a ratio of 1300 5' SH-OL per NP using several concentrations of 40 b.p. anti-parallel ssDNA. Graph A – 6 ng/µL; Graph B – 18 ng/µL; Graph C – 36 ng/µL. Graphs .I – UV-Vis spectra of the obtained samples. Black – Complementary ssDNA sample; Red – Mutated ssDNA sample. All spectra were obtained using a final nanoprobe concentration of 0.15 nM and a 100 µL sample volume. Graphs .II – Aggregation ratios calculated using the subtraction method for each sample. The results presented were obtained using an incubation time of 3 minutes instead of the usual 15 minutes.

The effect of the incubation temperature on the colorimetric response of the 40 nm Au-nanoprobes was then evaluated. The colorimetric assays obtained at distinct incubation temperatures can be seen in Figure 4.34.

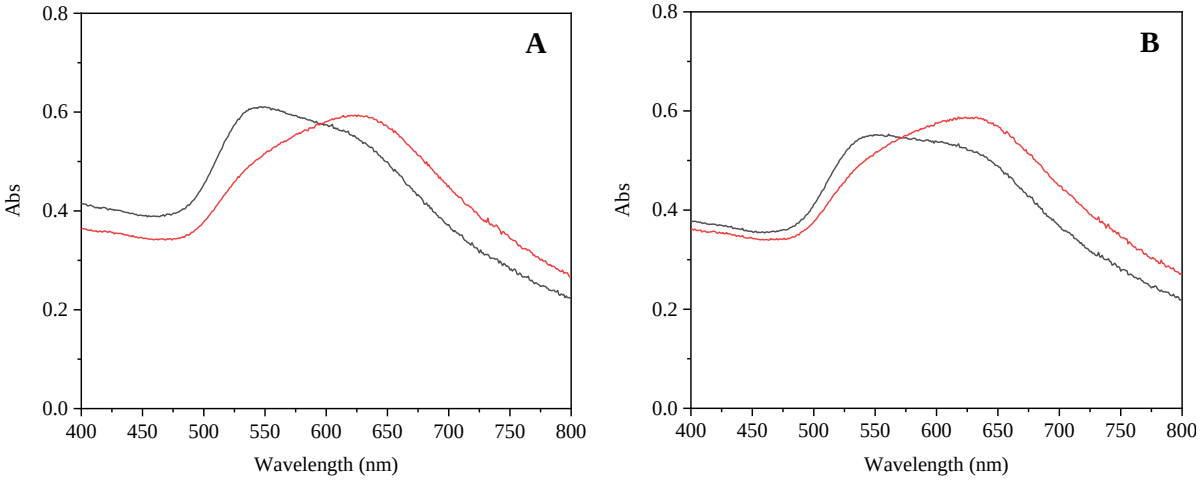

Figure 4.34 – Colorimetric assays of the 40 nm Au-nanoprobes obtained through the revised pH method with a ratio of 1300 5' SH-OL per NP using 40 b.p. anti-parallel ssDNA at different incubation temperatures. Graph A – 75 ºC; Graph B – 95 ºC. Black – Complementary ssDNA sample; Red – Mutated ssDNA sample. All spectra were obtained using a final Au-nanoprobe concentration of 0.15 nM, a ssDNA concentration of 18 ng/µL and a 100 µL sample volume. The results presented were obtained using an incubation time of 3 minutes instead of the usual 15 minutes.

The variation of the incubation temperature revealed that, for the tested conditions, this parameter does not seem to affect the colorimetric assays. As evidenced by Figure 4.34, for 75 and 95 ºC, the difference obtained between the assays is not significant. When percentual differences are evaluated, a small increase was seen from 75 to 85 ºC, but the increase was lost when transitioning to 95 ºC, whose results were similar to what was obtained at 75 ºC. As such, it is possible to postulate that the differences seen at a UV-Vis level may be attributed to small variations in the aggregations profile of the Au-nanoprobes, resulting from slight aggregation variability. These results are similar to the ones obtained using the 15 nm Au-nanoprobes and are an indication that the higher temperature, required for real patient samples, may be utilized without jeopardizing the colorimetric response seen.

4.6.2. Anti-parallel DNA with 120 base pairs

4.6.2.1. 15 nm gold nanoparticles

The effect of ssDNA length on the colorimetric response is an important parameter to evaluate since real patient samples would likely require DNA amplification. As such, the final amplified DNA would probably have hundreds of b.p. With this in mind, new 120 b.p. anti-parallel ssDNA targets were designed. The same evaluation used for the 40 b.p. anti-parallel ssDNA targets was then applied. The initial results obtained from the concentration curves can be seen in Figure 4.35.

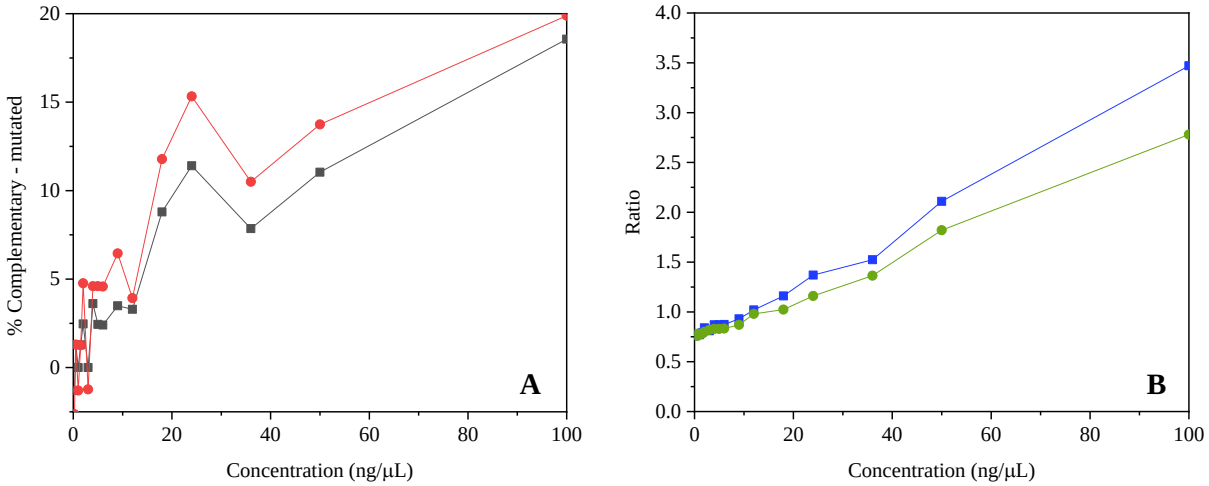

Figure 4.35 – Percentual difference calculated between the aggregation ratios of the complementary and mutated ssDNA samples (graph A) and aggregation ratios calculated for these samples using the subtraction method (graph B) for several ssDNA concentrations. These assays were performed using the 15 nm Au-nanoprobes obtained through the SA method using a ratio of 150 5' SH-OL per NP and the 120 b.p. anti-parallel ssDNA. Graph A: black – Percentual difference obtained using the ratio method; Red – Percentual difference obtained using the subtraction method. Graph B: blue – Complementary ssDNA samples aggregation ratios; Green – Mutated ssDNA samples aggregation ratios. All calculations were obtained using spectra with a final nanoprobe concentration of 2.5 nM and a 100 µL sample volume. The results presented were obtained using an incubation time of 9 minutes instead of the usual 15 minutes.

The concentration curve obtained reveal prominent differences between the colorimetric response obtained using the 120 b.p. and 40 b.p. anti-parallel ssDNA targets. This is indicative that the hybridization process is affected by the ssDNA length. As evidenced by graph A of Figure 4.35, the percentual difference between the aggregation ratios of the complementary and mutated ssDNA samples tends to widen with the increase of the ssDNA concentration. Unlike the 40 b.p. ssDNA, where for large ssDNA concentrations, this difference diminished, for 120 b.p. ssDNA this occurrence is not seen. The curve obtained illustrates a stabilization of the difference between samples when using higher ssDNA concentrations. The distinct behaviour visualized may be attributed to the number of ssDNA molecules in solution. The ssDNA concentrations utilized do not take into account the size of the ssDNA. This results in the effective number of molecules in solution being different for the tested ssDNA targets, even when the same concentration is applied. As such, since the 120 b.p. ssDNA is three times the size of the 40 b.p. ssDNA, a concentration of 100 ng/µL for the larger ssDNA may be similar to a concentration of 33 ng/µL of the smaller ssDNA.

The concentrations curves of the aggregation ratios, presented in graph B, also evidence that the Au-nanoprobe stabilization effect conferred by the 120 b.p. ssDNA targets is smaller than the stabilization effect obtained using the 40 b.p. ssDNA targets, which may also be justified by the beforementioned reason.

For these ssDNA targets, a concentration of 18 ng/µL was required to obtain a percentual difference of 10 % between the aggregation ratios of the complementary and mutated ssDNA samples. On top of this, only the highest tested concentration of 100 ng/µL was capable of inducing a difference of 20 %. These concentration values are significantly higher than the values obtained for the 40 b.p. ssDNA targets. This is undesirable since the patient samples, would utilize DNA targets larger than 120 b.p. The difference observed using the aggregation ratios does not translate to a good visual distinction between samples, which is unfavourable for the goal of producing a point-of-care test.

As stated by Sanromán-Iglesias et al., an increase in the DNA target length affects plasmon coupling, which has a negative effect on the limit of detection [95]. The capability of these larger DNAs to form stable secondary structures can also hinder detection. These effects could also explain the differences seen between the 40 and 120 b.p. ssDNA targets.

A comparison of the aggregation ratio calculation methods reveals that despite the subtraction method still resulting in a larger percentual difference between the complementary and mutated ssDNA samples, the difference between the ratio and subtraction method has diminished from 5 % for the 40 b.p. ssDNA targets to 1-3% using the 120 b.p. ones. While smaller, this difference still corresponds to a 1.05 to 1.15-fold increase.

The effect of the incubation temperature was evaluated between 3 and 9 minutes. The results obtained are presented in Figure 4.36.

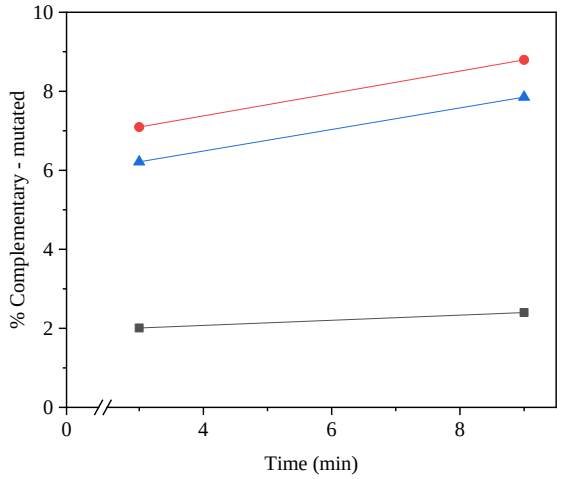

Figure 4.36 – Percentual difference calculated between the aggregation ratios of the complementary and mutated ssDNA samples at different incubation times for several ssDNA concentrations. These assays were performed using the 15 nm Au-nanoprobes obtained through the SA method with a ratio of 150 5' SH-OL per NP and the 120 b.p. anti-parallel ssDNA. Black – 6 ng/µL; Red – 18 ng/µL; Blue - 36 ng/µL. All calculations were obtained using spectra with a final Au-nanoprobe concentration of 2.5 nM and a 100 µL sample volume

The colorimetric assays obtained at the three- and nine-minute mark, presented in Figure 4.36, reveal that the aggregation ratios for the complementary and mutated samples, as well as the difference between them, remain stable independently of the incubation time applied. This effect is identical to what was observed utilizing the 40 b.p. ssDNA targets and the same justifications are valid. These results also further reinforce that the time-independent aggregation may be an inherent property of the 15 nm Au-nanoprobes since neither ssDNA concentration nor length seem to alter this behaviour.

The statistical significance of the colorimetric assays was then evaluated for the beforementioned ssDNA concentrations. The data obtained can be seen in Table 4.8. A colorimetric assay using each ssDNA concentration is presented in Figure 4.37.

Table 4.8 – Statistical significance of several replicates obtained for 6, 18 and 36 ng/µL of 120 b.p. anti-parallel ssDNA targets, using a t-Test at a 0.05 level, for the 15 nm Au-nanoprobes. Ratios were calculated according to the subtraction method. The results presented were obtained using an incubation time of 9 minutes instead of the usual 15 minutes.

DNA concentration (ng/µL)	Ratio Comp	Ratio Mut	Difference (%)	t-Test at 0.05 level	
				Equal variance assumed	Equal variance not assumed
6	0.90	0.84	6.7	0.1447	0.2065
	0.83	0.83	0		
	0.89	0.83	6.7		
18	1.12	1.00	10.7	0.0058	0.0079
	1.17	1.02	12.8		
	1.19	1.05	11.8		
36	1.51	1.30	13.9	0.0281	0.0389
	1.57	1.44	8.3		
	1.49	1.35	9.4		

The statistical analysis of the colorimetric assays performed for the 6, 18 and 36 ng/µL reveal that for the larger concentrations (18 and 36 ng/µL) the difference between the aggregation ratios of the complementary and mutated ssDNA samples is significant using a t-Test at a 0.05 level. The statistical insignificance visualized for the smaller concentration was expected, since the percentual difference between the two samples was extremely small due to intense aggregation. The results obtained for the larger concentrations reveal that, even though the difference between the two samples is smaller when using the 120 b.p. targets, the assay is more consistent with less variability. This is desirable and may be a good indication that although the difference between samples may be smaller when using the patient samples due to the larger DNA length, the assay may be more robust. Despite this, the colorimetric response obtained for any of the concentrations reveal that a clear visual distinction between the samples is not possible, requiring UV-Vis to visualize clear differences, as evidenced in Figure 4.37. On top of this, the differences visualized through UV-Vis are tame, which is not desirable.

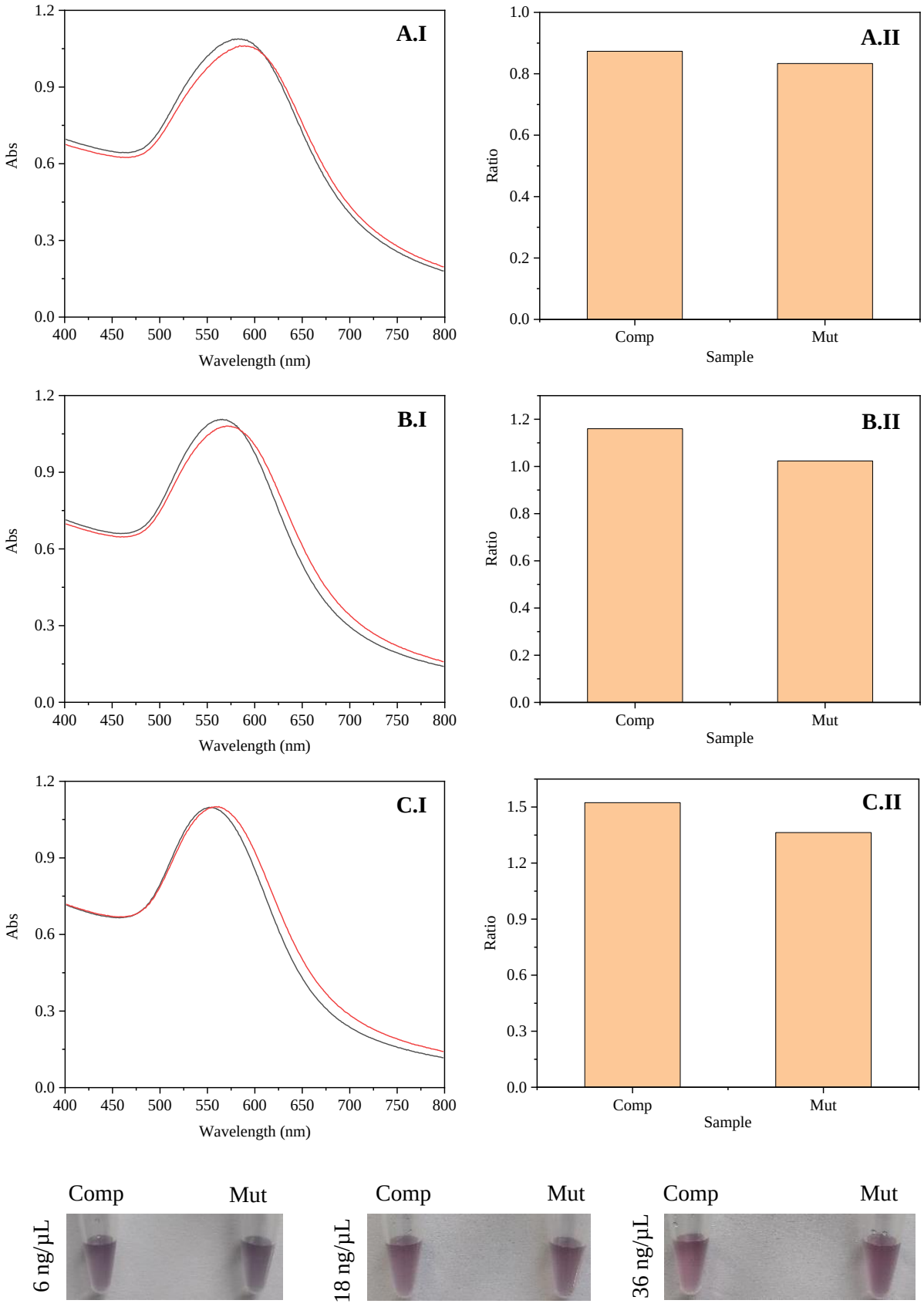

Figure 4.37 – Colorimetric assays and response of the 15 nm Au-nanoprobes obtained through the SA method with a ratio of 150 5' SH-OL per NP using several concentrations of 120 b.p. anti-parallel ssDNA. Graph A – 6 ng/µL; Graph B – 18 ng/µL; Graph C – 36 ng/µL. Graphs .I – UV-Vis spectra of the obtained samples. Black – Complementary ssDNA sample; Red – Mutated ssDNA sample. All spectra were obtained using a final Au-nanoprobe concentration of 2.5 nM and a 100 µL sample volume. Graphs .II – Aggregation ratios calculated using the subtraction method for each sample. The results presented were obtained using an incubation time of 9 minutes instead of the usual 15 minutes.

The effect of the incubation temperature was also evaluated using these 120 b.p. anti-parallel ssDNA targets. The results obtained can be seen in Figure 4.38.

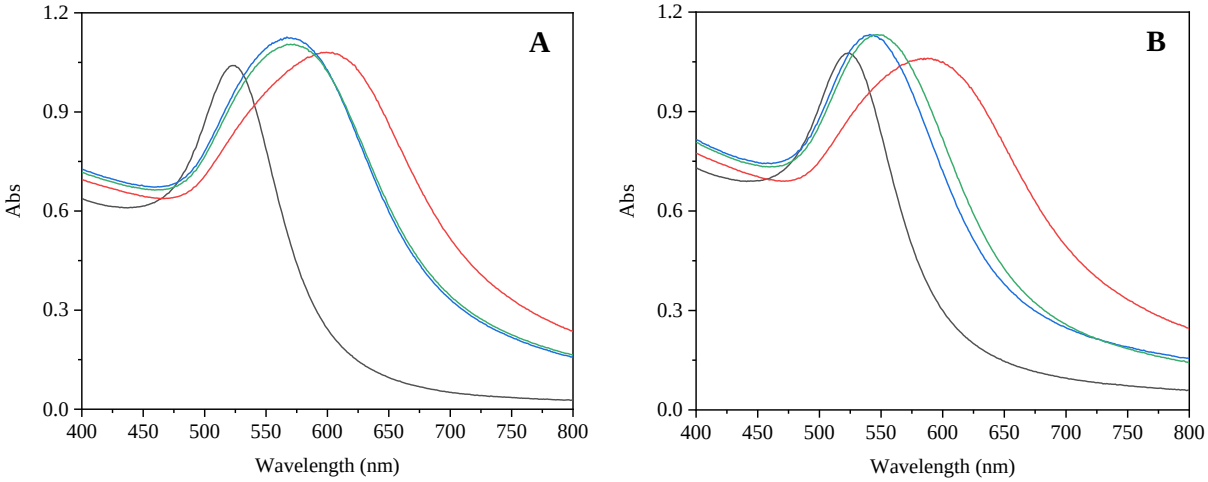

Figure 4.38 – Colorimetric assays of the 15 nm Au-nanoprobes obtained through the SA method with a ratio of 150 5' SH-OL per NP using 120 b.p. anti-parallel ssDNA at different incubation temperatures. Graph A – 75 ºC; Graph B – 95 ºC. Black – Control sample; Red – Salt sample; Blue – Complementary ssDNA sample; Green – Mutated ssDNA sample; Purple – Non-complementary ssDNA sample. All spectra were obtained using a final Au-nanoprobe concentration of 2.5 nM, a ssDNA concentration of 18 ng/µL and a 100 µL sample volume. The results presented were obtained using an incubation time of 9 minutes instead of the usual 15 minutes.

The incubation temperature variation from 75 to 95 ºC revealed that, for the 120 b.p. ssDNA targets, this parameter may be a significant factor in the colorimetric assays. As the temperature was increased, the percentual difference between the complementary and mutated ssDNA samples increased significantly, up to 2-fold. The increase was also almost linear with the increase in temperature. The results seen are correlated by the overall less aggregation of the samples, evidenced by the blue shift of the LSPR peaks. This temperature-dependent effect was not seen when 40 b.p. ssDNA targets were utilized, indicating that this property arose from the increase of the ssDNA length. As such, it is possible to postulate that the ssDNA – 5' SH-OL complex using 120 b.p. ssDNA targets is somehow affected by the incubation temperature applied. Since the difference between the two ssDNA lengths is the size of the resulting overhang after hybridization, it is plausible that the effect may be correlated to this portion of the ssDNA. A possible explanation may be that the increase in temperature causes the overhang to straighten instead of forming other stable secondary structures. This would lead to more available hybridization spots, resulting in a more intense stabilization of the Au-nanoprobes. The improved results obtained for the higher temperatures are desirable for the patient samples since, as mentioned before, the DNA obtained from patient samples has to be denatured using a temperature of 95 ºC, to allow hybridization with the SH-OL at the surface of the Au-nanoprobes.

4.6.2.2. 40 nm gold nanoparticles

The concentrations curves performed for the 40 nm Au-nanoprobes using the 120 b.p. anti-parallel ssDNA targets can be seen in Figure 4.39.

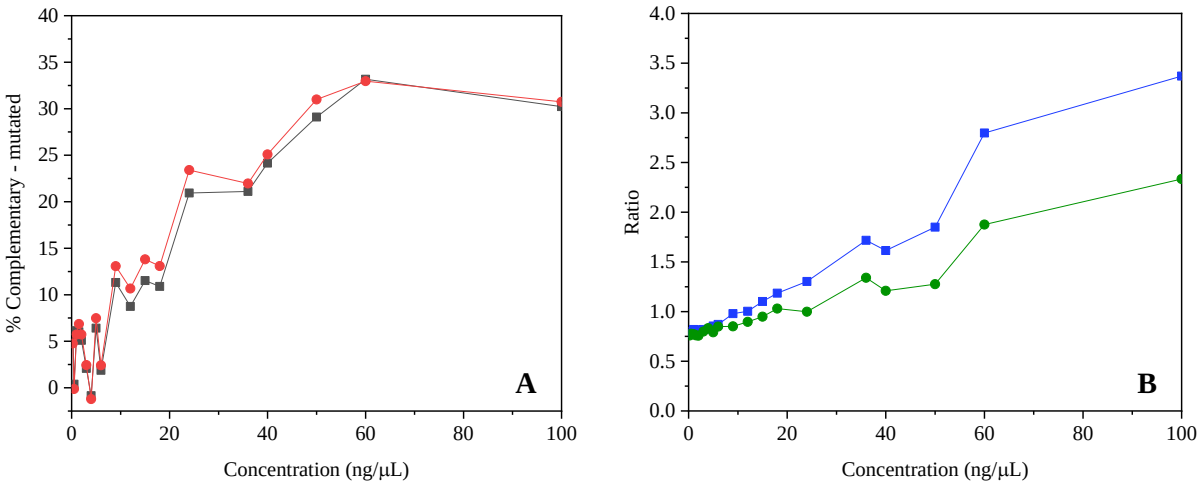

Figure 4.39 – Percentual difference calculated between the aggregation ratios of the complementary and mutated ssDNA samples (graph A) and aggregation ratios calculated for these samples using the subtraction method (graph B) for several ssDNA concentrations. These assays were performed using the 40 nm Au-nanoprobes obtained through the revised pH method with a ratio of 1300 5' SH-OL per NP and 120 b.p. anti-parallel ssDNA. Graph A: black – Percentual difference obtained using the ratio method; Red – Percentual difference obtained using the subtraction method. Graph B: blue – Complementary ssDNA samples aggregation ratios; Green – Mutated ssDNA samples aggregation ratios. All calculations were obtained using spectra with a final Au-nanoprobe concentration of 0.15 nM and a 100 µL sample volume. The results presented were obtained using an incubation time of 3 minutes instead of the usual 15 minutes.

The concentration curve obtained for the 120 b.p. ssDNA targets reveal a diminishing colorimetric response when compared to the 40 b.p. ssDNA targets. This is evidenced by the lowering of the percentual difference between aggregation ratios of the complementary and mutated ssDNA samples. These results are similar to the ones obtained using the 15 nm Au-nanoprobes and consolidate that the increase of the ssDNA target length severely affects the Au-nanoprobe stabilization effect. Similarly to the 40 b.p. ssDNA target, a plateau of the percentual difference was reached when high concentrations were applied. Contrarily to the 40 b.p. ssDNA targets where the plateau was reached at 20 ng/µL, this plateau is reached at 60 ng/µL using the 120 b.p. ssDNA targets. These results support the previous statement that the molecules of ssDNA in solution are a defining factor in the colorimetric assay. Since the ssDNA concentration utilized is not adjusted to ssDNA length, a requirement of three times the DNA concentration is to be expected to induce similar results to the 40 b.p. ssDNA targets, which possess one third of the size. When compared to the 15 nm Au-nanoprobes using the 120 b.p. ssDNA targets, an increase in the difference between samples from 20 % at 100 ng/µL to 35 % at 60 ng/µL is seen. This is an indication that the 40 nm Au-nanoprobes are capable of better discerning SNPs.

The aggregation ratios of the complementary and mutated samples show that an increase of the Au-nanoprobe stabilization effect is seen when using the 120 b.p. ssDNA targets. Unlike the 40 b.p. ssDNA targets, where the aggregation ratio of the samples reached a plateau, for the 120 b.p. targets the ratios saw a continuous growth, as the ssDNA concentration was increased. The major difference is seen for the mutated sample, where an increased stabilization occurred. This is the deciding factor in the diminishing of the percentual difference between samples visualized.

Detailed analysis of the percentual differences reveal that a concentration of 9 ng/µL is required to verify a 10 % difference between the aggregation ratios of the complementary and mutated ssDNA samples and a concentration of 24 ng/µL is required for a 20 % difference. Both these concentrations are superior to the values obtained for the 40 b.p. ssDNA targets. On top of this, the maximum percentual difference obtained was near 35 %, which is nearly half of the maximum value obtained for the 40 b.p. ssDNA targets. These results are not favourable for real patient samples. Nevertheless, when compared to the 15 nm Au-nanoprobes, the results obtained are an improvement and solidify the 40 nm Au-nanoprobes as the best option of the two.

Once again, the aggregation ratio calculation methods do not show substantial differences between them. On most of the tested DNA concentrations, the subtraction method only leads to a slightly increased percentual difference, around 2-3%. This smaller difference is less impactful on the 40 nm Au-nanoprobes, since the difference between the aggregation ratios of the complementary and mutated samples is substantially higher, when compared to the 15 nm ones.

The variation of the incubation time was also assessed for these 40 nm Au-nanoprobes using the 120 b.p. anti-parallel ssDNA targets. The results obtained are presented in Figure 4.40.

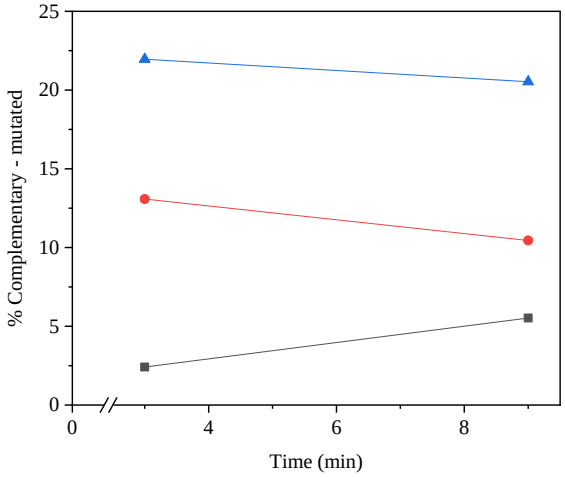

Figure 4.40 – Percentual difference calculated between the aggregation ratios of the complementary and mutated ssDNA samples at different incubation times for several ssDNA concentrations. These assays were performed using the 40 nm Au-nanoprobes, obtained through the revised pH method with a ratio of 1300 5' SH-OL per NP and 120 b.p. anti-parallel ssDNAs. Black – 6 ng/µL; Red – 18 ng/µL; Blue - 36 ng/µL. All calculations were obtained using spectra with a final Au-nanoprobe concentration of 0.15 nM and a 100 µL sample volume.

As evidenced in Figure 4.40, for the different incubation times tested, no remarkable differences were identifiable between the percentual differences/aggregation ratios for three- and nine-minute times. These results are distinct to the ones obtained using the 40 b.p. ssDNA targets, where a significant loss was seen, as the incubation time increased. This phenomenon may be tied to a smaller aggregation rate using the larger ssDNA targets, which may be related to the larger overhang that occurs when the SH-OL hybridizes with the 120 b.p. ssDNA targets. The effect seen is desirable, since it allows the adjustment of the incubation time of the assay, which was very short for the 40 b.p. ssDNA targets.

The evaluation of the statistical significance obtained for several replicates of colorimetric assays at defined ssDNA concentrations can be seen in Table 4.9. A colorimetric assay of each ssDNA concentration is presented in Figure 4.41.

Table 4.9 – Statistical significance of several replicates obtained for 6, 18 and 36 ng/µL, using a t-Test at a 0.05 level, for the 40 nm Au-nanoprobes, using 120 b.p. ssDNA targets. Ratios were calculated according to the subtraction method. The results presented were obtained using an incubation time of 3 minutes instead of the usual 15 minutes.

DNA concentration (ng/µL)	Ratio Comp	Ratio Mut	Difference (%)	t-Test at 0.05 level	
				Equal variance assumed	Equal variance not assumed
6	0.72	0.67	6.2	0.0222	0.0506
	0.69	0.68	2.7		
	0.72	0.68	5.3		
18	0.76	0.71	6.0	0.5401	0.5536
	0.79	0.80	-1.4		
	0.80	0.78	2.9		
36	1.21	0.87	28.3	0.0001	0.0002
	1.17	0.82	29.8		
	1.15	0.83	27.6		

From the several replicates at 6, 18 and 36 ng/µL, it was possible to assess that the colorimetric assays performed using 120 b.p. ssDNA targets have a statistically significant difference between the aggregation ratios of the complementary and the mutated ssDNA samples for 6 and 36 ng/µL, when a t-Test is applied at a 0.05 level. These results are on par with the ones obtained for the 40 b.p. ssDNA targets using 40 nm Au-nanoprobes. Some variability was seen using the 18 ng/µL, which resulted in the statistical insignificance seen. For 6 ng/µL, the difference between the complementary and mutated samples was rather small, near 5 %, but was constant across all three replicates. For 36 ng/µL, the difference was considerably higher, near 28 %. Nevertheless, good reproducibility paired with a better colorimetric response, when compared to the 15 nm Au-nanoprobes, lead to the conclusion that these Au-nanoprobes are more capable of discerning between SNPs. Despite this, the increase in length did make visual distinction between samples harder, as evidenced in Figure 4.41.

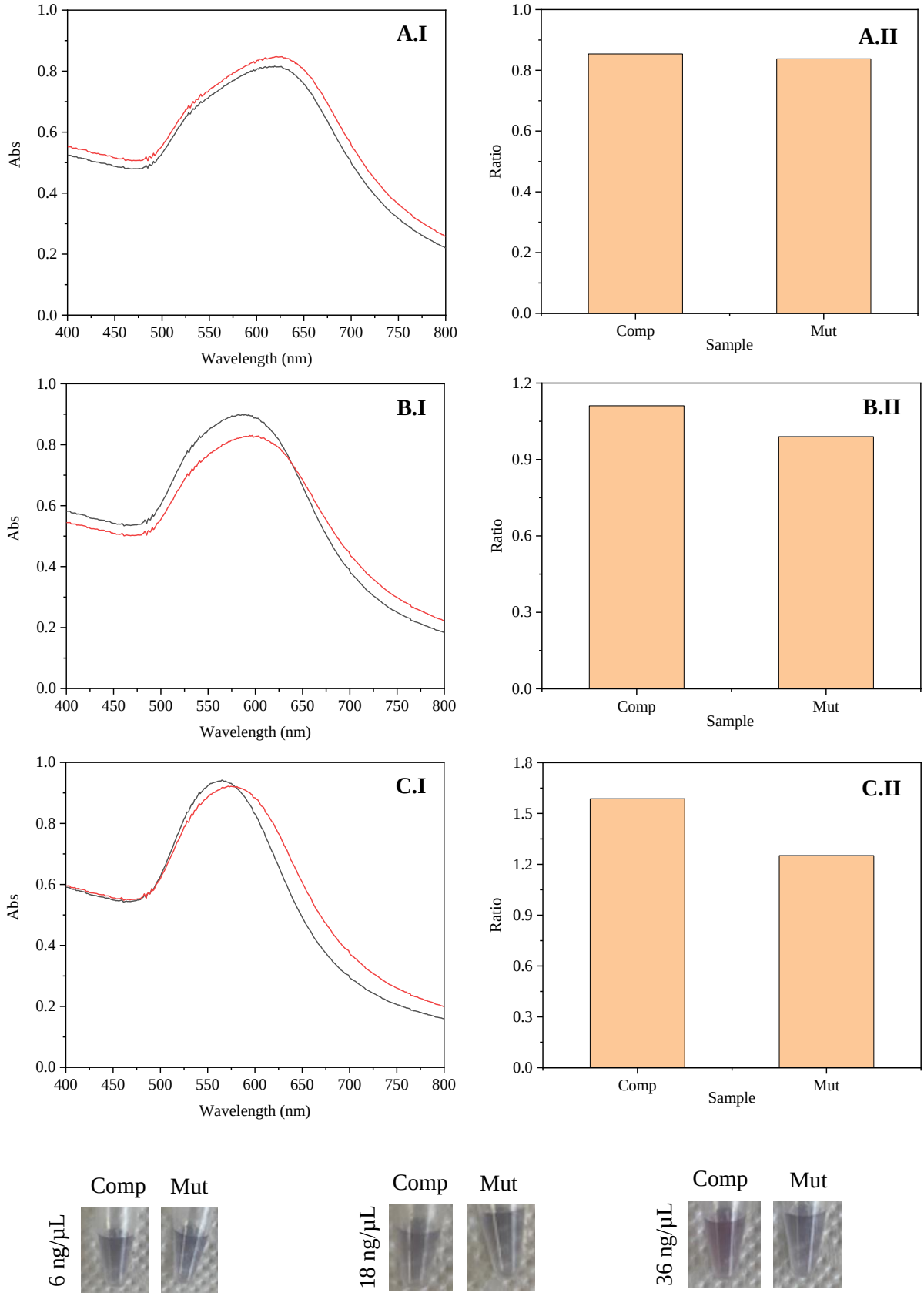

Figure 4.41 – Colorimetric assays and response of the 40 nm Au-nanoprobes obtained through the revised pH method with a ratio of 1300 5' SH-OL per NP using several concentrations of 120 b.p. anti-parallel ssDNA. Graph A – 6 ng/µL; Graph B – 18 ng/µL; Graph C – 36 ng/µL. Graphs .I – UV-Vis spectra of the obtained samples. Black – Complementary ssDNA sample; Red – Mutated ssDNA sample. All spectra were obtained using a final nanoprobe concentration of 0.15 nM and a 100 µL sample volume. Graphs .II – Aggregation ratios calculated using the subtraction method for each sample. The results presented were obtained using an incubation time of 3 minutes instead of the usual 15 minutes.

The effect of the incubation temperature was also assessed for these Au-nanoprobes using the 120 b.p. anti-parallel ssDNA targets. The results obtained can be seen in Figure 4.42.

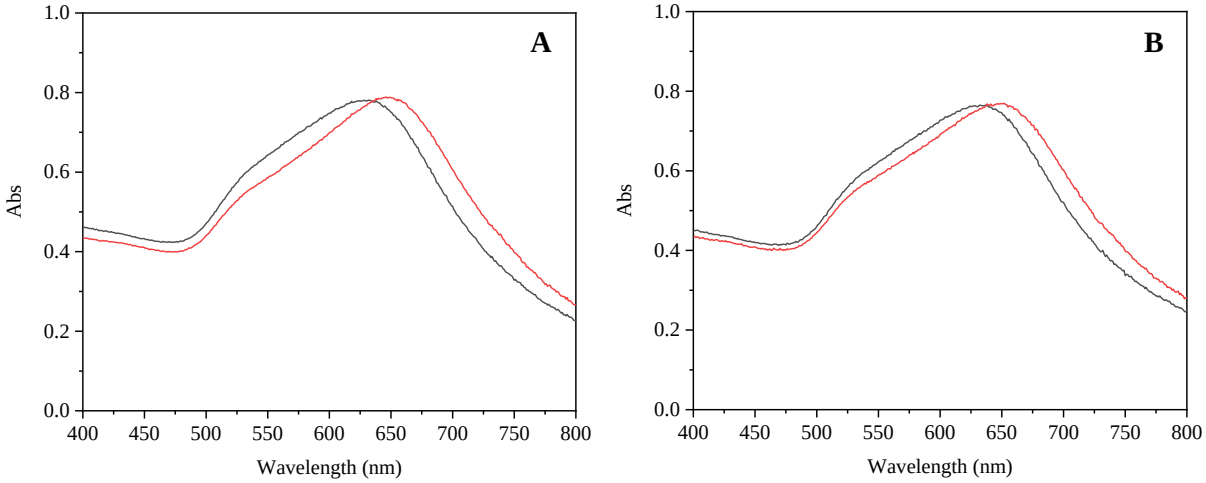

Figure 4.42 – Colorimetric assays of the 40 nm Au-nanoprobes obtained through the revised pH method with a ratio of 1300 5' SH-OL per NP using 120 b.p. anti-parallel ssDNA at different incubation temperatures. Graph A – 75 ºC; Graph B – 95 ºC. Black – Complementary ssDNA sample; Red – Mutated ssDNA sample. All spectra were obtained using a final Au-nanoprobe concentration of 0.15 nM, a ssDNA concentration of 18 ng/µL and a 100 µL sample volume. The results presented were obtained using an incubation time of 3 minutes instead of the usual 15 minutes.

The variation of the incubation temperature between 75 and 95 ºC revealed no correlation between the increase of the incubation temperature and distinct aggregation states. Since the aggregation ratios remained similar, the percentual differences between samples were also identical. Although a small decrease was seen when transitioning from 75 to 85 ºC, this difference was partially eliminated when 95 ºC where applied. The small variations seen could be attributed to slight variability of the aggregation that results from salt addition. The results obtained here are similar to the ones obtained using the 40 b.p. ssDNA targets but differ from the ones obtained using the 120 b.p. ssDNA targets with the 15 nm Au-nanoprobes, where a significant increase of the percentual difference between samples was verified with the increase of the incubation temperature. Nevertheless, since the increase in temperature did not result in smaller colorimetric distinction, it is a good indication that the assay would not suffer if real patient samples, which require such heating, were applied.

Chapter 5

Conclusions

The main purpose of this thesis was the development of an innovative colorimetric assay, based on AuNPs aggregation, capable of detecting a SNP related to LI in European populations.

To accomplish this, 15 and 40 nm AuNPs were synthetised and characterised. Through UV-Vis it was possible to estimate the size and concentration of the several synthetised AuNPs batches. For 15 nm AuNPs, the size estimations deviated only a maximum of 1.5 nm from the desired size while for 40 nm AuNPs, the maximum size deviation was 3.1 nm. The LSPR of the obtained AuNPs was on par with the values described in the literature (519 for 15 nm AuNPs and 528 for 40 nm AuNPs).

Before the functionalization of AuNPs, SH-OLs were pre-treated and purified. Nanodrop measurements allowed the assessment of the concentration and purity of the SH-OLs after purification and ssDNA targets. The results obtained revealed that 89 % of the SH-OL batches did not show any signs of contamination since the ratio 260/230 was above 1.8 and the ratio 260/280 above was 2.2 and were subsequently used. For the ssDNA targets, all samples used presented a minimum 260/230 ratio of 1.43 and a minimum 260/280 ratio of 1.87.

Following the synthesis of AuNPs and the purification of SH-OL, several ratios of SH-OL per NP were tested using two functionalization methods (SA and pH). Regarding the Au-nanoprobes obtained using the 5' SH-OL, for 15 nm AuNPs, it was possible to verify that the pH method allowed the obtention of stable Au-nanoprobes using a smaller ratio of 50, when compared to the SA method, which required a ratio of 150. Agarose gel electrophoresis confirmed the beforementioned results, since only stable nanoprobes resulted in well-defined bands that migrated in the gel. A comparison of the DLS and ELS measurements between functionalization methods show that the SA method produces Au-nanoprobes with increased hydrodynamic size (near 50 nm) and zeta potential (near -21 mV), when compared to both AuNPs (21.4 nm; -46 mV) and Au-nanoprobes obtained using the pH method (28 nm; -25 mV). The polydispersity index of both Au-nanoprobes saw an increase from 0.3 for the citrate capped AuNPs, to near 0.48 and 0.35 for the SA and pH method respectively. These differences were not found to be impactful in the stability assays, where the Au-nanoprobes obtained using either functionalization method had similar stability, only showing signs of aggregation when 500 mM of NaCl were added. The nanoprobe stability saw a 10-fold increase over the AuNPs, whose aggregation initiated at 50 mM of NaCl, demonstrating the stabilization effect of the SH-OLs.

Clear differences between both functionalization methods were seen in the colorimetric assays using 15 nm AuNPs, where the SA method produced Au-nanoprobes capable of better discerning distinct ssDNA targets. This was evidenced due to the increased Au-nanoprobe stabilization effect conferred by both the complementary and mutated ssDNA samples, while the non-complementary ssDNA did not alter Au-nanoprobe stabilization. On the other hand, for Au-nanoprobes obtained through the pH method, the complementary and mutated ssDNA targets only increased the stabilization of the Au-nanoprobes slightly and the non-complementary ssDNA target also had a slight stabilization effect, which should not occur. These results led to the conclusion that the SA method was the preferable functionalization method for the 15 nm AuNPs.

For the 40 nm AuNPs, inconsistencies during the functionalization step for the SA method were obtained from the beginning. The initially employed pH method, identical to the pH method of the 15 nm AuNPs, also suffered from variability. Upon revision of the pH method through the utilization of concentrated AuNPs, stable Au-nanoprobes were consistently obtained using a ratio of 1300 5' SH-OL per NP. The agarose gels also allowed differentiation between ratios. From DLS measurements, a hydrodynamic size increase was seen from the AuNPs (43 nm) to the Au-nanoprobes (near 50 nm). For the ratios capable of producing stable Au-nanoprobes (1300 and up), a decrease in both the polydispersity index and the zeta potential was seen, when compared to the AuNPs. The stability of the Au-nanoprobes was also higher than the AuNPs, with an increase in stability of 3.3-fold (from 90 mM to 300 mM for initial aggregation). The obtained results demonstrated that the revised pH method (using concentrated AuNPs) was the best performing functionalization method for 40 nm AuNPs.

The functionalization of AuNPs using the 3' SH-OL revealed that higher functionalization ratios had to be applied to obtain stable Au-nanoprobes. For 15 nm AuNPs, a ratio of 50 3' SH-OL per NP was still enough to produce stable Au-nanoprobes using the pH method, but an increase in the minimum ratio required was seen for the SA method, when compared to the Au-nanoprobes obtained using the 5' SH-OL (from 150 to 200). For 40 nm AuNPs, the minimum ratio also increased (from 1300 to 1500). The UV-Vis spectra of the Au-nanoprobes obtained using the 3' SH-OL also showed slight signs of aggregation, detected by the emergence of a sulk at greater wavelengths. As such, the Au-nanoprobes obtained using the 3' SH-OL seemed less stable than the ones previously obtained using the 5' SH-OL.

Once stable Au-nanoprobes were achieved, several ssDNA targets were tested trough NCL colorimetric assays. Initially, 50 b.p. parallel ssDNA targets, capable of parallel hybridization with the Au-nanoprobes were utilised. These targets produced a colorimetric distinction between the complementary and mutated ssDNA targets. Despite this, the non-complementary ssDNA had an Au-nanoprobe stabilization effect on par with the complementary ssDNA, which should not occur. As such, new 40 b.p. parallel ssDNA targets were designed, taking into account the whole gene sequence. Although these ssDNA targets saw a massive decline in the Au-nanoprobe stabilization effect of the non-complementary ssDNA target, the distinction between the complementary and mutated ssDNA samples saw a decline as well.

Since anti-parallel hybridization has been associated with stronger DNA interaction, 40 b.p. anti-parallel targets were designed in order to improve the hybridization between ssDNA target and Au-nanoprobe. The Au-nanoprobe stabilization effect of complementary and mutated ssDNA targets was so high using anti-parallel ssDNA that no aggregation was seen for salt concentrations at which the Au-nanoprobes showed intense aggregation. As such, new colorimetric assays were conducted using $MgCl_2$ instead of NaCl. A concentration of 30 mM and 50 mM was chosen for 15 and 40 nm Au-nanoprobes respectively. From the colorimetric assays it was possible to verify that not only was a distinction between the complementary and mutated ssDNA targets present, but also almost full aggregation of non-complementary ssDNA sample occurred.

The utilization of 6-mercapto-1-hexanol as an intercalating agent during the functionalization process was also evaluated. A ratio of 100 molecules of intercalating agent per NP were applied. The stability and colorimetric results obtained did not show any clear distinction between Au-nanoprobes with intercalating agent and Au-nanoprobes without it.

For both NPs' sizes, the CL assays did not result in Au-nanoprobe aggregation when using the complementary and mutated ssDNA targets. These results were an indication that problems with hybridization could be occurring. Since the Au-nanoprobes obtained using the 5' SH-OL had already been proven to be functioning correctly, the Au-nanoprobes obtained using the 3' SH-OL were tested using NCL colorimetric assays. For 15 nm Au-nanoprobes, both the complementary and non-complementary ssDNA targets had high Au-nanoprobe stabilization effect, while for the 40 nm Au-nanoprobes, neither target led to significant stabilization. These results are indicative that the Au-nanoprobes obtained with the 3' SH-OL had hybridization problems.

Following ssDNA optimization, the NCL colorimetric response using several ssDNA concentrations was evaluated. For the 15 nm Au-nanoprobes, an increase in the percentual difference between the aggregation ratios of the complementary and mutated ssDNA samples was seen until 36 ng/µL, after which the opposite effect was observed. A concentration of 4 ng/µL was required to achieve a 10 % difference between samples and 9 ng/µL were required for a difference of 25 %. For the tested concentrations (between 0.25 and 100 ng/µL), two aggregation ratios calculation methods were tested (subtraction and ratio method). The subtraction method led to a 1.12 to 1.2-fold increase of the percentual difference between samples, when compared to the ratio method. Following this, different incubation times were tested (between 3 and 15 minutes). Results revealed that these Au-nanoprobes did not show time-dependent aggregation or had a rate of aggregation that varied extremely slowly with time. The statistical significance was also evaluated for 6, 18 and 36 ng/µL using the aggregation ratios obtained from three replicates. The results obtained showed no statistically significant difference between the aggregation ratios of the complementary and mutated ssDNA samples for any of the concentrations tested. Lastly, the incubation temperature of the colorimetric assay was varied (between 75 and 95 ºC) and no temperature-dependent effect was seen for the complementary and mutated ssDNA samples.

For the 40 nm Au-nanoprobes, an increase in the percentual difference between the aggregation ratios of the complementary and mutated ssDNA samples was seen up until 12 ng/µL, after which the percentual difference stabilized. For these Au-nanoprobes, a concentration of 1.5 ng/µL of ssDNA was enough to achieve a 20 % difference between samples, while 12 ng/µL and up resulted in a 60 % difference. In this case, the calculation methods of the aggregation ratios had extremely similar results, with no clear distinction between them. Time-dependent aggregation was verified, where a diminishing difference between samples with the increase of the incubation time was seen. Statistical significance was obtained for ssDNA concentrations of 6 and 36 ng/µL. No temperature-dependent aggregation behaviour was seen for the complementary and mutated ssDNA samples.

When the ssDNA target length was increased to 120 b.p. diminishing percentual differences between samples were seen. For the 15 nm Au-nanoprobes, an increase of the difference was seen until 24 ng/µL, after which it seemed to stabilise. A ssDNA concentration of 18 ng/µL was required to achieve a 10 % difference between samples, and a 20 % difference was only achieved at 100 ng/µL. Once again, the subtraction method led to a 1.05 to 1.15-fold increase in the difference between samples, making it a better option for the calculation of aggregation ratios. The same incubation time independence was visualised for the tested conditions (between 3 and 15 minutes), but statistically significant differences were seen for 18 and 36 ng/µL. Incubation temperature testing also revealed an increase in the distinction of the samples when higher temperatures (95 ºC) were applied.

For 40 nm Au-nanoprobes, an increase of the percentual difference between the aggregation ratios of the complementary and mutated samples was seen until 60 ng/µL, after which the difference stabilized in the tested conditions (until 100 ng/µL). A DNA concentration of 9 ng/µL was required to induce a 10 % difference and a maximum of 33 % difference was attained for 60 ng/µL. In these assays, the subtraction method led to a slight increase in the percentual difference between samples, although it was not as significant as what had been seen for the 15 nm Au-nanoprobes. Contrarily to what was seen using the 40 b.p. ssDNA targets, the incubation time did not appear to hinder the distinction between samples. Statistically significant differences were seen for 6 and 36 ng/µL, similarly to the 40 b.p. ssDNA targets. The incubation temperature did not seem to affect the aggregation state of the complementary and mutated ssDNA samples.

Overall, the results obtained revealed the following: (1) the SA method was better for the functionalization of 15 nm AuNPs, while the revised pH method worked best for 40 nm AuNPs; (2) anti-parallel hybridization led to more stable SH-OL – ssDNA complexes and better colorimetric distinction between the complementary and mutated samples; (3) the Au-nanoprobes obtained using the 3’ SH-OL did not show ssDNA selectivity; (4) an increase in target ssDNA concentration usually led to greater distinction between the complementary and mutated samples; (5) an increase in ssDNA target length led to less distinction between samples; (6) 40 nm Au-nanoprobes achieved a better colorimetric distinction than 15 nm nanoprobes; (7) the subtraction method for the calculation of aggregation ratios wielded better results than the ratio method.

Regarding future perspectives, several possibilities would be beneficial to further elucidate the employed colorimetric system. The following propositions are ordered from a logical standpoint:

(1) Redesign of the 3’ SH-OL to obtain stable Au-nanoprobes for the CL assay. This could be achieved by increasing the GC content to raise the melting temperature of the SH-OL either by replacing DNA bases or introducing a poly C/G tail. The first option would increase the SH-OL size, which may hinder the colorimetric distinction between samples while the second one would decrease the number of complementary bases which could have the same effect. As such, both possibilities should be considered and tested.

(2) Utilization of fluorescent SH-OL to investigate further differences between the SA and the pH functionalization methods. This would allow the calculation of the percentage of SH-OLs that adhere to the surface of the AuNPs.

(3) Diagnostic of heterozygous samples using the optimized colorimetric assay. Real patients can be homozygous lactose tolerant or intolerant, but heterozygous tolerant individuals also exist. Differences between all these samples should be smaller than between only the homozygous samples but their study is necessary.

(4) Test real patient samples to evaluate the performance of the developed colorimetric system in a real scenario, without using synthetic ssDNA targets. This would allow the comparison between real samples and synthetic ssDNA and evaluate the applicability of our test for a point-of-care application.

(5) Evaluate the limit of detection of the developed assay to verify the lowest DNA concentration required to induce a measurable response for real patient samples. This is an important parameter to verify the competitiveness of the assay with other methods already available for the detection of LI.

(6) Obtain DLS and ELS measurements upon the addition of DNA targets and during the colorimetric assay. These measurements would not only allow to verify the hybridization of the DNA targets with the Au-nanoprobes, but also assess the difference of the aggregation state of the Au-nanoprobes upon salt addition, allowing further comparison between the complementary and mutated DNA samples.

The proposed studies would lead to a better understanding of the employed colorimetric system and allow further optimizations that could result in a better colorimetric distinction between samples, broadening the application of these systems for other genetic diseases with SNPs.

Chapter 6

References

(1) Unlocking Nature. Enriching Life. | ADM https://www.adm.com/news/news-releases/emerging-consumer-behavior-shifts-six-ways-food-beverage-innovation-is-evolving-in-the-face-of-covid-19-2 (accessed Mar 10, 2021).
(2) Venda de leite caiu 11% em 2016. Indústria fala em "demonização" do leite | Consumo | PÚBLICO https://www.publico.pt/2018/01/19/sociedade/noticia/venda-de-leite-caiu-11-em-2016-industria-fala-em-demonizacao-do-leite-1799926 (accessed Mar 10, 2021).
(3) Lomer, M. C. E.; Parkes, G. C.; Sanderson, J. D. Review Article: Lactose Intolerance in Clinical Practice - Myths and Realities. *Alimentary Pharmacology and Therapeutics*. 2008. https://doi.org/10.1111/j.1365-2036.2007.03557.x.
(4) Storhaug, C. L.; Fosse, S. K.; Fadnes, L. T. Country, Regional, and Global Estimates for Lactose Malabsorption in Adults: A Systematic Review and Meta-Analysis. *Lancet Gastroenterol. Hepatol.* **2017**, *2* (10), 738–746. https://doi.org/10.1016/S2468-1253(17)30154-1.
(5) *NIH Consensus Development Conference Statement on Lactose Intolerance and Health NIH Consensus and State-of-the-Science Statements*.
(6) Lember, M. Hypolactasia: A Common Enzyme Deficiency Leading to Lactose Malabsorption and Intolerance. *Polish Arch. Intern. Med.* **2012**, *122* (Suppl. 1), 60–64. https://doi.org/10.20452/pamw.1517.
(7) Johnson, J. M.; Conforti, F. D. LACTOSE. In *Encyclopedia of Food Sciences and Nutrition*; Elsevier, 2003; pp 3472–3476. https://doi.org/10.1016/b0-12-227055-x/00674-x.
(8) Steyn, N. P.; Temple, N. J. Dietary Sugar: Public Health Perspective. In *Encyclopedia of Toxicology: Third Edition*; Elsevier, 2014; pp 125–127. https://doi.org/10.1016/B978-0-12-386454-3.01243-4.
(9) Hettinga, K. A. Lactose in the Dairy Production Chain. In *Lactose: Evolutionary Role, Health Effects, and Applications*; Elsevier, 2019; pp 231–266. https://doi.org/10.1016/B978-0-12-811720-0.00006-4.
(10) Labrie, V.; Buske, O. J.; Oh, E.; Jeremian, R.; Ptak, C.; Gasinas, G.; Maleckas, A.; Petereit, R.; Avirbliene, A.; Adamonis, K.; Kriukiena, E.; Konceviaius, K.; Gordeviaius, J.; Nair, A.; Zhang, A.; Ebrahimi, S.; Oh, G.; Šikšnys, V.; Kupainskas, L.; Brudno, M.; Petronis, A. Lactase Nonpersistence Is Directed by DNA-Variation-Dependent Epigenetic Aging. *Nat. Struct. Mol. Biol.* **2016**, *23* (6), 566–573. https://doi.org/10.1038/nsmb.3227.
(11) Gerbault, P.; Liebert, A.; Itan, Y.; Powell, A.; Currat, M.; Burger, J.; Swallow, D. M.; Thomas, M. G. Evolution of Lactase Persistence: An Example of Human Niche Construction. *Philosophical Transactions of the Royal Society B: Biological Sciences*. Royal Society March 27, 2011, pp 863–877. https://doi.org/10.1098/rstb.2010.0268.
(12) Vandenplas, Y. Lactose Intolerance. *Asia Pac. J. Clin. Nutr.* **2015**, *24* (December), S9–S13. https://doi.org/10.6133/apjcn.2015.24.s1.02.
(13) Sala Coromina, J.; Vinaixa Vergés, A.; Garcia Puig, R. Congenital Lactase Deficiency: Identification of a New Mutation. *An. Pediatría (English Ed.* **2015**, *82* (5), 365–366. https://doi.org/10.1016/j.anpede.2014.10.010.
(14) Järvelä, I. E. Molecular Genetics of Adult-Type Hypolactasia. *Annals of Medicine*. Ann Med 2005, pp 179–185. https://doi.org/10.1080/07853890510007359.
(15) Usai-Satta, P. Lactose Malabsorption and Intolerance: What Should Be the Best Clinical Management? *World J. Gastrointest. Pharmacol. Ther.* **2012**, *3* (3), 29. https://doi.org/10.4292/wjgpt.v3.i3.29.
(16) Schultheis, P. J.; Bowling, B. V. Analysis of a SNP Linked to Lactase Persistence: An Exercise for Teaching Molecular Biology Techniques to Undergraduates. *Biochem. Mol. Biol. Educ.* **2011**, *39* (2), 133–140. https://doi.org/10.1002/bmb.20456.
(17) Kuokkanen, M.; Kokkonen, J.; Enattah, N. S.; Ylisaukko-Oja, T.; Komu, H.; Varilo, T.; Peltonen, L.; Savilahti, E.; Järvelä, I. *Report Mutations in the Translated Region of the Lactase Gene (LCT) Underlie Congenital Lactase Deficiency*; 2006; Vol. 78.
(18) Järvelä, I.; Enattah, N. S.; Kokkonen, J.; Varilo, T.; Savilahti, E.; Peltonen, L. *Assignment of the Locus for Congenital Lactase Deficiency to 2q21, in the Vicinity of but Separate from the Lactase-Phlorizin Hydrolase Gene*; 1998; Vol. 63.
(19) Robayo-Torres, C. C.; Nichols, B. L. Molecular Differentiation of Congenital Lactase Deficiency from Adult-Type Hypolactasia. *Nutrition Reviews*. Nutr Rev February 2007, pp 95–

98. https://doi.org/10.1111/j.1753-4887.2007.tb00286.x.
(20) Swallow, D. M. Genetics of Lactase Persistence and Lactose Intolerance. *Annual Review of Genetics*. December 2003, pp 197–219. https://doi.org/10.1146/annurev.genet.37.110801.143820.
(21) Ortolani, C.; Pastorello, E. A. Food Allergies and Food Intolerances. *Best Pract. Res. Clin. Gastroenterol.* **2006**, *20* (3), 467–483. https://doi.org/10.1016/j.bpg.2005.11.010.
(22) Dawson, D. J.; Lobley, R. W.; Burrows, P. C.; Miller, V.; Holmes, R. Lactose Digestion by Human Jejunal Biopsies: The Relationship between Hydrolysis and Absorption M13 9WL. *Gut* **1986**, *27*, 521–527. https://doi.org/10.1136/gut.27.5.521.
(23) Kuokkanen, M.; Myllyniemi, M.; Vauhkonen, M.; Helske, T.; Kääriäinen, I.; Karesvuori, S.; Linnala, A.; Härkönen, M.; Järvelä, I.; Sipponen, P. A Biopsy-Based Quick Test in the Diagnosis of Duodenal Hypolactasia in Upper Gastrointestinal Endoscopy. *Endoscopy* **2006**, *38* (7), 708–712. https://doi.org/10.1055/s-2006-925354.
(24) Mattar, R.; Mazo, D. F. de C.; Carrilho, F. J. Lactose Intolerance: Diagnosis, Genetic, and Clinical Factors. *Clinical and Experimental Gastroenterology*. Dove Medical Press Ltd July 4, 2012, pp 113–121. https://doi.org/10.2147/CEG.S32368.
(25) Newcomer, A. D.; McGill, D. B.; Thomas, P. J.; Hofmann, A. F. Prospective Comparison of Indirect Methods for Detecting Lactase Deficiency. *N. Engl. J. Med.* **1975**, *293* (24), 1232–1236. https://doi.org/10.1056/nejm197512112932405.
(26) Law, D.; Conklin, J.; Pimentel, M. Lactose Intolerance and the Role of the Lactose Breath Test. *American Journal of Gastroenterology*. Nature Publishing Group August 2010, pp 1726–1728. https://doi.org/10.1038/ajg.2010.146.
(27) Szilagyi, A.; Malolepszy, P.; Hamard, E.; Xue, X.; Hilzenrat, N.; Ponniah, M.; Macnamara, E.; Chong, G. Comparison of a Real-Time Polymerase Chain Reaction Assay for Lactase Genetic Polymorphism With Standard Indirect Tests for Lactose Maldigestion. **2007**. https://doi.org/10.1016/j.cgh.2006.06.009.
(28) Farooq, M. U.; Novosad, V.; Rozhkova, E. A.; Wali, H.; Ali, A.; Fateh, A. A.; Neogi, P. B.; Neogi, A.; Wang, Z. Gold Nanoparticles-Enabled Efficient Dual Delivery of Anticancer Therapeutics to HeLa Cells. *Sci. Rep.* **2018**, *8* (1), 1–12. https://doi.org/10.1038/s41598-018-21331-y.
(29) Chang, C. C.; Chen, C. P.; Wu, T. H.; Yang, C. H.; Lin, C. W.; Chen, C. Y. Gold Nanoparticle-Based Colorimetric Strategies for Chemical and Biological Sensing Applications. *Nanomaterials*. MDPI AG June 1, 2019. https://doi.org/10.3390/nano9060861.
(30) Jeevanandam, J.; Barhoum, A.; Chan, Y. S.; Dufresne, A.; Danquah, M. K. Review on Nanoparticles and Nanostructured Materials: History, Sources, Toxicity and Regulations. *Beilstein Journal of Nanotechnology*. Beilstein-Institut Zur Forderung der Chemischen Wissenschaften April 3, 2018, pp 1050–1074. https://doi.org/10.3762/bjnano.9.98.
(31) Yeh, Y. C.; Creran, B.; Rotello, V. M. Gold Nanoparticles: Preparation, Properties, and Applications in Bionanotechnology. *Nanoscale*. Royal Society of Chemistry March 21, 2012, pp 1871–1880. https://doi.org/10.1039/c1nr11188d.
(32) Bar-Ilan, O.; Albrecht, R. M.; Fako, V. E.; Furgeson, D. Y. Toxicity Assessments of Multisized Gold and Silver Nanoparticles in Zebrafish Embryos. *Small* **2009**, *5* (16), 1897–1910. https://doi.org/10.1002/smll.200801716.
(33) Elhani, S.; Ishitobi, H.; Inouye, Y.; Ono, A.; Hayashi, S.; Sekkat, Z. Surface Enhanced Visible Absorption of Dye Molecules in the Near-Field of Gold Nanoparticles. *Sci. Rep.* **2020**, *10* (1), 1–11. https://doi.org/10.1038/s41598-020-60839-0.
(34) Petryayeva, E.; Krull, U. J. Localized Surface Plasmon Resonance: Nanostructures, Bioassays and Biosensing-A Review. *Analytica Chimica Acta*. Elsevier November 7, 2011, pp 8–24. https://doi.org/10.1016/j.aca.2011.08.020.
(35) Fong, K. E.; Yung, L. Y. L. Localized Surface Plasmon Resonance: A Unique Property of Plasmonic Nanoparticles for Nucleic Acid Detection. *Nanoscale* **2013**, *5* (24), 12043–12071. https://doi.org/10.1039/c3nr02257a.
(36) Link, S.; El-Sayed, M. A. Size and Temperature Dependence of the Plasmon Absorption of Colloidal Gold Nanoparticles. *J. Phys. Chem. B* **1999**, *103* (21), 4212–4217. https://doi.org/10.1021/jp984796o.

(37) Yao, G.; Liu, Q.; Zhao, Z. Studied Localized Surface Plasmon Resonance Effects. **2018**. https://doi.org/10.3390/catal8060236.
(38) Senut, M. C.; Zhang, Y.; Liu, F.; Sen, A.; Ruden, D. M.; Mao, G. Size-Dependent Toxicity of Gold Nanoparticles on Human Embryonic Stem Cells and Their Neural Derivatives. *Small* **2016**, *12* (5), 631–646. https://doi.org/10.1002/smll.201502346.
(39) Nehl, C. L.; Hafner, J. H. Shape-Dependent Plasmon Resonances of Gold Nanoparticles. *Journal of Materials Chemistry*. 2008, pp 2415–2419. https://doi.org/10.1039/b714950f.
(40) Bang, N. A.; Thi, P.; Hoang, T. &; Nhat, N. A Comparative Study of Classical Approaches to Surface Plasmon Resonance of Colloidal Gold Nanorods. https://doi.org/10.1007/s13404-013-0082-0.
(41) Hao, F.; Nehl, C. L.; Hafner, J. H.; Nordlander, P. Plasmon Resonances of a Gold Nanostar. *Nano Lett.* **2007**, *7* (3), 729–732. https://doi.org/10.1021/nl062969c.
(42) Favi, P. M.; Gao, M.; Johana Sepúlveda Arango, L.; Ospina, S. P.; Morales, M.; Pavon, J. J.; Webster, T. J. Shape and Surface Effects on the Cytotoxicity of Nanoparticles: Gold Nanospheres versus Gold Nanostars. *J. Biomed. Mater. Res. - Part A* **2015**, *103* (11), 3449–3462. https://doi.org/10.1002/jbm.a.35491.
(43) Ali, M. R. K.; Rahman, M. A.; Wu, Y.; Han, T.; Peng, X.; Mackey, M. A.; Wang, D.; Shin, H. J.; Chen, Z. G.; Xiao, H.; Wu, R.; Tang, Y.; Shin, D. M.; El-Sayed, M. A. Efficacy, Long-Term Toxicity, and Mechanistic Studies of Gold Nanorods Photothermal Therapy of Cancer in Xenograft Mice. *Proc. Natl. Acad. Sci. U. S. A.* **2017**, *114* (15), E3110–E3118. https://doi.org/10.1073/pnas.1619302114.
(44) Mahmoud, A. Y. F.; Rusin, C. J.; McDermott, M. T. Gold Nanostars as a Colloidal Substrate for In-Solution SERS Measurements Using a Handheld Raman Spectrometer. *Analyst* **2020**, *145* (4), 1396–1407. https://doi.org/10.1039/c9an02439e.
(45) Wang, X.; Li, G.; Ding, Y.; Sun, S. Understanding the Photothermal Effect of Gold Nanostars and Nanorods for Biomedical Applications. *RSC Adv.* **2014**, *4* (57), 30375–30383. https://doi.org/10.1039/c4ra02978j.
(46) Ghosh, S. K.; Pal, T. Interparticle Coupling Effect on the Surface Plasmon Resonance of Gold Nanoparticles: From Theory to Applications. *Chemical Reviews*. American Chemical Society November 2007, pp 4797–4862. https://doi.org/10.1021/cr0680282.
(47) Xu, J. X.; Siriwardana, K.; Zhou, Y.; Zou, S.; Zhang, D. Quantification of Gold Nanoparticle Ultraviolet-Visible Extinction, Absorption, and Scattering Cross-Section Spectra and Scattering Depolarization Spectra: The Effects of Nanoparticle Geometry, Solvent Composition, Ligand Functionalization, and Nanoparticle Aggregation. *Anal. Chem.* **2018**, *90* (1), 785–793. https://doi.org/10.1021/acs.analchem.7b03227.
(48) Baptista, P. V.; Koziol-Montewka, M.; Paluch-Oles, J.; Doria, G.; Franco, R. Gold-Nanoparticle-Probe-Based Assay for Rapid and Direct Detection of Mycobacterium Tuberculosis DNA in Clinical Samples [5]. *Clinical Chemistry*. July 2006, pp 1433–1434. https://doi.org/10.1373/clinchem.2005.065391.
(49) Gaviña, P.; Parra, M.; Gil, S.; M. Costero, A. Red or Blue? Gold Nanoparticles in Colorimetric Sensing. In *Gold Nanoparticles - Reaching New Heights*; IntechOpen, 2019. https://doi.org/10.5772/intechopen.80052.
(50) XiuJuan, S.; Dan, L.; Jing, X.; Shawn, W.; ZhaoQiang, W.; Hong, C. Polymer Chemistry. *Chin Sci Bull* **2012**, *57* (10), 1109–1115. https://doi.org/10.1007/s11434-011-4741-3.
(51) Herizchi, R.; Abbasi, E.; Milani, M.; Akbarzadeh, A. Current Methods for Synthesis of Gold Nanoparticles. *Artif. Cells, Nanomedicine, Biotechnol.* **2016**, *44* (2), 596–602. https://doi.org/10.3109/21691401.2014.971807.
(52) Daruich De Souza, C.; Ribeiro Nogueira, B.; Rostelato, M. E. C. M. Review of the Methodologies Used in the Synthesis Gold Nanoparticles by Chemical Reduction. *Journal of Alloys and Compounds*. Elsevier Ltd August 25, 2019, pp 714–740. https://doi.org/10.1016/j.jallcom.2019.05.153.
(53) Abkenar, A. K.; Naderi, M. Chemical Synthesis of Gold Nanoparticles with Different Morphology from a Secondary Source. *J. Iran. Chem. Soc.* **2016**, *13* (12), 2173–2184. https://doi.org/10.1007/s13738-016-0935-6.
(54) Oliveira, J. P.; Prado, A. R.; Keijok, W. J.; Ribeiro, M. R. N.; Pontes, M. J.; Nogueira, B. V.;

Guimarães, M. C. C. A Helpful Method for Controlled Synthesis of Monodisperse Gold Nanoparticles through Response Surface Modeling. *Arab. J. Chem.* **2020**, *13* (1), 216–226. https://doi.org/10.1016/j.arabjc.2017.04.003.

(55) Kimling, J.; Maier, M.; Okenve, B.; Kotaidis, V.; Ballot, H.; Plech, A. Turkevich Method for Gold Nanoparticle Synthesis Revisited. *J. Phys. Chem. B* **2006**, *110* (32), 15700–15707. https://doi.org/10.1021/jp061667w.

(56) NAKAGAWA, T.; TAKAGAI, Y. Simple Synthesis of Gold Nanoparticles by Sodium Borohydride Reduction Method and Their Ligand Exchange Reaction. *BUNSEKI KAGAKU* **2019**, *68* (10), 751–755. https://doi.org/10.2116/bunsekikagaku.68.751.

(57) Zong, R.; Wang, X.; Shi, S.; Zhu, Y. Kinetically Controlled Seed-Mediated Growth of Narrow Dispersed Silver Nanoparticles up to 120 Nm: Secondary Nucleation, Size Focusing, and Ostwald Ripening. *Phys. Chem. Chem. Phys.* **2014**, *16* (9), 4236–4241. https://doi.org/10.1039/c3cp54846e.

(58) Niu, W.; Zhang, L.; Xu, G. Seed-Mediated Growth of Noble Metal Nanocrystals: Crystal Growth and Shape Control. *Nanoscale* **2013**, *5* (8), 3172–3181. https://doi.org/10.1039/c3nr00219e.

(59) Jana, N. R.; Gearheart, L.; Murphy, C. J. Evidence for Seed-Mediated Nucleation in the Chemical Reduction of Gold Salts to Gold Nanoparticles. *Chem. Mater.* **2001**, *13* (7), 2313–2322. https://doi.org/10.1021/cm000662n.

(60) Grzelczak, M.; Pérez-Juste, J.; Mulvaney, P.; Liz-Marzán, L. M. Shape Control in Gold Nanoparticle Synthesis. *Chem. Soc. Rev.* **2008**, *37* (9), 1783–1791. https://doi.org/10.1039/b711490g.

(61) Wang, P.; Wang, X.; Wang, L.; Hou, X.; Liu, W.; Chen, C. Interaction of Gold Nanoparticles with Proteins and Cells. *Science and Technology of Advanced Materials*. Institute of Physics Publishing June 1, 2015, p 034610. https://doi.org/10.1088/1468-6996/16/3/034610.

(62) Carnerero, J. M.; Jimenez-Ruiz, A.; Castillo, P. M.; Prado-Gotor, R. Covalent and Non-Covalent DNA–Gold-Nanoparticle Interactions: New Avenues of Research. *ChemPhysChem* **2017**, *18* (1), 17–33. https://doi.org/10.1002/cphc.201601077.

(63) Li, H.; Rothberg, L. Colorimetric Detection of DNA Sequences Based on Electrostatic Interactions with Unmodified Gold Nanoparticles. *Proc. Natl. Acad. Sci. U. S. A.* **2004**, *101* (39), 14036–14039. https://doi.org/10.1073/pnas.0406115101.

(64) Hurst, S. J.; Lytton-Jean, A. K. R.; Mirkin, C. A. Maximizing DNA Loading on a Range of Gold Nanoparticle Sizes. *Anal. Chem.* **2006**, *78* (24), 8313–8318. https://doi.org/10.1021/ac0613582.

(65) Mirkin, C. A.; Letsinger, R. L.; Mucic, R. C.; Storhoff, J. J. A DNA-Based Method for Rationally Assembling Nanoparticles into Macroscopic Materials. *Nature* **1996**, *382* (6592), 607–609. https://doi.org/10.1038/382607a0.

(66) Liu, B.; Liu, J. Methods for Preparing DNA-Functionalized Gold Nanoparticles, a Key Reagent of Bioanalytical Chemistry. *Analytical Methods*. Royal Society of Chemistry May 14, 2017, pp 2633–2643. https://doi.org/10.1039/c7ay00368d.

(67) Zhang, X.; Servos, M. R.; Liu, J. Instantaneous and Quantitative Functionalization of Gold Nanoparticles with Thiolated DNA Using a PH-Assisted and Surfactant-Free Route. *J. Am. Chem. Soc.* **2012**, *134* (17), 7266–7269. https://doi.org/10.1021/ja3014055.

(68) Zhang, X.; Gouriye, T.; Göeken, K.; Servos, M. R.; Gill, R.; Liu, J. Toward Fast and Quantitative Modification of Large Gold Nanoparticles by Thiolated DNA: Scaling of Nanoscale Forces, Kinetics, and the Need for Thiol Reduction. *J. Phys. Chem. C* **2013**, *117* (30), 15677–15684. https://doi.org/10.1021/jp403946x.

(69) Xia, F.; Zuo, X.; Yang, R.; Xiao, Y.; Kang, D.; Vallée-Bélisle, A.; Gong, X.; Yuen, J. D.; Hsu, B. B. Y.; Heeger, A. J.; Plaxco, K. W. Colorimetric Detection of DNA, Small Molecules, Proteins, and Ions Using Unmodified Gold Nanoparticles and Conjugated Polyelectrolytes. *Proc. Natl. Acad. Sci. U. S. A.* **2010**, *107* (24), 10837–10841. https://doi.org/10.1073/pnas.1005632107.

(70) Liu, G.; Lu, M.; Huang, X.; Li, T.; Xu, D. Application of Gold-Nanoparticle Colorimetric Sensing to Rapid Food Safety Screening. *Sensors (Switzerland)*. MDPI AG December 1, 2018, p 4166. https://doi.org/10.3390/s18124166.

(71) Storhoff, J. J.; Elghanian, R.; Mucic, R. C.; Mirkin, C. A.; Letsinger, R. L. One-Pot Colorimetric Differentiation of Polynucleotides with Single Base Imperfections Using Gold Nanoparticle

Probes. *J. Am. Chem. Soc.* **1998**, *120* (9), 1959–1964. https://doi.org/10.1021/ja972332i.
(72) Sato, K.; Hosokawa, K.; Maeda, M. Rapid Aggregation of Gold Nanoparticles Induced by Non-Cross-Linking DNA Hybridization. *J. Am. Chem. Soc.* **2003**, *125* (27), 8102–8103. https://doi.org/10.1021/ja034876s.
(73) Wang, G.; Akiyama, Y.; Shiraishi, S.; Kanayama, N.; Takarada, T.; Maeda, M. Cross-Linking versus Non-Cross-Linking Aggregation of Gold Nanoparticles Induced by DNA Hybridization: A Comparison of the Rapidity of Solution Color Change. *Bioconjug. Chem.* **2017**, *28* (1), 270–277. https://doi.org/10.1021/acs.bioconjchem.6b00410.
(74) Zhou, Z.; Wei, W.; Zhang, Y.; Liu, S. DNA-Responsive Disassembly of AuNP Aggregates: Influence of Nonbase-Paired Regions and Colorimetric DNA Detection by Exonuclease III Aided Amplification. *J. Mater. Chem. B* **2013**, *1* (22), 2851–2858. https://doi.org/10.1039/c3tb20206b.
(75) Doria, G.; Franco, R.; Baptista, P. Nanodiagnostics: Fast Colorimetric Method for Single Nucleotide Polymorphism/Mutation Detection. *IET Nanobiotechnology* **2007**, *1* (4), 53–57. https://doi.org/10.1049/iet-nbt:20070001.
(76) Bastus, G. N.; Comenge, J.; Puntes, V. Kinetically Controlled Seeded Growth Synthesis of Citrate-Stabilized Gold Nanoparticles of up to 200 Nm. *Langmuir* **2011**, *27*, 11098–11105.
(77) Khlebtsov, N. G. Determination of Size and Concentration of Gold Nanoparticles from Extinction Spectra. *Anal. Chem.* **2008**, *80* (17), 6620–6625. https://doi.org/10.1021/ac800834n.
(78) Zhang, X.; Gouriye, T.; Göeken, K.; Servos, M. R.; Gill, R.; Liu, J. Toward Fast and Quantitative Modification of Large Gold Nanoparticles by Thiolated DNA: Scaling of Nanoscale Forces, Kinetics, and the Need for Thiol Reduction. *J. Phys. Chem. C* **2013**, *117* (30), 15677–15684. https://doi.org/10.1021/jp403946x.
(79) Koetsier, G.; Cantor, E. A Practical Guide to Analyzing Nucleic Acid Concentration and Purity with Microvolume Spectrophotometers. *New Engl. Biolabs* **2019**, *1* (1), 1–8.
(80) Ghosh, D.; Sarkar, D.; Girigoswami, A.; Chattopadhyay, N. A Fully Standardized Method of Synthesis of Gold Nanoparticles of Desired Dimension in the Range 15 Nm-60 Nm. *J. Nanosci. Nanotechnol.* **2011**, *11* (2), 1141–1146. https://doi.org/10.1166/jnn.2011.3090.
(81) Pellegrino, T.; Sperling, R. A.; Alivisatos, A. P.; Parak, W. J. Gel Electrophoresis of Gold-DNA Nanoconjugates. **2007**, *2007*. https://doi.org/10.1155/2007/.
(82) Zheng, T.; Bott, S.; Huo, Q. Techniques for Accurate Sizing of Gold Nanoparticles Using Dynamic Light Scattering with Particular Application to Chemical and Biological Sensing Based on Aggregate Formation. *ACS Appl. Mater. Interfaces* **2016**, *8* (33), 21585–21594. https://doi.org/10.1021/acsami.6b06903.
(83) Danaei, M.; Dehghankhold, M.; Ataei, S.; Hasanzadeh Davarani, F.; Javanmard, R.; Dokhani, A.; Khorasani, S.; Mozafari, M. R. Impact of Particle Size and Polydispersity Index on the Clinical Applications of Lipidic Nanocarrier Systems. *Pharmaceutics* **2018**, *10* (2), 1–17. https://doi.org/10.3390/pharmaceutics10020057.
(84) Ivanov, M. R.; Bednar, H. R.; Haes, A. J. Investigations of the Mechanism of Gold Nanoparticle Stability and Surface Functionalization in Capillary Electrophoresis. *ACS Nano* **2009**, *3* (2), 386–394. https://doi.org/10.1021/nn8005619.
(85) Liu, B.; Liu, J. Interface-Driven Hybrid Materials Based on DNA-Functionalized Gold Nanoparticles. *Matter* **2019**, *1* (4), 825–847. https://doi.org/10.1016/j.matt.2019.08.008.
(86) Park, S.; Hamad-Schifferli, K. Evaluation of Hydrodynamic Size and Zeta-Potential of Surface-Modified Au Nanoparticle-DNA Conjugates via Ferguson Analysis. *J. Phys. Chem. C* **2008**, *112* (20), 7611–7616. https://doi.org/10.1021/jp8004426.
(87) Stakenborg, T.; Peeters, S.; Reekmans, G.; Laureyn, W.; Jans, H.; Borghs, G.; Imberechts, H. Increasing the Stability of DNA-Functionalized Gold Nanoparticles Using Mercaptoalkanes. *J. Nanoparticle Res.* **2008**, *10* (SUPPL. 1), 143–152. https://doi.org/10.1007/s11051-008-9425-9.
(88) Jameel, Z. N. Synthesis of the Gold Nanoparticles with Novel Shape via Chemical Process and Evaluating the Structural, Morphological and Optical Properties. *Energy Procedia* **2017**, *119*, 236–241. https://doi.org/10.1016/j.egypro.2017.07.075.
(89) Samuels, D. C. Life Span Is Related to the Free Energy of Mitochondrial DNA. *Mech. Ageing Dev.* **2005**, *126* (10), 1123–1129. https://doi.org/10.1016/j.mad.2005.05.003.
(90) Hughes, R. A.; Ellington, A. D. Synthetic DNA Synthesis and Assembly: Putting the Synthetic

in Synthetic Biology. *Cold Spring Harb. Perspect. Biol.* **2017**, *9* (1). https://doi.org/10.1101/cshperspect.a023812.

(91) Cárdenas, M.; Barauskas, J.; Schullén, K.; Brennan, J. L.; Brust, M.; Nylander, T. Thiol-Specific and Nonspecific Interactions between DNA and Gold Nanoparticles. *Langmuir* **2006**, *22* (7), 3294–3299. https://doi.org/10.1021/la0530438.

(92) Szabat, M.; Pedzinski, T.; Czapik, T.; Kierzek, E.; Kierzek, R. Structural Aspects of the Antiparallel and Parallel Duplexes Formed by DNA, 2'-O-Methyl RNA and RNA Oligonucleotides. *PLoS One* **2015**, *10* (11), 1–16. https://doi.org/10.1371/journal.pone.0143354.

(93) Ghosh, M.; Madauß, L.; Schleberger, M.; Lebius, H.; Benyagoub, A.; Wood, J. A.; Lammertink, R. G. H. Understanding Mono- And Bivalent Ion Selectivities of Nanoporous Graphene Using Ionic and Bi-Ionic Potentials. *Langmuir* **2020**, *36* (26), 7400–7407. https://doi.org/10.1021/acs.langmuir.0c00924.

(94) Wang, X.; Lim, H. J.; Son, A. Characterization of Denaturation and Renaturation of DNA for DNA Hybridization. *Env. Anal Heal. Toxicol* **2014**, *29* (0), e2014007-0. https://doi.org/10.5620/eht.2014.29.e2014007.

(95) Sanromán-Iglesias, M.; Lawrie, C. H.; Liz-Marzán, L. M.; Grzelczak, M. Nanoparticle-Based Discrimination of Single-Nucleotide Polymorphism in Long DNA Sequences. *Bioconjug. Chem.* **2017**, *28* (4), 903–906. https://doi.org/10.1021/acs.bioconjchem.7b00028.

GOLD NANOPROBES FOR MOLECULAR DETECTION OF SNPS RELATED TO LI

ANDRÉ DIAS

2022